The Effects of Mechanical Forces on Human Embryonic Stem Cell Behavior

By

Tuğba Topal

A dissertation submitted in partial fulfillment
of the requirements for the degree of
Doctor of Philosophy
(Biomedical Engineering)
in the University of Michigan
2018

Doctoral Committee:

Professor Cheri X. Deng, Co-Chair
Professor Paul H. Krebsbach, Co-Chair, University of California, Los Angeles
Associate Professor Jianping Fu
Professor Andy Putnam
Professor Shuichi Takayama, Georgia Institute of Technology

Tuğba Topal

tugba@umich.edu

ORCID iD: 000-0002-8865-9656

…dedicated to the people who seriously make an effort to be a part of my life.

Acknowledgements

I would like to express my deepest gratitude to my advisor, Dr. Paul Krebsbach for believing in me, and giving me the opportunity to work in his lab and helping me to be an independent researcher and a team player. It was my greatest luck that I had a chance to work with him. I would like to extend very big and special thanks to Prof. Cheri X. Deng for all the guidance, support, and mentorship she offered me in my last two years of graduate school. I would like to thank to my committee members: I owe special thanks to Dr. Shuichi Takayama for your steadfast resolve to do great science and your guidance and support. I would like to thank Dr. Andy Putnam for opening my mind while taking his class with norm-breaking discussions during the early graduate school, and also his valuable input on my dissertation. I would like to thank Dr. Jianping Fu for his valuable input and insights on my dissertation. I would also like to a special thanks to Prof. Joerg Lahann for ample resources to complete my research projects in my final year of graduate school.

I extend my gratitude to my past and current colleagues, including Dr. Luis Villa-Diaz, Dr. Adeline Hong, and Dr. Zhenzhen Fan. I would like to highlight a very special thanks to more than a colleague- my buddy; Joe Nguyen, I would not be able come this far without your constant support, patience, and encouragement. I would like to thank to my life-long friend from undergraduate, Zeynep Öztop, she is an incredible human being and I want to thank to her for too many reasons to list.

I need to acknowledge funding sources that were critical to my success: Ministry of Education the Republic of Turkey, Graduate Research Fellowship (1416) in the USA and NIH (R01 EB019436).

My family: Mom, Dad, and my sister and brothers, thank you for your constant support and encouragement during this journey.

TABLE OF CONTENTS

5.3 Rapid Formation of Neural Rosettes via Cyclic Strain

LIST OF FIGURES

ABSTRACT

The development of an organism from a zygote into a fully functional 3D individual is a process in which a strong coupling of morphogens and mechanical forces is coordinated with embryo shape. During development, cells communicate with each other through cell-cell junctions and with their microenvironment via mechanical cues to regulate cell fate, re-organize the extracellular matrix, and guide developmental process. Most studies on human embryonic stem cells (hESCs) focused on how external soluble factors including growth factors and small inhibitors, gene and protein expression, and signaling pathways to maintain stemness or initiate differentiation of these cells. A various array of environmental factors including the effect of geometry and mechanical properties of extracellular matrix on stem cells contributes to altering stem cell fate. Recently, increasing evidence has revealed the importance of mechanical factors in affecting migration, proliferation and stem cell differentiation *in vitro*.

In this dissertation, we focus on the development and application of novel bioengineering approaches to understand the effects of mechanical forces on hESC behaviors and the directed differentiation of hESCs. Specifically, by employing a microfluidic device to induce controlled and regulated forces that apply global mechanical forces to adherent hESCs, we find that uniaxial substrate stretching disrupts the pluripotency circuit and initiates the exit of transcription factors, Nanog and Oct4, from the nucleus into the cytoplasm via a nuclear export protein (CRM1) as early as 30 min after stretch application and for 2 hours on a flexible substrate coated with Matrigel, and is not reliant on exogenous soluble factors. In order to pinpoint to the receptors responsible for mechanical sensing, we employ a novel technique, acoustic tweezing cytometery (ATC), that utilizes ultrasound pulses to actuate functionalized microbubbles targeted to integrin in order to apply cyclic strain to hESCs. We find that ATC-mediated cyclic forces applied for 30 min induced immediate global responses in the colony, including increased contractile force, enhanced calcium activity, as well as decreased nuclear expression of pluripotency transcription factors Oct4 and Nanog, leading to rapid differentiation and characteristic epithelial-mesenchymal transition (EMT) events that depend on focal adhesion kinase activation and cytoskeleton tension. These results reveal a unique, rapid mechanoresponsiveness and community behavior of hESCs to integrin-targeted cyclic forces. Furthermore, we demonstrate an integrative mechanotransduction that induced neural rosette formation of hESCs via the application of ATC and induction medium. We observe upregulation of Pax6 and Sox1 in as early as 6 hours, following by neural rosettes formation in 48 hours, which is much faster compared to the typical 10-15 days needed with conventional neural rosettes formation protocols.

Together, this dissertation presents novel findings and insights regarding the effects of external mechanical forces on hESCs. Such information may help elucidate the mechanobiology of hESCs, and thus advance our knowledge of human embryogenesis, regenerative medicine, and tissue engineering.

CHAPTER I

Introduction

“In the case of all things, in which totally is not, as it were, a mere heap, but the whole thing is something besides the parts, there is a cause” Aristotle [*Metaphysics, VIII.6, 1045a8-10*]. The question of “human development” is one that not only excites philosophers to understand human behavior and nature, but also stimulates scientists to develop and improve new approaches for modern medicine.

Embryonic development is one of the most dramatic processes in the genesis of complex spatial organization in biology. The complete development of a human embryo is a 40-weeks of process, and each stage of this journey is critical and sophisticated. Notwithstanding of such importance, our understanding of development of humans is limited due to lack of techniques and ethical controversies. The goal of this dissertation is therefore to fill such a gap in knowledge and technology, by taking advantage of the recent human embryonic stem cells biology and engineering approaches to develop *in vitro* methods for studying how external mechanical cues alter and control hESC fate - a critical developmental cue that ensues throughout the development.

In this chapter, the background and the outline of this dissertation is briefly summarized.

1.1 Background and Motivation of Research

1.1.1Human Embryogenesis in the First Five Days

Development of an embryo from a sperm and an egg initiates a complex process of self-assembly in which living cells form into heterogeneous tissues and organs with highly specialized forms and functions (*1-3*) The first mechanical effect before embryogenesis begins as a sperm penetrates into the oocyte; by utilizing spring forces of mechanical energy stored in actin filaments within actin bundles (*4*) and triggering the complex process of fertilization. After fertilization, the fertilized egg (also known as the zygote) starts to divide, and the number of cells (known as blastomeres) in the embryo rapidly increases, but the width of the embryo is maintained at 100 μm in diameter (Figure 1-1). At the late 8-cell stage, compaction starts via cadherin receptors at the adhesion sites and the embryo continues its progression into the morula stage (*5*). During this process, cells are initially separated from each other, and then they stick to each other and begin to flatten out. Tight junctions strengthen the contact among them and this contact leads to their compaction. The first cell lineage differentiation, known as the trophectoderm epithelium, occurs at this stage by cell polarity changes (*6, 7*). The outermost blastomeres of the zygote only contact cells internally (*8*), whereas the innermost blastomeres of the zygote experience tensile and compression forces by neighboring cells, which are strengthened by tight junctions. This mechanical contraction is required for pre-implantation development (*9*). These inner and outer blastomeres in the morula stage embryo divide and rearrange to form a hollow cluster, and the embryo enters into the following stage, called “blastocyst”. The innermost blastomeres form what it is known as the inner cell mass (ICM), which will subsequently differentiate into the three germ layers: endo-, ecto-, and meso- derm (*7*). While the outer blastomeres form the trophectoderm. In the ICM, the initial diversification and distribution of cells acquired a "salt and pepper" pattern(*10-12*) (Figure 1-2 B).In the late ICM stage the layer of cells lining in the cavity is called the hypoblast, and will form the primitive endoderm, while the cluster of cells situated inside are named the epiblast(*13*)(Figure 1-2).

The well-established dogma is that soluble morphogens (diffusible signaling molecules in a concentration gradient) spatially control the changes in cell growth, migration, differentiation and cell fate switching(*15*). This theory suggests that soluble factors stimulate biochemical responses and changes in gene expression in cells that drive tissue patterning during development. Even though it has been shown that these factors are crucial for embryo development, by now it is well established how mechanical forces, either extrinsic from the environment or intrinsic from cellular structures, generated within the cells and tissues of the embryo are equally important as those delivered by chemicals cues in deciding the cell fate in development (*16, 17*) (Figure 1-3).

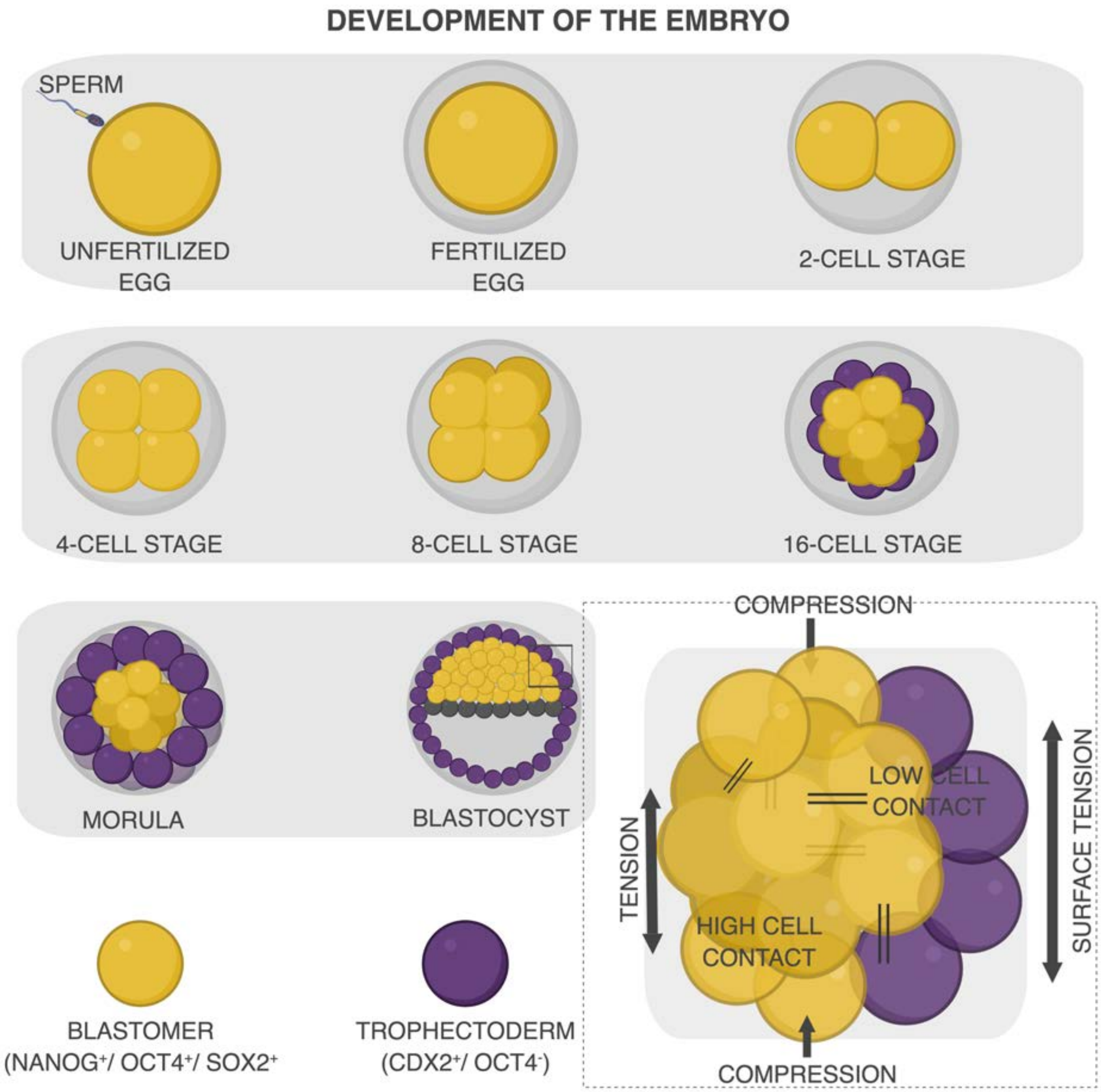

Figure 1-1 Mechanical Transcriptional Control in Early Embryo Development during the first five days. After fertilization, one single cell starts dividing into two, then four, and the number of the cells at the blastocyst stage is more than 100 in ~100 µm size embryo. Reproduced from Rossant et al.(*14*)

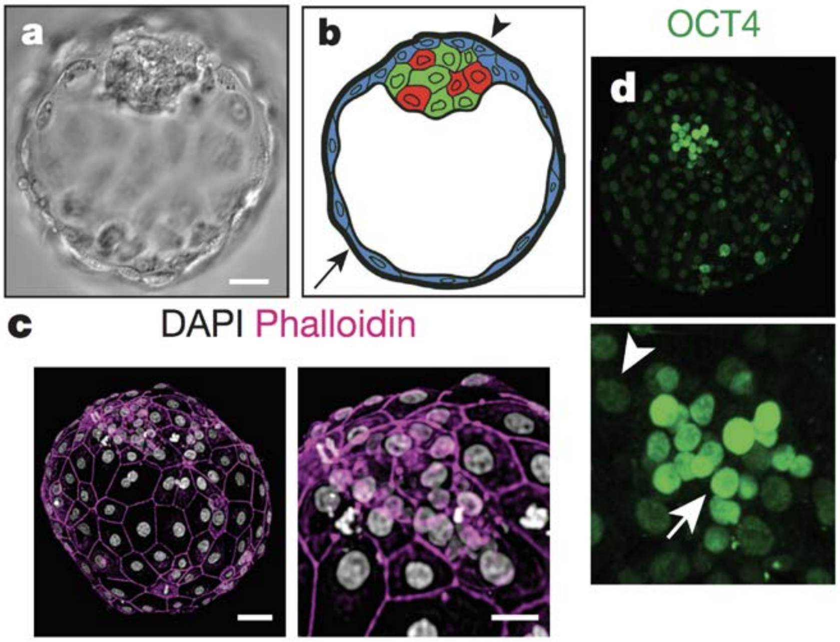

Figure 1-2 In vitro cultured human embryos in day post fertilization 6 (d.p.f.6) by Deglincerti et al(*18*) (a-d) DIC image of a d.p.f. 6 human blastocyst (a), cartoon of d.p.f.6 human embryo with salt-pepper distribution of Oct4 (green), Gata6 (red) (b), immunostaining of d.p.f.6 blastocyst DAPI (white) and phalloidin (magenta, actin) (c), and 3D rendering of a d.p.f 6 blastocyst (top) and ICM-zoom (bottom) (d). Scale bars: 50 µm (embryo), 20 µm (zoom). *Reproduced from Deglincerti et al(*18*).

Particularly, morphogenic events are mediated by mechanical cues that include physical forces (e.g. tension, compression or shear stress) that are translated into biochemical signals to coordinate regulation of proliferation, differentiation, and rearrangement of cells in the correct shaped embryos (*19*). The alignment of this cell lining solely by gene expression or chemical cues is hard to explain, rather we propose that cell generated forces (tensional and compressional) between cells in the ICM is also involved in this organization.

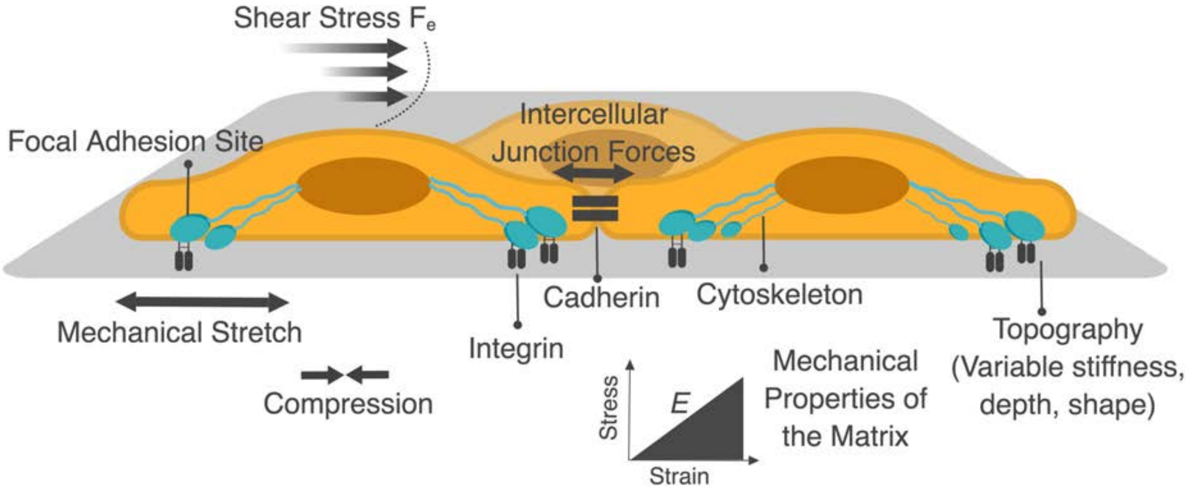

Figure 1-3 Schematic showing biophysical signals regulating stem cell fate in their niche and the involved reciprocal interactions. Biophysical signals in the stem cell microenvironment including matrix rigidity, tension and compression, flow shear stress, and other mechanical forces such as intercellular junctional forces via cadherins. Stem cells can sense these external/ internal biomechanical stimuli via focal adhesions, cell surface receptors, cell-cell junctions, and actin cytoskeleton, and alter gene/ protein expression, proliferation, and differentiation. Reproduced from Vining et al. (*17*)

1.1.2 Human Embryonic Stem Cells: Resource to Understand Human Development and for Tissue Engineering and Regenerative Medicine Applications

Human embryonic stem cells (hESC), are pluripotent stem cells that are derived from the inner cell mass of the developing blastocyst and are able to self-renew and to maintain their pluripotency under certain conditions indefinitely, and able to differentiate into all human germ layers (Endoderm, Ectoderm, and Mesoderm) and extraembryonic lineage including trophectoderm and primitive ectodermal-like cells *in vitro* and *in vivo* *(20-24)*. Although it is known that pluripotent stem cells are only transiently present in embryo development, and quickly differentiation into various somatic cells through developmental process (*22, 23*), isolating *ex vivo* pluripotent embryonic stem cells from inner cells mass of blastocyst in human embryos and maintaining pluripotency in laboratory under certain conditions is possible (*25, 26*). These cells are capable of expression high level of key transcription factors including NANOG, OCT4 (POU5F1), SOX2, and SSEA3/4 that are identified as significant to maintain the inner cell pluripotency(*27-29*). These features have directed to anticipations that hESCs might be valuable to study early human development since hESCs may provide a valid model to comprehend complex signaling pathways in human embryos due to their ability to differentiate into specific cells that take place during early development. Although utilizing hESCs have raised various ethical concerns and controversies including destruction of human embryos, and these cells provide an expedient source for several potential applications both for basic science and medical treatment. However, these cells have important hurdles including immune rejections after transplantation. Research on human hESCs and with the discovery of induced pluripotent stem cells (iPSCs) has attracted attention for regenerative medicine due to their capacity to differentiate into any cell type, and for developmental biologists to understand how embryogenesis progresses(*20*). Since iPSC derived from somatic cells of patient, it is assumed that these cells hold a great promise to comprehend disease mechanism due to their unlimited capacity of self-renew and differentiate, to screen effective and safe drugs, to leverage the self-organization of organoids for cell replacement therapies, to treat patients of numerous diseases and injuries such as Parkinson, ALS, and spinal cord injury in regenerative medicine and tissue engineering (*30-36*). Although iPSC technology has an enormous potential, there are some challenges including teratoma formation since even small number of undifferentiated cells could result in the teratoma formation in the long-term application (*37*). Furthermore, despite these cells have a great potential and show promising results, there are many evidences that hiPSC derived cardiac or neuron cells do not exhibit the morphological and functional features of adult cardiomyocytes (*38, 39*).

1.1.3 Controlling Embryonic Stem Cell Fate

The difficulty and inability to access human embryonic cells during development makes it challenging to test and determine how mechanical forces alter embryo shape and how sensitive embryonic cells are during early development. Albeit, traditional stem cell biologists have been utilizing soluble factors to understand cell fate, recent evidence suggest that regulation of stem cell fate is strongly influenced by the coexisting mechanical cues, topological, and external cyclic forces *in vitro*, even in the absence of soluble growth factors (*40-43*). Accumulating experimental evidence suggests that mechanical forces have a critical role in development by utilizing data from cultured embryonic stem cells (hESCs), which are derived from early blastocyst stage of the embryo, to study biological responses of mechanical cues (*19, 44*).

1.1.3.1 Stiffness and Nanotopography of Extracellular Matrix

hESCs have the ability to sense micro- and nano-scale geometric cues from their microenvironment. Accumulating experimental evidences show that ECM mechanical properties alter stem cell fate due to being a major niche element to provide cellular support, maintenance of self-renewal, proliferation, and differentiation (*45-48*). Cells on the substrates that exert tensile stress on the cytoskeleton result in exerting tensile stress in the cytoskeleton by altering contractility. Studies on compliant substrates demonstrated neural induction of hESCs and hiPSCs in the presence of small inhibitors, such as Smad inhibitor, through Hippo and Yap signaling pathways (*49, 50*). Further *Ali et al*. reported neural differentiation of mouse ESC on variety of rigidities (*51*). However, a recent study showed that compliant substrate induces mesodermal differentiation, while enhancing endothelial specification in the absence of small inhibitors without manipulating Wnt signaling pathway (*52*).

The influence of topography on stem cell differentiation and behavior has been comprehensively reviewed (*41, 44, 53-55*). The Nano-topography of ECM have been shown to change alignment and elongation of hESC on 600 nm PDMS gratings by altering various cytoskeleton components scuh as F-actin, α- and γ- tubulin (*56*). Studies on nano-topography-induced differentiation in pluripotent stem cells have demonstrated that substrate topography can enhance neural differentiation of stem cells, and/or are differentiated into neurons by groove patterns in the absence of bFGF (*57*). Abagnale *et al.,* demonstrated that submicrometer groove-ridge structures with a periodicity in 650nm and height of 200nm can modulate the shape of hiPSC colonies by regulating cell polarity and guiding the orientation of actin fibers (*58*). Further, Ankam *et al.* examined the role of various topographical cues on the differentiation of hESCs into neuronal or glial lineage by culturing these cells on continuous anisotropic gratings patterned on PDMS (Nano-gratings: Depth:0.25-2 μm, Width: 0.25-2 μm, Pitch 0.25-2μm) and discontinuous anisotropic microscale sized pillars (Micro-gratings: Depth:0.08-2 μm, Width: 1-2 μm, Pitch 1-2μm) (*59*). This study shows that the anisotropic gratings promote hESCs into neuronal differentiation while the isotropic patters, the pillars and wells, promote glial differentiation (*60*). Moreover, Chen *et al*. showed that culturing hESCs on smooth surfaces promoted self-renewal and maintenance of pluripotency, while rough surfaces induce spontaneous differentiation (*60*). In a recent report, the same group has shown that hESCs differentiated into neural lineage in response to synergistic of nano-topography combined with growth factors. The author reported that neural differentiation differs based on the nano roughness (R_q) of the surface, and it was reported that while unprocessed smooth glass surface R_q =1nm maintains pluripotency, nano rough surface, R_q = 200nm forms polarized neural tube-like rosettes in day 8 (*61*). Overall, combining these approaches and optimizing the culture conditions with these biomechanical cues in the presence of soluble growth factors must be understood to enrich specific neural lineages and explore the mechanism underneath.

1.1.3.2 Spatial Organization of hESCs

In addition to the influence of ECM stiffness and nanotopography, there is significant evidence that may also contribute on cell shape. The stem cell niches play a critical role in directing hESC fate and in controlling the differentiation of pluripotent stem cell through cell patterning, which has been used as a model to study mammalian embryogenesis and to precisely control the area of cell attachment in order to understand embryonic spatial patterning *in vitro*. Changes in the geometry of stem cells may change morphogenetic factor distribution and cell-cell interactions. Spatial patterning of individual embryonic stem cells changes to drive morphogenesis by altering tissue architecture (*62*). Adhesive islands with micro patterning confirmed that variation of local internal stress is distributed over the cytoskeleton and resisted by cell-cell and cell-ECM adhesions (*63*). Colony size in a serum- and cytokine-free environment directs self-renewal and differentiation toward the extraembryonic endoderm lineage *in vitro* (*64*).

For the first time, it has shown that microcontact printing (μCP) technology is able to direct hESC fate by controlling the colony size and differentiate into either the mesoderm or the endoderm lineage in the presence of bone morphogenetic protein 2 (BMP2) and Activin A (*65*). The authors have shown that while 1200-μm-diameter colonies (large) give rise to mesoderm lineage, 200-μm colonies (small) give rise to definitive endoderm. Further study has demonstrated that hESCs grown on micropatterned surfaces demonstrate reproducible spatial differentiation upon treatment with BMP4 and geometrical confided hESC colonies self-organize to germ layers: cells at the outer rim differentiated into trophoctoderm, while cells at the inner rim differentiated into ectodermal and cells that express mesendoderm primitive streak markers located in between these two rims, depending of the size of the micropattern (*66*). More recently, this μCP technique has been extended to model neural ectodermal organization on 400 μm of two-dimensional PDMS substrates by applying neural differentiation protocols on confined hESCs (*67*). Overall, confinement of hESC colonies is affected by space, area, and aspect ratio of the topographical features and lead to differentiation of these cells. Although these studies demonstrate that endogenous biophysical cues may be ruling stem cell fate by more than biochemical inhibitors such as SMAD/ TGFB/ Nodal inhibitors, how these geometrical confinement and colony size affects traction forces at the edges of the colony alter cell size and shape, change cytoskeletal contractile forces, and re-organize morphogenetic factors remains elusive.

1.1.3.3 The Effect of External, Local, Small Mechanical Cues

Cells exert, sense, and respond to physical forces through numerous different mechanisms, and to measure cellular push and pull forces, a large number of experimental techniques including optical magnetic tweezing cytometry, atomic force microscopy, and magnetic tweezers have emerged with various ranges of frequencies (0.01- 1,000Hz) and large range of forces (up to ~100 nN) to make easily interpretable measurements (*68-73*).

As discussed earlier, cell shape and stiffness of microenvironment can be a potent regulator of differentiation in hESCs. Biophysical forces play a vital role in the early stage of the embryo development. However, cell-generated forces, specifically tensile forces, and their effect on embryonic stem cells differentiation remain elusive. Levenberg and her colleagues recently have shown how tensile forces alter mouse embryonic stem cells differentiation in three-dimensional (3D) environment (*40, 74*). The authors exerted uniaxial and cyclic tensile forces on mESCS in cell-embedded collagen scaffolds. Their work has shown that cyclic stretching was exerted on mESCS for six days, and they determined that cells were differentiated into mesoderm differentiation by looking at expression of Brachyury (Brach-T); they confirmed this result with immunohistochemistry experiment.

Moreover, *Chowdhury et al*. indicated that adherent mouse embryonic stem cells (mESCS) were softer and more sensitive than applied local cyclic stress via magnetic tweezers mESC-derived differentiated cells (*75*). This local cyclic force was applied through focal adhesions and leads to cell differentiation with downregulation of Oct4 and accompanying cell spreading. Overall this study validate that a local, small, cyclic stress plays a critical role in inducing strong biological responses in soft mESCs and in shaping embryogenesis in early mammalian development. However, we have yet to understand what the intracellular molecular strain sensor(s) in a mES-cell exist. Even though the authors showed down regulation of Oct3/4 after the applied cyclic forces, it is unclear what kind of lineage the cell entering. A study suggests that E-cadherin mediated cell-cell contact prevents an increase in surface contractility at cell-cell to facilitate compaction. The study revealed that the quantitative map in space and time of each cell surface tension in a living mouse embryo by utilizing from pipette aspiration is driven by increased actomyosin contractility at the cell-surface interface, as opposed to an increased cell-cell adhesion as commonly thought (*76*). Self-organization of the embryo and specification of the germ layers into a blastocyst rely on intrinsic and extrinsic contractile mechanical forces before embryo implants to uterus (*77*). Further, applying external 15% cyclic strain to hiPSC and hESC utilizing FlexCell system demonstrated inhibition of pluripotency transcription factors in 12 hours (*78, 79*). Contrary, there are experimental evidences suggesting mechanical strain supports self-renewal and maintains pluripotency depending on the type of the external mechanical stimuli, (e.g. equibiaxial cyclic, uniaxial stretch), the length of a time of strain exposure (e.g hours and days), and given growth factors and small inhibitors (TGFβ, Smad2/3) (*80, 81*). For example, Saha et al report that continuous application of a 10% equibiaxial cyclic strain at frequencies above 6 cycles per minute by using FlexCell system for 12 days maintains pluripotency through action of TGFb/ Activin A/ Nodal pathway (*80, 81*), although another study that was also utilized FlexCell system demonstrated that 15% applied strains at 12 cycles per minute for 12 hours reduced pluripotency gene expression by activating Rho/ROCK and decreasing phosphorylation of AKT (*78*).

1.2 Research Topics and Dissertation Outline

1.2.1 Rapid Nuclear Export of Nanog and Oct4 by External Uniaxial Force

During pre-implantation development, blastomers experience mechanical forces that alter cell fates within an embryo. Maintenance of stem cell pluripotency requires the activity of all three of the transcription factors, Nanog, Oct4, and Sox2. During differentiation, the levels of all three factors decrease but in different orders depending on the direction of differentiation. What could be the role of mechanical forces in regulating the timing of changes in levels of these three key transcription factors? We hypothesized that mechanical forces transmitted through different combinations of cell surface receptors may play a role. Upon performing experiments, we were surprised to find that mechanical strain applied to human embryonic stem cells for as short as 30-min induces rapid and irreversible nuclear-to-cytoplasmic translocation of Nanog and Oct4 but not Sox2. On Matrigel coated substrates, these translocations are directed by intracellular transmission of biophysical signals from cell surface integrins to nuclear CRM1 and is not reliant on exogenous soluble factors. Interestingly, on E-cadherin coated substrates, presumably with minimal integrin engagement, mechanical strain induced rapid nuclear-to-cytoplasmic translocation of all three transcription factors. These findings provide fundamental insights into early developmental processes and may facilitate mechanotransduction-mediated bioengineering approaches to influencing stem cell fate determination.

Therefore, in chapter 2, we will describe investigations explicitly aimed at understanding the mechanosensitive properties of hESCs. To demonstrate mechanosensitive properties of hESCs, we utilized from a stretchable micro-molded poly(dimethylsiloxane) (PDMS) chips to recreated “outside-in” mechanical stimuli to hESCs in the form of uniaxial stretching. We determined that hESCs are mechonosensitive to external uniaxial stretch and these forces disrupt the pluripotency transcription complex circuitry and initiate the exit from pluripotency via nuclear export signaling, CRM1 (XPO1). Our results highlighted the important mechanism between external uniaxial stretch and the pluripotency of hESCs and a novel approach to comprehend mechanotransduction and its involvement in hESCs function.

1.2.2 Cyclic Forces Induces Rapid Differentiation of Human Embryonic Stem Cells

Mechanical forces are critical to modulate gene expression, proliferation and migration, and differentiation in hESCs. Existing tools including optical and magnetic tweezers that can apply mechanical forces to single cells simultaneously are still limited due to the lack of multidisciplinary approaches involving the combination of stem cell biology, physics, and material sciences. Considering the importance of mechanical cues to regulate mechanoresponsiveness of hESCs, it is necessary to improve new tools that are capable of controlling subcellular mechanical forces to apply on a large number of cells, and colonies in hESCs.

Hence, in chapter 3, we will discuss a novel ultrasound technique, which is called Acoustic Tweezing Cytometery (ATC), to stimulate functionalized lipid microbubbles that are attached to integrins on single live hESCs and hESC colonies to apply subcellular mechanical forces in the nanonewton (nN) range (*82*). Our results demonstrated that ATC mediated forces could generate rapid mechanoresponses in single hESCs and hESC colonies by leading these cells rapid differentiation by the loss of Nanog and Oct4 and characteristic epithelial-to-mesenchymal transition (EMT) event that depend on focal adhesion and cytoskeleton contractility. Further, orchestration of mechanoresposnes in hESC colonies revealed that integrin-bound microbubbles displacement via ATC on hESC colonies generate cyclic strains and transmit these forces in the center of the colony via cell-cell contact and increased contractility (*82*).

1.2.3 Rapid Formation of Neural-tube Like Rosettes via Cyclic Strain

The role of mechanical forces that are involved in organogenesis are crucial to understanding of how movements of cells leading to mechanical deformation during embryo development. The effects of the external mechanical cues on the differentiation of hESCs are not completely established, and defined protocols utilizing soluble growth factors are not sufficient to explain early embryo development especially considering the speed of differentiation in vivo.

In chapter 4, we combined the ATC technique with growth factors to study how mechanical forces regulate hESC cell fate in a short period of time. We discovered that supplementing neural induction medium for 48 hours with ATC applied hESCs formed neural-tube like rosettes. These results quantitatively reveal how mechanical forces initiates differentiation and synergize with biochemical cues rapidly. Further, these data also suggest that applied cyclic forces are significant biophysical cues that influence neural induction and therefore this tool may be used as an innovative platform for future large-scale culture of hPSCs.

1.3 References

1. S. F. Gilbert, M. J. F. Barresi, *Developmental biology*. (Sinauer Associates, Inc., Publishers, Sunderland, Massachusetts, ed. Eleventh edition., 2016), pp. xxiii, 810 pages, 100 variously numbered pages.
2. J. M. W. Slack, *Essential developmental biology*. (Wiley, Hoboken, NJ, ed. 3rd, 2012), pp. xi, 479 p.
3. L. Wolpert, *Principles of development*. (Oxford University Press, Oxford ; New York, ed. 4th, 2011), pp. xxv, 616 p.
4. J. H. Shin *et al.*, Force of an actin spring. *Biophys J* **92**, 3729-3733 (2007).
5. N. G. Kan *et al.*, Gene replacement reveals a specific role for E-cadherin in the formation of a functional trophectoderm. *Development* **134**, 31-41 (2007).
6. L. M. Wiley, Trophoctoderm: The first epithelium to develop in the mammalian embryo. *Scanning Microscopy* **2**, 417-426 (1988).
7. Y. Marikawa, V. B. Alarcon, Establishment of trophectoderm and inner cell mass lineages in the mouse embryo. *Mol Reprod Dev* **76**, 1019-1032 (2009).
8. T. P. J. Fleming, M.H, From egg to epithelium. (1988).
9. D. Riethmacher, Brinkmann, V and Birchmeier, C, A targeted mutation in the mouse E-cadherin gene results in defective preimplantation development. *PNAS*, (1995).
10. C. Chazaud, Y. Yamanaka, T. Pawson, J. Rossant, Early lineage segregation between epiblast and primitive endoderm in mouse blastocysts through the Grb2-MAPK pathway. *Dev Cell* **10**, 615-624 (2006).
11. K. Kurimoto *et al.*, An improved single-cell cDNA amplification method for efficient high-density oligonucleotide microarray analysis. *Nucleic Acids Res* **34**, e42 (2006).
12. B. Plusa, A. Piliszek, S. Frankenberg, J. Artus, A. K. Hadjantonakis, Distinct sequential cell behaviours direct primitive endoderm formation in the mouse blastocyst. *Development* **135**, 3081-3091 (2008).
13. G. S. Kwon, M. Viotti, A. K. Hadjantonakis, The endoderm of the mouse embryo arises by dynamic widespread intercalation of embryonic and extraembryonic lineages. *Dev Cell* **15**, 509-520 (2008).
14. J. Rossant, P. P. Tam, Blastocyst lineage formation, early embryonic asymmetries and axis patterning in the mouse. *Development* **136**, 701-713 (2009).
15. N. Perrimon, C. Pitsouli, B. Z. Shilo, Signaling mechanisms controlling cell fate and embryonic patterning. *Cold Spring Harb Perspect Biol* **4**, a005975 (2012).
16. M. Simunovic, A. H. Brivanlou, Embryoids, organoids and gastruloids: new approaches to understanding embryogenesis. *Development* **144**, 976-985 (2017).
17. K. H. Vining, D. J. Mooney, Mechanical forces direct stem cell behaviour in development and regeneration. *Nat Rev Mol Cell Biol* **18**, 728-742 (2017).
18. A. Deglincerti *et al.*, Self-organization of the in vitro attached human embryo. *Nature* **533**, 251-254 (2016).
19. M. A. Wozniak, C. S. Chen, Mechanotransduction in development: a growing role for contractility. *Nat Rev Mol Cell Biol* **10**, 34-43 (2009).

20. K. Takahashi *et al.*, Induction of pluripotent stem cells from adult human fibroblasts by defined factors. *Cell* **131**, 861-872 (2007).
21. J. A. Thomson *et al.*, Embryonic stem cell lines derived from human blastocysts. *Science* **282**, 1145-1147 (1998).
22. M. Amit *et al.*, Clonally derived human embryonic stem cell lines maintain pluripotency and proliferative potential for prolonged periods of culture. *Dev Biol* **227**, 271-278 (2000).
23. J. Itskovitz-Eldor *et al.*, Differentiation of human embryonic stem cells into embryoid bodies compromising the three embryonic germ layers. *Mol Med* **6**, 88-95 (2000).
24. M. F. Pera *et al.*, Regulation of human embryonic stem cell differentiation by BMP-2 and its antagonist noggin. *J Cell Sci* **117**, 1269-1280 (2004).
25. S. M. Morgani, J. M. Brickman, The molecular underpinnings of totipotency. *Philos Trans R Soc Lond B Biol Sci* **369**, (2014).
26. J. Nichols, A. Smith, Pluripotency in the embryo and in culture. *Cold Spring Harb Perspect Biol* **4**, a008128 (2012).
27. P. D. Tonge, M. Shigeta, T. Schroeder, P. W. Andrews, Functionally defined substates within the human embryonic stem cell compartment. *Stem Cell Res* **7**, 145-153 (2011).
28. L. F. Batista, Telomere biology in stem cells and reprogramming. *Prog Mol Biol Transl Sci* **125**, 67-88 (2014).
29. I. International Stem Cell *et al.*, Characterization of human embryonic stem cell lines by the International Stem Cell Initiative. *Nat Biotechnol* **25**, 803-816 (2007).
30. B. Connor, Concise Review: The Use of Stem Cells for Understanding and Treating Huntington's Disease. *Stem Cells* **36**, 146-160 (2018).
31. G. H. Underhill, S. R. Khetani, Bioengineered Liver Models for Drug Testing and Cell Differentiation Studies. *Cell Mol Gastroenterol Hepatol* **5**, 426-439 e421 (2018).
32. K. G. Chen *et al.*, Pluripotent Stem Cell Platforms for Drug Discovery. *Trends Mol Med*, (2018).
33. R. A. Barker, M. Gotz, M. Parmar, New approaches for brain repair-from rescue to reprogramming. *Nature* **557**, 329-334 (2018).
34. N. Jongkamonwiwat, P. Noisa, Biomedical and clinical promises of human pluripotent stem cells for neurological disorders. *Biomed Res Int* **2013**, 656531 (2013).
35. N. Sayed, C. Liu, J. C. Wu, Translation of Human-Induced Pluripotent Stem Cells: From Clinical Trial in a Dish to Precision Medicine. *J Am Coll Cardiol* **67**, 2161-2176 (2016).
36. L. M. Ferreira, M. A. Mostajo-Radji, How induced pluripotent stem cells are redefining personalized medicine. *Gene* **520**, 1-6 (2013).
37. J. Y. Li, N. S. Christophersen, V. Hall, D. Soulet, P. Brundin, Critical issues of clinical human embryonic stem cell therapy for brain repair. *Trends Neurosci* **31**, 146-153 (2008).
38. O. Caspi *et al.*, Transplantation of human embryonic stem cell-derived cardiomyocytes improves myocardial performance in infarcted rat hearts. *J Am Coll Cardiol* **50**, 1884-1893 (2007).

39. Y. Shiba *et al.*, Human ES-cell-derived cardiomyocytes electrically couple and suppress arrhythmias in injured hearts. *Nature* **489**, 322-325 (2012).
40. D. Dado, M. Sagi, S. Levenberg, A. Zemel, Mechanical control of stem cell differentiation. *Regen Med* **7**, 101-116 (2012).
41. D. E. Discher, D. J. Mooney, P. W. Zandstra, Growth factors, matrices, and forces combine and control stem cells. *Science* **324**, 1673-1677 (2009).
42. F. Guilak *et al.*, Control of stem cell fate by physical interactions with the extracellular matrix. *Cell Stem Cell* **5**, 17-26 (2009).
43. G. C. Reilly, A. J. Engler, Intrinsic extracellular matrix properties regulate stem cell differentiation. *J Biomech* **43**, 55-62 (2010).
44. R. Goetzke, A. Sechi, L. De Laporte, S. Neuss, W. Wagner, Why the impact of mechanical stimuli on stem cells remains a challenge. *Cell Mol Life Sci*, (2018).
45. M. M. Stevens, J. H. George, Exploring and engineering the cell surface interface. *Science* **310**, 1135-1138 (2005).
46. N. D. Evans *et al.*, Substrate stiffness affects early differentiation events in embryonic stem cells. *Eur Cell Mater* **18**, 1-13; discussion 13-14 (2009).
47. W. H. Guo, M. T. Frey, N. A. Burnham, Y. L. Wang, Substrate rigidity regulates the formation and maintenance of tissues. *Biophys J* **90**, 2213-2220 (2006).
48. E. Hadjipanayi, V. Mudera, R. A. Brown, Close dependence of fibroblast proliferation on collagen scaffold matrix stiffness. *J Tissue Eng Regen Med* **3**, 77-84 (2009).
49. Y. Sun *et al.*, Hippo/YAP-mediated rigidity-dependent motor neuron differentiation of human pluripotent stem cells. *Nat Mater* **13**, 599-604 (2014).
50. S. Musah *et al.*, Substratum-induced differentiation of human pluripotent stem cells reveals the coactivator YAP is a potent regulator of neuronal specification. *Proc Natl Acad Sci U S A* **111**, 13805-13810 (2014).
51. S. Ali, I. B. Wall, C. Mason, A. E. Pelling, F. S. Veraitch, The effect of Young's modulus on the neuronal differentiation of mouse embryonic stem cells. *Acta Biomater* **25**, 253-267 (2015).
52. Q. Smith *et al.*, Compliant substratum guides endothelial commitment from human pluripotent stem cells. *Sci Adv* **3**, e1602883 (2017).
53. D. Hoffman-Kim, J. A. Mitchel, R. V. Bellamkonda, Topography, cell response, and nerve regeneration. *Annu Rev Biomed Eng* **12**, 203-231 (2010).
54. Y. Yang, K. Wang, X. Gu, K. W. Leong, Biophysical Regulation of Cell Behavior-Cross Talk between Substrate Stiffness and Nanotopography. *Engineering (Beijing)* **3**, 36-54 (2017).
55. Y. Shao, J. Fu, Integrated micro/nanoengineered functional biomaterials for cell mechanics and mechanobiology: a materials perspective. *Adv Mater* **26**, 1494-1533 (2014).
56. S. Gerecht *et al.*, The effect of actin disrupting agents on contact guidance of human embryonic stem cells. *Biomaterials* **28**, 4068-4077 (2007).
57. M. R. Lee *et al.*, Direct differentiation of human embryonic stem cells into selective neurons on nanoscale ridge/groove pattern arrays. *Biomaterials* **31**, 4360-4366 (2010).

58. G. Abagnale *et al.*, Surface Topography Guides Morphology and Spatial Patterning of Induced Pluripotent Stem Cell Colonies. *Stem Cell Reports* **9**, 654-666 (2017).
59. S. Ankam *et al.*, Substrate topography and size determine the fate of human embryonic stem cells to neuronal or glial lineage. *Acta Biomater* **9**, 4535-4545 (2013).
60. W. Chen *et al.*, Nanotopography influences adhesion, spreading, and self-renewal of human embryonic stem cells. *ACS Nano* **6**, 4094-4103 (2012).
61. W. Chen *et al.*, Nanotopography regulates motor neuron differentiation of human pluripotent stem cells. *Nanoscale* **10**, 3556-3565 (2018).
62. I. Salazar-Ciudad, J. Jernvall, S. A. Newman, Mechanisms of pattern formation in development and evolution. *Development* **130**, 2027-2037 (2003).
63. C. M. Nelson *et al.*, Emergent patterns of growth controlled by multicellular form and mechanics. *Proc Natl Acad Sci U S A* **102**, 11594-11599 (2005).
64. R. Peerani *et al.*, Niche-mediated control of human embryonic stem cell self-renewal and differentiation. *EMBO J* **26**, 4744-4755 (2007).
65. L. H. Lee *et al.*, Micropatterning of human embryonic stem cells dissects the mesoderm and endoderm lineages. *Stem Cell Res* **2**, 155-162 (2009).
66. A. Warmflash, B. Sorre, F. Etoc, E. D. Siggia, A. H. Brivanlou, A method to recapitulate early embryonic spatial patterning in human embryonic stem cells. *Nat Methods* **11**, 847-854 (2014).
67. X. Xue *et al.*, Mechanics-guided embryonic patterning of neuroectoderm tissue from human pluripotent stem cells. *Nat Mater* **17**, 633-641 (2018).
68. E. K. Paluch *et al.*, Mechanotransduction: use the force(s). *BMC Biol* **13**, 47 (2015).
69. A. V. Taubenberger, D. W. Hutmacher, D. J. Muller, Single-cell force spectroscopy, an emerging tool to quantify cell adhesion to biomaterials. *Tissue Eng Part B Rev* **20**, 40-55 (2014).
70. N. Bufi, P. Durand-Smet, A. Asnacios, Single-cell mechanics: the parallel plates technique. *Methods Cell Biol* **125**, 187-209 (2015).
71. A. R. Harris *et al.*, Characterizing the mechanics of cultured cell monolayers. *Proc Natl Acad Sci U S A* **109**, 16449-16454 (2012).
72. J. L. Tan *et al.*, Cells lying on a bed of microneedles: an approach to isolate mechanical force. *Proc Natl Acad Sci U S A* **100**, 1484-1489 (2003).
73. C. Grashoff *et al.*, Measuring mechanical tension across vinculin reveals regulation of focal adhesion dynamics. *Nature* **466**, 263-266 (2010).
74. D. Dado-Rosenfeld, I. Tzchori, A. Fine, L. Chen-Konak, S. Levenberg, Tensile forces applied on a cell-embedded three-dimensional scaffold can direct early differentiation of embryonic stem cells toward the mesoderm germ layer. *Tissue Eng Part A* **21**, 124-133 (2015).
75. F. Chowdhury *et al.*, Soft substrates promote homogeneous self-renewal of embryonic stem cells via downregulating cell-matrix tractions. *PLoS One* **5**, e15655 (2010).
76. J. L. Maitre, R. Niwayama, H. Turlier, F. Nedelec, T. Hiiragi, Pulsatile cell-autonomous contractility drives compaction in the mouse embryo. *Nat Cell Biol* **17**, 849-855 (2015).

77. J. L. Maitre *et al.*, Asymmetric division of contractile domains couples cell positioning and fate specification. *Nature* **536**, 344-348 (2016).
78. T. Teramura *et al.*, Mechanical stimulation of cyclic tensile strain induces reduction of pluripotent related gene expressions via activation of Rho/ROCK and subsequent decreasing of AKT phosphorylation in human induced pluripotent stem cells. *Biochem Biophys Res Commun* **417**, 836-841 (2012).
79. A. M. Singh *et al.*, Signaling network crosstalk in human pluripotent cells: a Smad2/3-regulated switch that controls the balance between self-renewal and differentiation. *Cell Stem Cell* **10**, 312-326 (2012).
80. S. Saha, L. Ji, J. J. de Pablo, S. P. Palecek, Inhibition of human embryonic stem cell differentiation by mechanical strain. *J Cell Physiol* **206**, 126-137 (2006).
81. S. Saha, L. Ji, J. J. de Pablo, S. P. Palecek, TGFbeta/Activin/Nodal pathway in inhibition of human embryonic stem cell differentiation by mechanical strain. *Biophys J* **94**, 4123-4133 (2008).
82. T. Topal *et al.*, Acoustic Tweezing Cytometry Induces Rapid Initiation of Human Embryonic Stem Cell Differentiation. *Scientific Reports* **8**, (2018).

CHAPTER II

Rapid Nuclear Export of Nanog and Oct4 by External Uniaxial Force

2.1 Introduction

In human embryo development, pre-implantation is one of the critical development milestones for embryogenesis in the first 5 days. During this process, the number of cells in the embryo increases and these cells reorganize themselves and evolve to form 2-disticnt lineages at 16 cells stage- trophectoderm (TE) and inner cell mass (ICM). At blastocysts stage, cells in ICM distributed as salt and pepper manner, and later they self-organize themselves by physical mechanisms after the specification of the two cell types: the primitive endoderm and epiblast (*1*).

Human embryonic stem cells (ESCs) are derived from ICM and due their ability to give rise to 3-different germ layers; they are a promising resource for regenerative medicine and to study developmental biology. Pluripotency, described as the ability of a stem cell to generate all of the cell types of an organism (*2*), is regulated by a group of transcription factors- NANOG, OCT4, and SOX2- expressed in pluripotent stem cells and the inner cell mass of the blastocyst stage embryo, and down-regulated upon differentiation and gastrulation, respectively(*3-5*). These transcription factors have fundamental roles in early development and are required for the propagation of undifferentiated ESCs in culture(*6*). OCT4 and NANOG are essential regulators of early development and ESC identity, and have distinct roles maintaining pluripotency since disruption of OCT4 or NANOG regulatory circuitry results in the differentiation of inner cell mass and ESCs to trophectoderm and extra embryonic endoderm, respectively (*2, 6, 7*). Therefore, better understanding of factors that alter the expression of the pluripotent-related transcription factors and hESC's fate may help comprehending early embryo development processes(*8, 9*).

Embryonic development is a dynamic, self-organizational process involving cell division, cell fate decisions, and morphogenic-patterning events coordinated through physical and soluble signals (*10, 11*). Biochemical signals known as morphogens modulate cell activities within developing embryo(*10, 12*), however, emerging evidence increasingly suggests that physical factors can dictate cellular fates in response to alterations within the internal and external environment in embryogenesis(*11*). Cells experience extrinsic tensile-compressive forces from their neighboring cells and they exert intrinsic forces to the extracellular matrix (ECM) through several mechanisms including acto-myosin contractility and cytoskeletal assembly(*13*). A computer simulation model has shown that surface plasticity and pressure from the zona pellucida recapitulates the blastocyst development from morula to blastocyst stage that includes blastocoel and ICM(*14*). Further, before hatching, blastocyst undergoes repeated collapse (Rapid; <5 min) and re- expansion (several hours) *in vitro(15).* Advanced understanding of the mechanisms by which hESCs respond to local forces will inform knowledge of development and lineage determination.

In past years, hPSCs have been successfully utilized for modeling microenvironment to understand cell-matrix interaction(*16, 17*). However, embryonic development is a dynamic process involving cell divisions and proliferations, cells in this stage experience extrinsic and intrinsic tensile- compressive forces from their neighboring cells, and however, understanding the effect of these forces on the hESCs remain elusive. Inspired by the recently implicated ability of directing stem cell fate in the absence of soluble factors by utilizing from mechanical cues, including the stiffness of substrate and the nanotopography of adhesion surface *in vitro* (*18, 19*), which gives rise the effects of purely mechanical cues on stem cells response, the goal of this chapter is to adapt a biomimicry approach to induce controlled and regulated forces into hESCs *in vitro* system for efficient application of "Outside-in" mechanical stimuli to hESCs in the concept of mechanotransduction.

During pre-implantation development, blastomers experience mechanical forces that alter cell fates within an embryo. Maintenance of stem cell pluripotency requires the activity of all three of the transcription factors, Nanog, Oct4, and Sox2. During differentiation, the levels of all three factors decrease but in different orders depending on the direction of differentiation. What could be the role of mechanical forces in regulating the timing of changes in levels of these three key transcription factors? We hypothesized that mechanical forces transmitted through different combinations of cell surface receptors may play a role. Upon performing experiments, we were surprised to find that mechanical strain applied to human embryonic stem cells for as short as 30-min induces rapid and irreversible nuclear-to-cytoplasmic translocation of Nanog and Oct4 but not Sox2. On Matrigel coated substrates, these translocations are directed by intracellular transmission of biophysical signals from cell surface integrins to nuclear CRM1 and is not reliant on exogenous soluble factors. Interestingly, on E-cadherin coated substrates, presumably with minimal integrin engagement, mechanical strain induced rapid nuclear-to-cytoplasmic translocation of all three transcription factors. These findings provide fundamental insights into early developmental processes and may facilitate mechanotransduction-mediated bioengineering approaches to influencing stem cell fate determination.[†]

[†] The results presented in this chapter are adapted from a manuscript that we recently submitted. The research presented in this chapter has received technical assistance from Dr. Byoung Choul Kim, Dr. Luis Villa Diaz. I would like to thank Dr. Cheri Deng, Dr. Shuichi Takayama, and Dr. Paul H. Krebsbach for their comments on the research presented in this chapter.

2.2 Materials and Methods

2.2.1 Microfabrication and PDMS device preparation

PDMS devices were fabricated using standard soft lithographic techniques(*20*). Briefly, a rectangular pattern (13 mm x 3 mm) was designed using commercial computer aided design software, AutoCAD (Autodesk, Inc) and printed on a transparent film (CAD Art, Inc). With the transparent film mask, a SU-8 master structure with a thickness of 200 µm was developed on a silicon wafer. A 10:1 mixture of a PDMS prepolymer base (Sylard 184, Dow Corning) and a curing agent was deposited on the silicon mold and cured overnight at 60°C flat oven. Glass slides were salinized overnight, and then a 10:1 mixture of a PDMS prepolymer base and a curing agent was deposited on the salinized glass slide, then spin coated at 650 Rpm for 40 seconds to obtain 100 mm thick membrane and cured overnight at 60°C flat oven. Glass slides were salinized overnight, and then a 10:1 mixture of a PDMS prepolymer base and a curing agent was deposited on the salinized glass slide, then spin coated at 650 Rpm for 40 seconds to obtain 100 mm thick membrane and cured overnight at 60°C flat oven. After peeling the finished PDMS from the mold, two holes at each end of the pattern were punched on the PDMS. The peeled PDMS slabs and membrane were rendered hydrophilic by exposure to oxygen plasma (SPI supplies, West Chester, PA) for 5 min and then the slabs were bonded to a PDMS membrane, then two tip reservoirs were connected to each hole. Shortly afterwards, channels were filled with PBS to maintain their hydrophilic state and devices were sterilized with UV light for 30 min.

2.2.2. ECM coating on channel

Microchannels were coated with hESC qualified Matrigel (Corning) and recombinant human E-cadherin protein (R&D Systems).

Matrigel coating: Matrigel solution (1:20) in cold DMEM/F12; 50ul per inlet) and incubated at room temperature for 2 hours. To remove excess Matrigel, the channel system was washed three times with PBS.

E-cadherin coating: Company's protocol was followed for Human recombinant E-cadherin protein coating. Briefly, Human recombinant E-cadherin protein was reconstituted at 250ug/ml in PBS with Ca^{++} and Mg^{++} and then added to microchannels for incubation at 37^0C for 90min. To remove excess E-cadherin, the channel system was washed three times with PBS with Ca^{++} and Mg^{++}.

2.2.3 hESC Culture

Human embryonic stem cells (hESCs) lines H1, H9 (NIH code: WA09; WiCell Research Institute, Madison, WI) and CHB10 (NIH Code: NIHhESC-09-0009, Children's Hospital Corporation) were cultured on the synthetic surface PMEDSAH as described previously(*21*) with human-cell- conditioned medium (HCCM, MTI-Global Stem, Gaithersburg, MD, http://www.mti-globalstem.com) supplemented with 5 ng/mL of human recombinant basic fibroblast growth factor (FGF2; InvitrogenTM, Carlsbad, CA, http://www.invitrogen.com), and 1%antibiotic-antimycotic (Gibco). The hPSC culture medium was replaced every other day and all cell culture was performed in designated incubators at 37^0C in 5% CO2 and high humidity. Differentiated cells were mechanically removed using a sterile pulled-glass pipet under a stereomicroscope (LeicaMZ9.5, Leica Microsystems Inc., Buffalo Grove, IL).

2.2.4 hESC Seeding in the channel and Cell Stretching

100 ul of HCCM with roughly 10 undifferentiated hESC's clusters (100–150 mm) were loaded into the channel from one end of the device for attachment overnight at 37^0C in 5% CO2 and high humidity. After observing cell attachment in the channel, hESC colonies were subjected to uniaxial strain (ε ~ 10%) using a stretcher (S.T. Japan USA LLC, FL, USA) (Supl. Fig.1)(*22*)

2.2.5 Drug Inhibition Assay

PF-562271 (Sigma-Aldrich) was added to the culture media at 1 μM an hour before stretching the cells to inhibit focal adhesion kinase phosphorylation.
To block nuclear export signal via interaction with a cysteine residue in the CRM1 (exportin1), LMB (Exportin1 inhibitor) was added to the media at 100 nM an hour before applying mechanical strain.

2.2.6 Cell immunocytochemistry analysis

hESCs in microchannel were washed with PBS for 5 min and aspirated out the supernant and addded 1 ml of Z-Fix solution (Anatech LTD: cat# 170) for 10 min at RT shaking. Next, cells were washed 3x with 1 mL of PBS for 15 min each at RT. This was followed by sequential incubation with unmasking solution (PBS, 2N HCL, 0.5% TritonX) for 15 min, its removal, quenching solution (TBS, 0.1% Sodium Borohydride) for 15 min, its removal, and permeabilization solution (PBS, 0.02% TritonX) for 15 min. Then, blocking solution (5% BSA in 1X PBS) was added for 1hour. Microchannels were then incubated in primary antibodies overnight at 4˚C shaking. Channels were then washed with 1X PBS 3 times for 15 min at RT while shaking. We then incubated in secondary antibodies covered in foil for at least one hour at RT while shaking. Afterwards, channels were washed twice in PBS for 20 min, incubated in DAPI solution for 20 min and washed in 1X PBS for 20 min. We used Nikon Ti Eclipse Confocal Microscope, 20x and 60x magnification lenses, with water to capture images with or without 3x digital zoom, ¼ frames per second, 512x512 image capture, 1.2 Airy Units, 2x line averaging, appropriate voltage and power settings optimized per antibody. No modification was done, except image sizing reduction, rotation, or gray scale change for figure preparation. All original and unaltered blots are found in the supplementary figures.

All antibodies were used as following with a working volume of 1 mL in 5% BSA in PBS, unless noted otherwise:

Primary antibodies for immunofluorescence: Oct4 (Santa Cruz, Cat #sc8629, 1:500), Nanog (Abcam, Cat# ab62724, 1:100), Sox2 (Milipore, ab56603, 1:500), pFAK (TYR397) (Invitrogen, Cat # 700255, 1:200), Beta-Catenin (Santa Cruz, Cat# sc7963, 1:500), and Cdx2 (SantaCruz, Cat#393572, 1:500)

Secondary antibodies for immunofluorescence: All antibodies were used at a concentration of 1:1,500 with a working volume of 1.5 mL in 5% BSA in PBS. DAPI stain was used for DNA. Donkey anti-Rabbit IgG Secondary Antibody, Alexa Fluor® 488 (TFS: cat# A-21207), Donkey anti-Goat IgG Secondary Antibody, Alexa Fluor® 594

(TFS: cat# A-11058), and Donkey anti-Mouse IgG Secondary Antibody, Alexa Fluor® 647 (TFS: cat# R37114).

2.2.7 Image Analysis

Image J was used to quantify fluorescent intensity(*23, 24*). Briefly, after selecting the cell of interest using any of the polygon drawing/selection tools, “set measurement” was selected from the Analyze menu by selecting area, integrated density and mean gray value. Then, "Measure" was selected from the analyze menu, and a region next to the cell that has no fluorescence was selected for background. This step was repeated for each single cells in the field and then the all data were analyzed on excel, and this formula was followed for the corrected total cell fluorescence (CTCF).

CTCF = Integrated Density - (Area of selected cell X Mean fluorescence of background readings)

2.2.8 Extraction and purification of total RNA

Plates were washed with PBS and 1000µl of Trizol Reagent (Invitrogen, Carlsbad, CA) was added to the plates, and RNAs were collectfed after vigorous pipetting. 200 µl Chloroform was added to this solution followed by centrifugation (13,000 g-15 min). Aqueous phase containing RNA was separated and 500 µl isopropanol was added and stored at 200C at least overnight. Then, the manufacturer’s RNA Clean-up protocol, RNeasy Mini-Kit (Qiagen, Valencia, CA), with the optional On-column DNAse treatment was followed. RNA quality and concentration were checked using a Synergy NEO HTS Multi-Mode Microplate Reader (BioTek Instruments, Winooski, VT).

2.2.9 Reverse-transcription PCR (RT-PCR) analysis

Reverse transcription from 2.5 μg of total RNA in a 20 μL reaction into cDNA was performed using SuperScript™ VILO™ Master Mix (ThermoFisher Cat#11755050). The synthesis of first-stranded cDNA was carried out in the PCR tube after combining SuperScript VILO, RNA, and DEPC-treated water, in the first cycle at 25ºC for 10 min, incubating at 42ºC for 60 min, and terminating the reaction at 85ºC for 5 min. Quantitative PCR was performed triplicate for for each sample using TaqMan probes (Applied Biosystems) and TaqMan Universal PCR Master Mix (Applied Biosystems) on 7900 HT Fast Real Time PCR system (Applied Biosystems). Relative quantification of Nanog, Oct4, Sox2, FAK, Snai1, T, ITGAV, and Pax6 gene expression data were normalized to the GAPDH expression and calculated using the 2-ΔΔCT expression level(*25*)

List of primers used in qRT-PCR in Table 2. All primers were purchased from ThermoFisher Life Technologies: Nanog (Assay ID: Hs02387400_g1 (FAM-MGB), UniGeneID: Hs.635882), POU5F1 (OCT 3/4) (Assay ID: Hs03005111_g1 (FAM-MGB) , UniGeneID: Hs.249184), SOX2 (Assay ID: Hs01053049 (FAM-MGB), UniGeneID: Hs.518438), FAK (PTK2) (Assay ID: Hs03657683 (FAM-MGB), UniGeneID: Hs. 395482), and GAPDH (Assay ID: Hs02786624_g1 (FAM-MGB), UniGeneID: Hs.544577).

2.2.10 Statistical Analysis

Results are presented as Mean ± SEM. Unpaired two-tailed student's t test was performed for comparisons, and unpaired *t* test *p* values < 0.05 (*), <0.01 (**), <0.001(***), n.s. not significant.

2.3 Results and Discussion

Due to difficulty and inability to access human blastomeres in inner cell mass during development, it is challenging to test and determine how mechanical forces alter embryo shape, how sensitive embryonic stem cells are, and how quick this process is during early development. Previous work utilizing cultured embryonic stem cells *in vitro* has provided interesting results that aim to fill this gap but has also led to apparently contradictory outcomes where mechanical stretch has led to either maintenance of pluripotency(*26, 27*)or promotion of differentiation(*28, 29*). Because of multiple differences between the studies such as type of external mechanical stimuli, the length of a time stimulated (hours, days), and growth factors and small inhibitors (TGFβ, Smad2/3) administered to the cells it is not clear what parameters promote differentiation versus(*30*) maintenance of pluripotency(*26, 27*). For example, Saha *et al*. report that continuous application of a 10% equibiaxial cyclic strain at frequencies above 6 cycles/min for 12 days maintains pluripotency through action of the TGFb/Activin/Nodal signaling pathway(*26, 27*). On the other hand, 15% applied strains at 12 cycles/min for 12 hours reduces pluripotency gene expression via activation of Rho/ROCK and subsequent decrease of AKT phosphorylation(*28*). Chowdhury *et al.* also showed that a 17.5 Pa force applied to cells via RGD coated microbeads at 18 cycles/min for 1 hr reduced Oct 3/4 expression(*29*). In this work, we study the effect of a non-cyclical 10% uniaxial strain based on the rationale that during gastrulation, strain is more of a one-time stretch rather than a cyclical stretch-relax event that repeats every few seconds.

To investigate the role of mechanical forces in hESCs, we applied a 10% uniaxial stretch and held the cells in that stretched state thereafter (Figure 2-1 and Figure 2-2). This mechanical stimulation led to a surprisingly fast-induced translocation of NANOG and OCT4, from the nucleus to cytoplasm that was significant within 30 min (Figure 2-3) and continuing beyond 2 hours (Figure 2-2). In contrast, SOX2 remained in the nucleus regardless of application of stretch for the cells attached to Matrigel coated substrates. Culturing hESCs in a non-strain condition for an additional 24 hours beyond the 2 hours of applied strain demonstrated that the translocations were practically irreversible (Figure 2-3). Mechanical strain also elevated the translation of CDX2, a transcription factor antagonist of OCT4(*31*) and a determinant in trophoectoderm lineage(*32*) (Figure 2-2). Gene expression analysis showed no change in Sox2, while Nanog and Oct4 expression decreased, and Cdx2 and Ptk2 (FAK) gene expressions are elevated (Fig. 2-2). These effects are a direct effect of the mechanical forces and not reliant on exogenous chemical cues, since cells in the absence or presence of mechanical forces were grown in the same self-renewal supporting culture medium (Materials and Methods).

OCT4 is transported through nuclear pores by the nuclear export protein (NES) CRM1(XPO1)(*33*), (*34*)and nuclear import protein, importainα(*35*). Previous reports showed OCT4 is imported into the nucleus by nuclear transport mechanism via the function of importinα and leaded to cell differentiation(*35-37*). Therefore, we investigated the involvement of CRM1 in the translocation of pluripotency-related transcription factors in hESCs during uniaxial forces. In the presence of Leptomysin B (LMB), a chemical inhibitor of CRM1, NANOG AND OCT4 remained in the nucleus, while both proteins translocated to the cytoplasm in the control group (Figure 2-4). To determine what cellular machinery might be involved in sensing the micro-environmental forces we analyzed nuclear lamins which sense forces through the cytoskeleton and extracellular matrix (*38*). Lamin A/C in particular plays a central role in the organization of the nuclear structure and gene function, and it is activated during hESCs differentiation (*39*). Here, Lamin A/C increased in response to mechanical strain, concurrent to translocation of pluripotent related-factors to the cytoplasm (Figure 2-5). These results suggest that phosphorylation of mechanosensitive focal adhesion kinase mediates Nanog and Oct4 translocation by responding externally applied forces with the involvement of CRM1 and Lamin A/C. Thus, we next analyzed phosphorylation of focal adhesion kinase (FAK), a mechanotransductive protein associated with translocation of OCT4 to the cytoplasm and differentiation (*40*). Uniaxial force application to hESCs induced the phosphorylation of FAK (Figure 2-6A) concurrent with NANOG and OCT4 translocation to the cytoplasm. This is consistent with our previous report that shows translocation of Oct4 to the cytoplasm in response to phosphorylation of FAK, triggered in that study by Mn^{+2}-mediated activation of integrins in hESCs rather than through external stretch (*40*). When FAK phosphorylation was inhibited by pre-treatment of hESCs with a chemical inhibitor, PF562271, this restrained stretch-induced NANOG and OCT4 cytoplasmic translocation (Figure 2-6B). Thus, uniaxial strain-mediated effects on hESCs cultured on Matrigel-coated substrates involve FAK activation to transmit the extracellular information from outside to inside the cell.

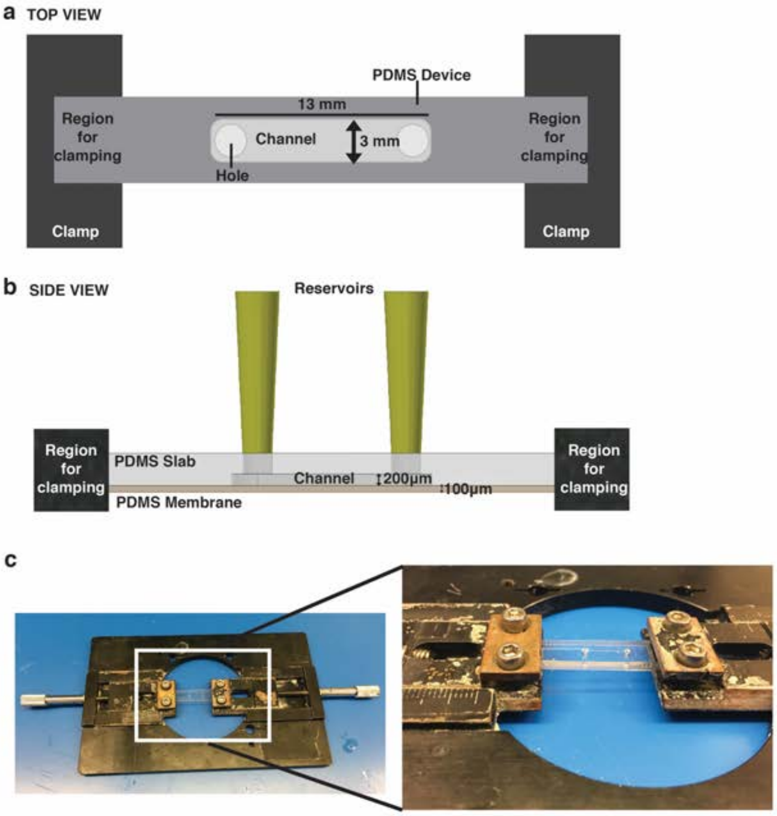

Figure 2-1 Schematic design of PDMS stretching chip**. (a),** Schematic top view depicting uniaxial stretch on the rectangle chip**. (b),** Schematic side of PDMS chips view with and without applied uniaxial in-plane strain, showing displacement of the flexible PDMS substrates and the adhered monolayer of cells. (**c),** Stretching device with microchannel on it.

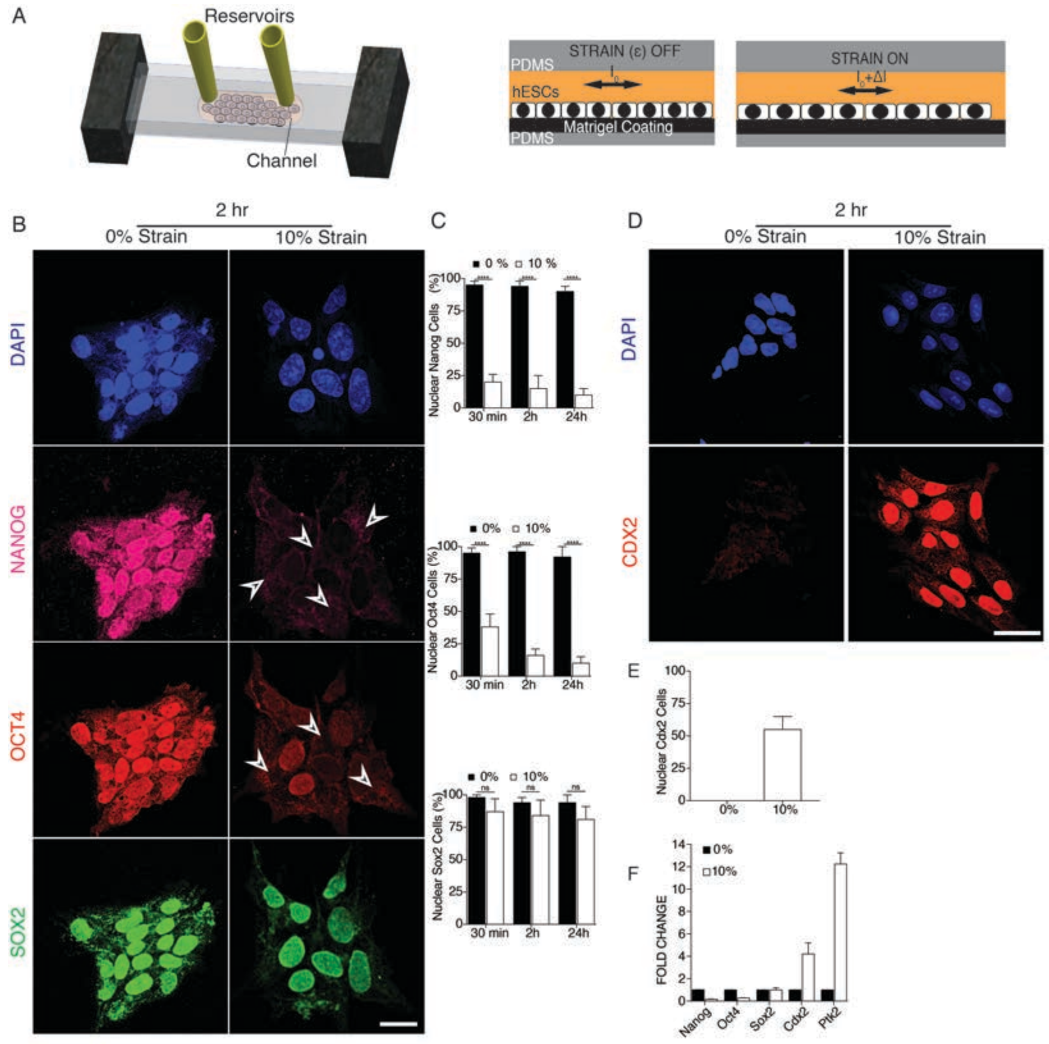

Figure 2-2. Uniaxial mechanical force exerted on hESC. (**a**) Schematic of chip to exert 10% uniaxial strain to hESCs. Side view with and without stretch applied illustrates how distortion of flexible substrates results in stretch of the adherent hESCs. Top view depicts the reservoirs where cells are loaded and supplied with medium. (**b**) Representative micrographs showing expression of NANOG, OCT4 and SOX2 in hESC colonies during 2 hours of no strain (0%) and 10% strain applied via uniaxial forces. DAPI stained nuclei. Scale bar= 50 μm. (**c**) Percentages of cells with nuclear localization of the indicated transcription factor in each condition at different time points. (**d**) Representative micrographs showing expression of CDX2 in cells under 10% strain, and (**e**) its quantification from three independent replicates. Unpaired *t* test *p* values < 0.05 (*), <0.01 (**), <0.001(***), n.s. not significant.

Cell strain may be sensed not only through cell-ECM interactions but also through cell-cell contacts. For example, β-catenin contains binding sites for E-cadherin and provides a connection to control cell adhesion and gene transcription (*41*). The β-catenin and α-catenin complex interacts with formin to link cadherin-catenin complexes with actin cytoskeleton at the plasma membrane (*42*). Beta-catenin expression in hESCs is associated with differentiation (*43*) and the phosphorylation of FAK has been related to the activation and nuclear translocation of β-catenin (*44, 45*). During uniaxial stretching of hESCs, β-catenin became expressed (Figure 2-7). Together this suggests that mechanical forces applied to hESCs resulted in FAK phosphorylation, translocation of pluripotent-related transcription factor, and activation of β-catenin.

Similar to during embryogenesis and early development, our stretch experiments activated mechanism that sense changes in both cell-cell adhesions (*46, 47*) and cell-ECM interaction (*48, 49*). To better tease out the effects of just cell-cell interactions with less involvement of cell-ECM interactions, we performed experiments with substrates coated with E-cadherin. In absence of mechanical strain, NANOG, OCT4, and SOX2 remained in the nucleus. However, upon mechanical straining of these cells plated on E-cadherin, all three-transcription factors translocated to the cytoplasm within 2 hours (Figure 2-8). This contrasted with results observed on Matrigel-coated chips, where SOX2 remained nuclear, while NANOG and OCT4 translocated to the cytoplasm. This suggests that strain sensed through integrin-mediated and E-cadherin-mediated mechanisms have different effects on hESCs, with E-cadherin-mediated sensing being more differentiation promoting. From a practical viewpoint, these results suggest that the response of hESCs to stretch may differ depending on cell confluency where the extent of

E-cadherin interactions between cells would be higher for confluent monolayers due to differentiation occurs more efficiently at the edges of hESC colony (*50*). Interestingly, the differentiation promoting experiments by Teramura et al(*28*) use confluent layers of cells while the pluripotency promoting experiments by Saha et al(*26*) use less confluent culture of colonies, although there are too many other variables to conclude this is the definitive factor. Mechanical cues on cell-ECM interaction are well known to be involved in mechanotransduction via integrins and focal adhesions(*51, 52*), however, pathway of strain-induced differentiation through cell-cell interaction remains elusive. Our results and methods open new avenues for exploring the distinct role of mechanical cues from cell-cell interactions vs cell-ECM interactions.

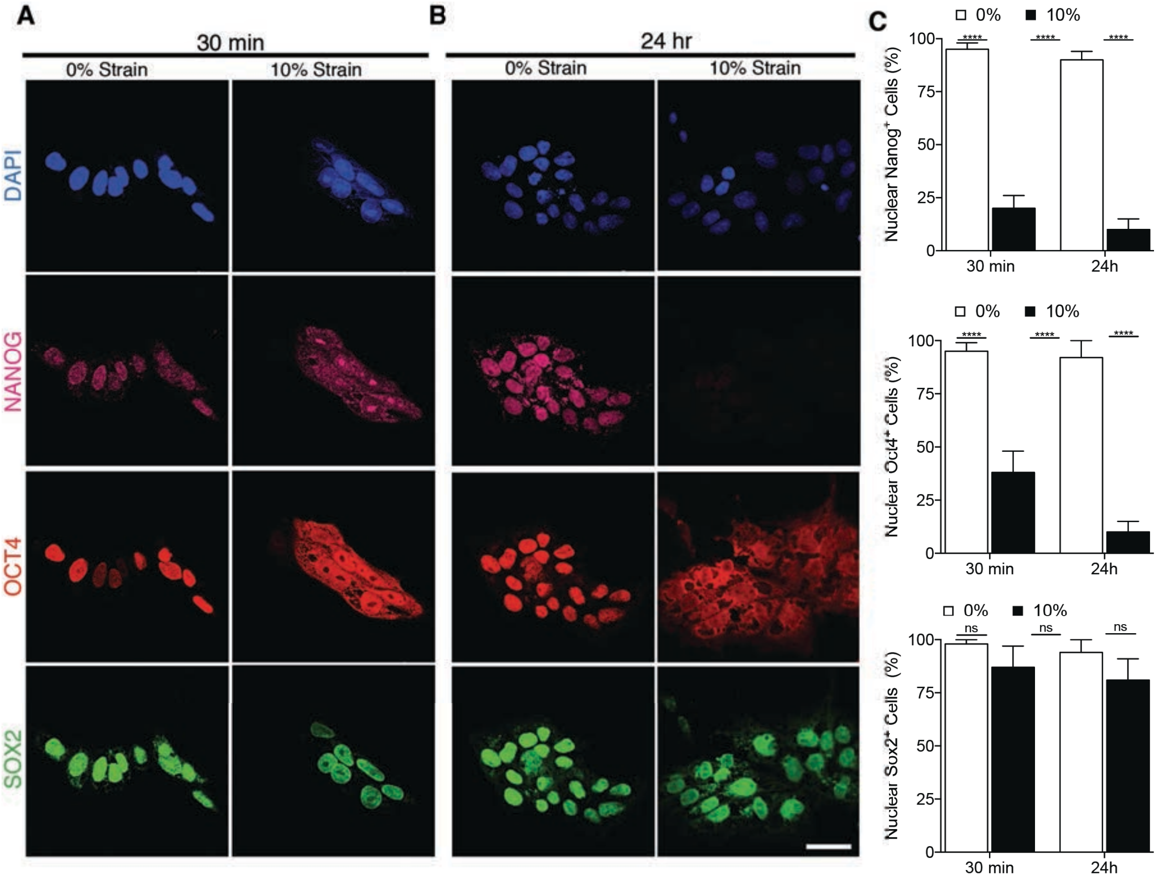

Figure 2-3 Effect of external mechanical forces on pluripotent related transcription factors. Representative micrographs showing the effect of uniaxial stretching of hESCs during a, 30 min and b, 24 hours in Nanog, Oct4 and Sox2. Note the cytoplasmic translocation of Nanog and Oct4 in stretched cells. **c,** Representative micrographs of hESCs stretched for 2 hours and then sub-cultured for additional 24 hours in a non-strain condition, showing that the cytoplasmic shuttling is not reversible. Scale bars equal to 50 µm.

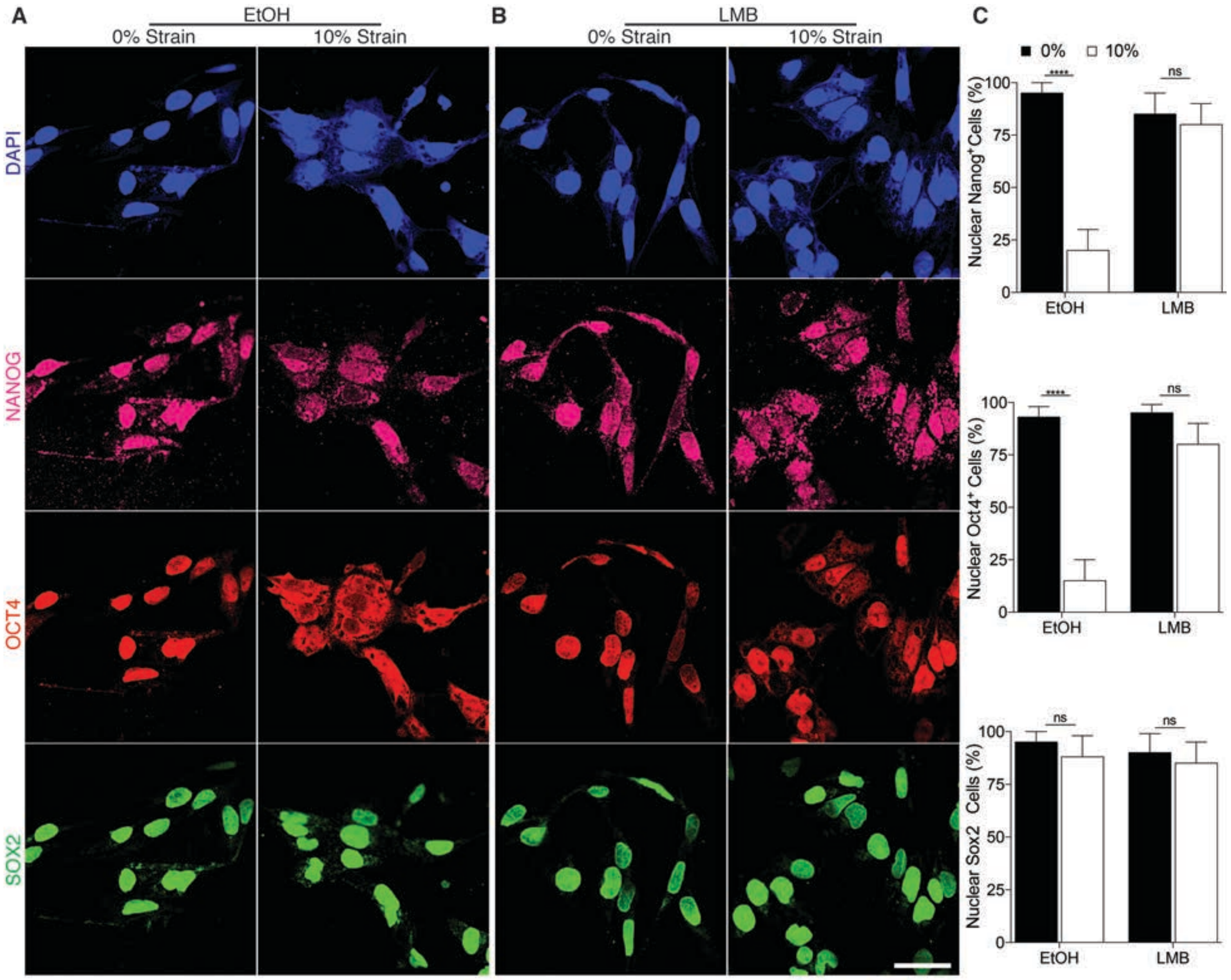

Figure 2-4 CRM1 inhibitor, Leptomyosin (LMB), abolished the effect of mechanical strain in pluripotent transcription factors. **(a),** Representative micrographs showing the shuttling of NANOG and OCT4 to the cytoplasm of hESCs under mechanical strain during 2 hours in the absence of LMB inhibitor but treated with ethanol (EtOH) as diluent. (**b),** Pre-treatment of hESCs with LMB inhibitor abolished the shuttling mechanism of transcription factors during 2 hours of 10% strain forces. (**c),** Percentage of cells with nuclear localization of NANOG, OCT4, and SOX2 within 2 hours upon mechanical strain with and without LMB. Scale bars equal to 50 µm. All quantifications were from at least 3 independent experiments with two replicates per experiments. Unpaired t test p values <0.05 (*), <0.01(**), <0.001 (***). n.s. not significant.

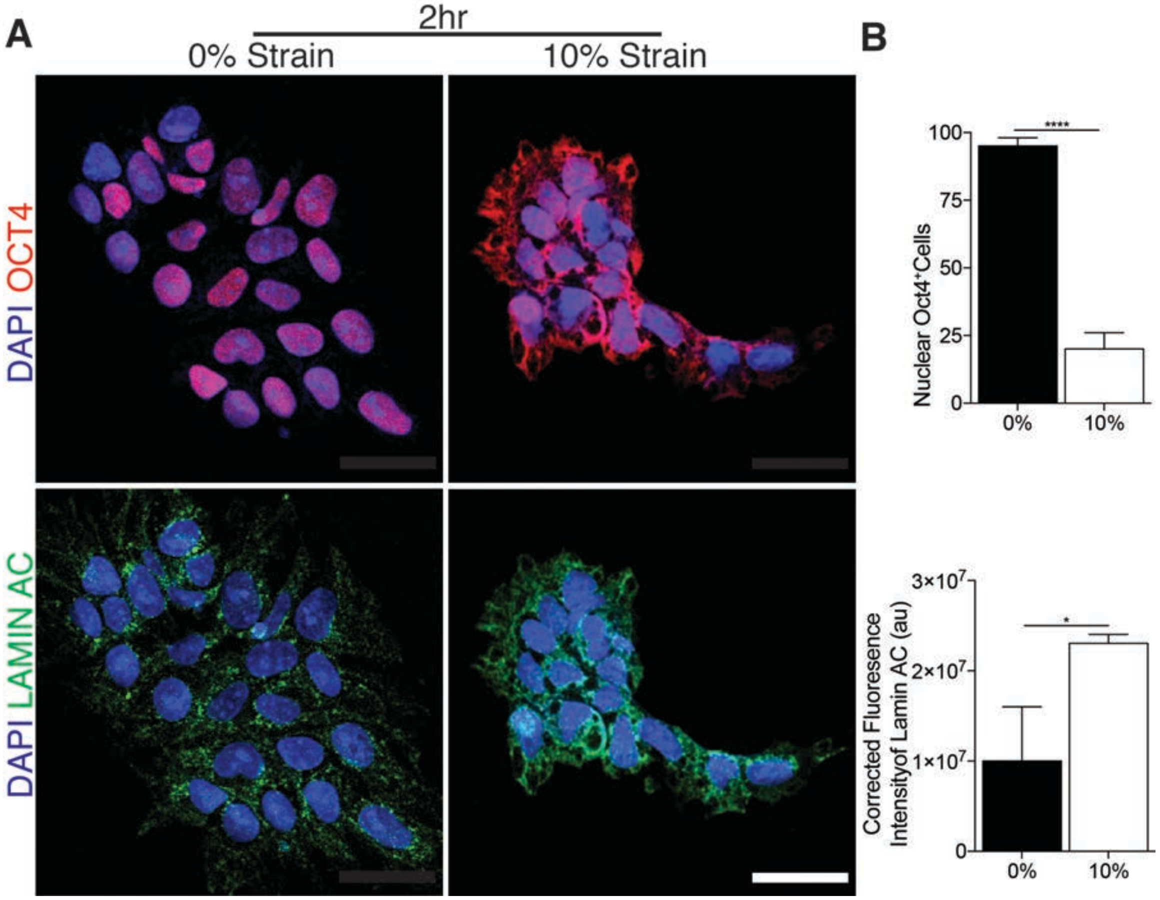

Figure 2-5 Effect of uniaxial mechanical force on mechanotransductive molecular components. (**a**) Representative micrographs showing expression of Lamin A/C and Oct4 in cells during 2 hours without (0% strain) and with (10% strain) mechanical strain. DAPI stained nuclei. Scale bar = 50 mm. Unpaired *t* test *p* values < 0.05 (*), >0.01 (**), <0.001(***),n.s. not significant. (**b**) Quantification of fluorescence for each protein after 10% uniaxial strain.

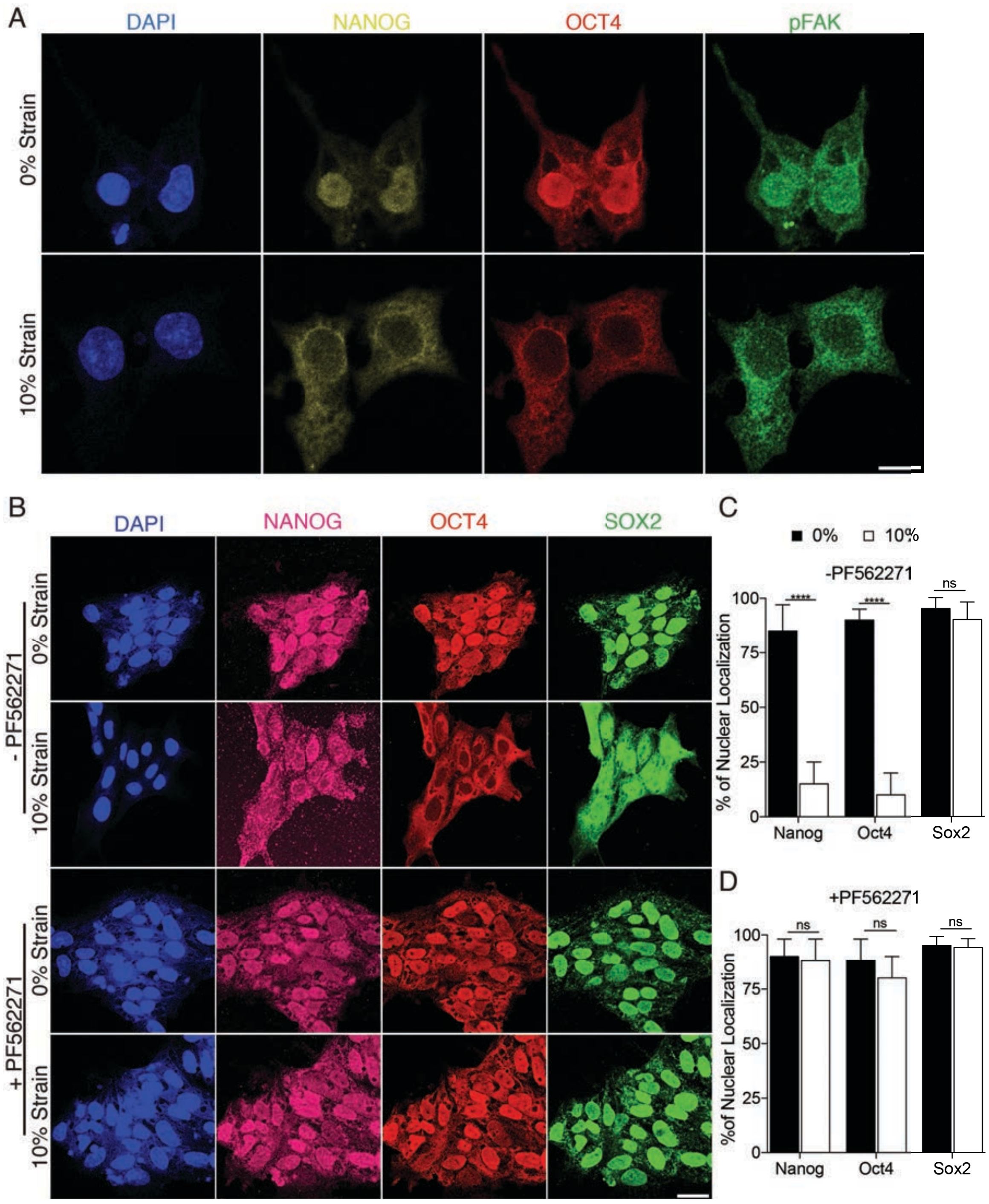

Figure 2-6 FAK translocate to cytoplasm after strain forces are applied and prevention of FAK phosphorylation eliminates the effects of mechanical strain shuttling pluripotent transcription factors from nucleus to cytoplasm. (**a**), NANOG, OCT4, and pFAK shuttle to cytoplasm after mechanical strain exerted**, (b),** NANOG and OCT4 shuttled to cytoplasm under the mechanical strain within 2 hours in the absence of PF562271, chemical inhibitor of FAK phosphorylation (treated with DMSO, as diluent)**;** while their localization of these markers remains in the nuclei within 2 hours under 10% strain in the

presence of PF562271 (**c & d)** Percentage of cells with nuclear localization of NANOG, OCT4, and SOX2 within 2 hours upon mechanical strain with and without PF562271. Scale bars equal to 50 µm. All quantifications were from at least 3 independent experiments with two replicates per experiments. Unpaired t test p values <0.05 (*), <0.01(**), <0.001 (***). n.s. not significant

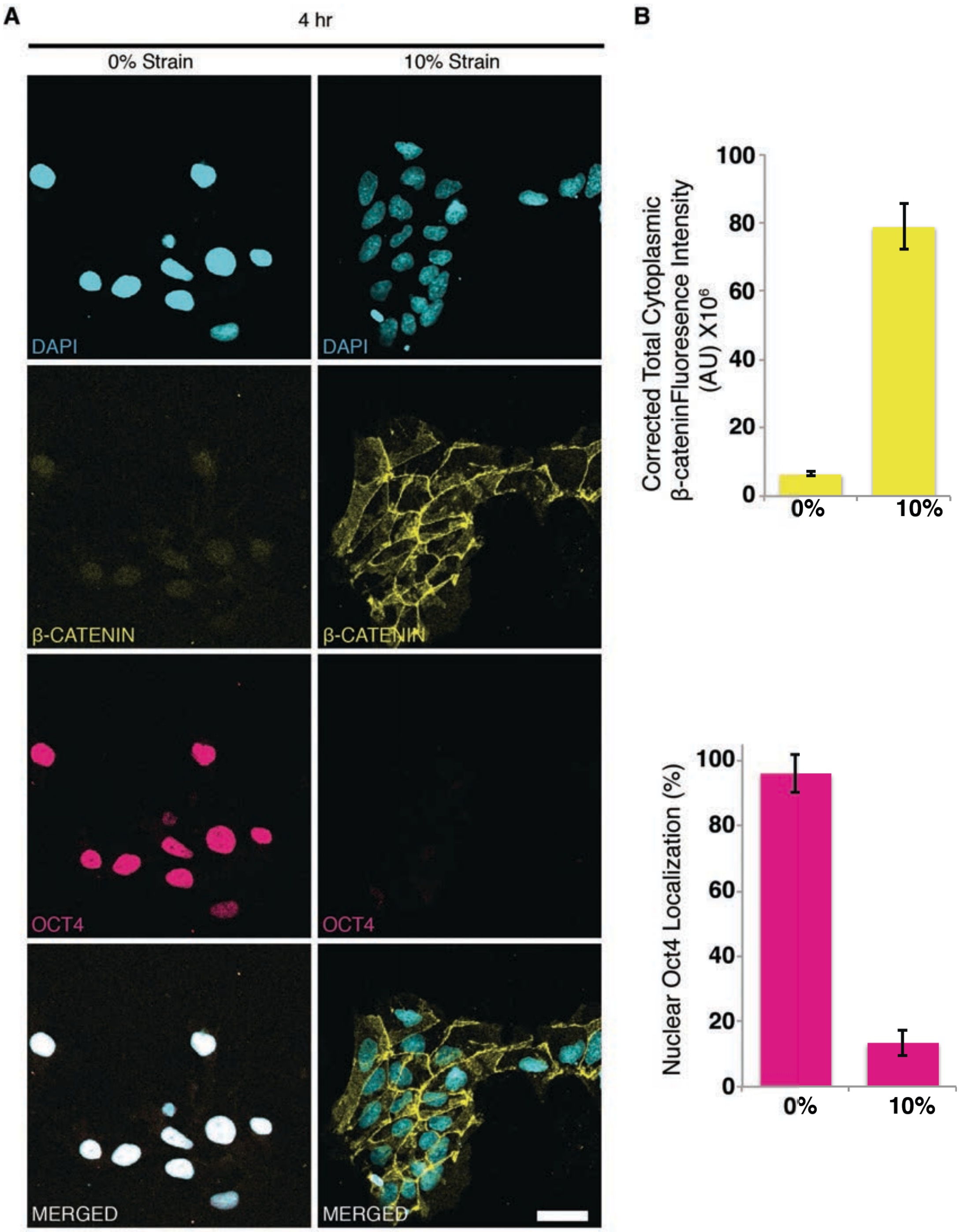

Figure 2-7 Effect of uniaxial mechanical strain β-catenin expression in hESCs. **(a),** Representative micrographs of hESCs with and without mechanical strain applied within 4 hours. β-catenin localized at the plasma membrane within 4 hours upon after 10% strain applied. (**b),** Graph indicating corrected total cytoplasmic fluorescence intensity of β-catenin and percentage of cells with nuclear localization of Oct4. Scale bars equal to 50 μm. All quantifications were from at least 3 independent experiments with two replicates per experiments. Unpaired t test p values <0.05 (*), <0.01(**), <0.001 (***). n.s. not significant.

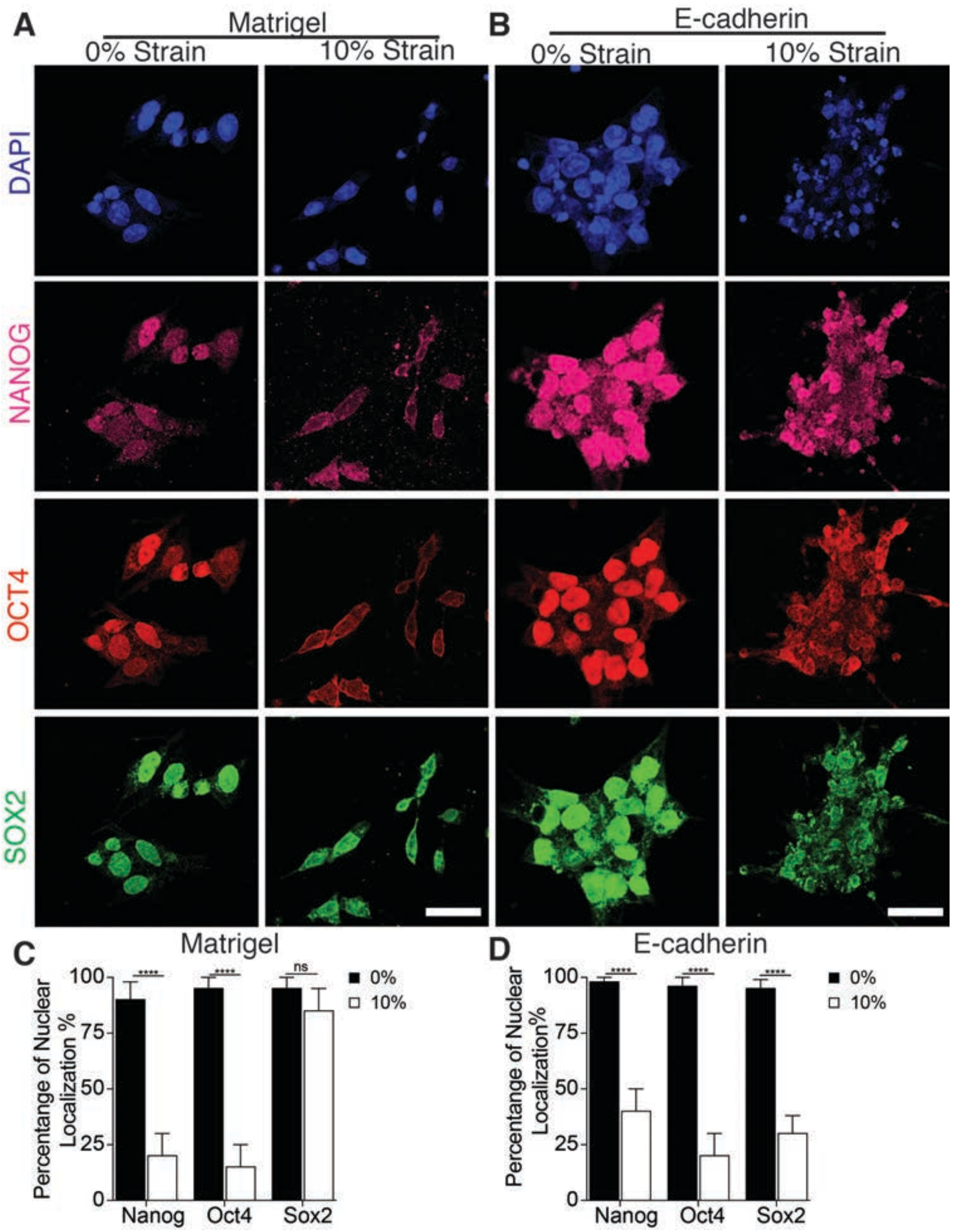

Figure 2-8 Effect of uniaxial mechanical strain of hESCs on Matrigel- and E-cadherin-coated substrates**. (a),** Representative micrographs of hESCs with and without 10% mechanical strain applied during 2 hours. Cytoplasmic localization of Nanog and Oct4 was observed on Matrigel- coated PDMS chips. (**b),** Graph indicating percentage of cell with nuclear localization of Nanog, Oct4, and Sox2 within 2 hours upon mechanical strain, compared to control group. (**c),** Representative micrographs showing shuttled to cytoplasm of Nanog, Oct4, and Sox2 on E-cadherin coated PDMS chip within 2 hours of mechanical strain. (**d),** Graph indicating percentage of cell with nuclear localization of Nanog, Oct4, and Sox2 within 2 hours upon mechanical strain on cell cultured on E-cadherin-coated chips, compared to control group. Scale bars equal to 50 µm. All quantifications were from at least 3 independent experiments with two replicates per

experiments. Unpaired *t* test *p* values <0.05 (*), <0.01(**), <0.001 (***). n.s. not significant.

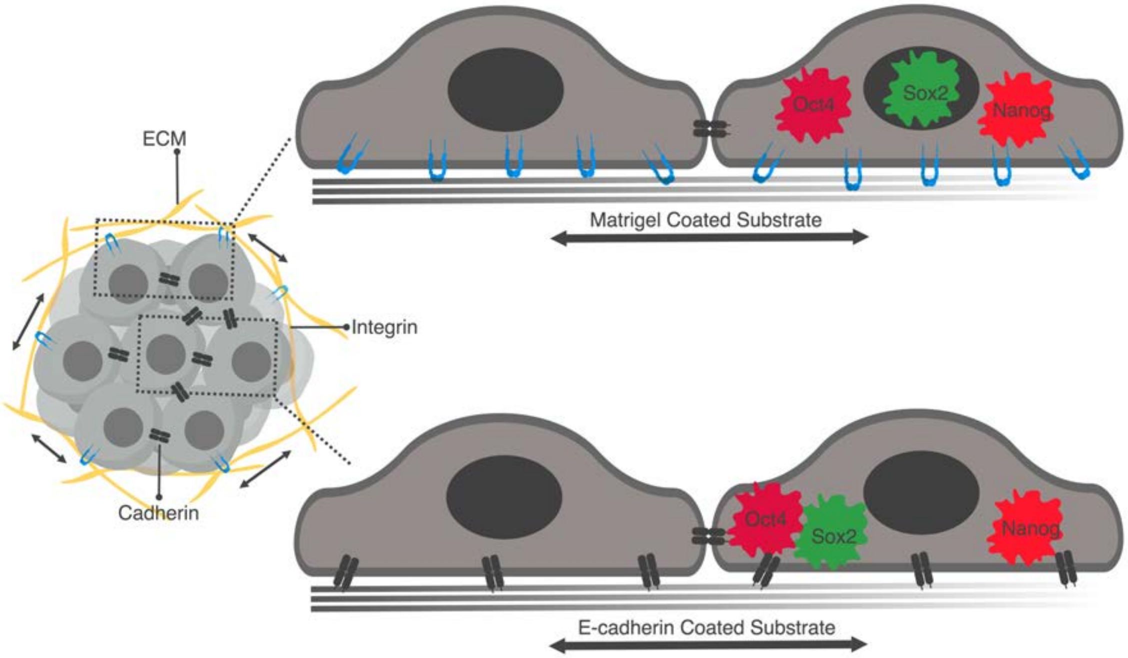

Figure 2-9. Schematic illustration of mechanotransductive signals activated in hESCs by uniaxial mechanical strain.

2.4 Conclusion

Embryonic stem cells are pluripotent cells that derived from the inner cell mass of the mammalian blastocyst, and they are capable of self-renewal in vitro under certain conditions(*53, 54*). The precise balance of transcription factors, Nanog, Oct4, and Sox2, plays essential roles in regulation hESC pluripotency, and down-regulation and/or over-expression of any of these factors leads a loss of maintenance of pluripotency and initiates differentiation, such as overexpression of Sox2 prompts neuroectodermal specification(*55*), while overexpression/ downregulation of Oct4 and Nanog leads mesodermal differentiation(*3, 56*).

The delicate interactions between these transcription factors suggest that not only the transcription factor levels but subcellular localization changes may also play key roles

(*34, 57*), particularly in the early stages of differentiation. Studies of pluripotency-related transcription factor translocation, however, is limited to a few reports such as a recent report that an ERK phosphorylation mutant leads to KLF4 and NANOG translocation from the nucleus to the cytoplasm and subsequent differentiation in mouse ESCs(*34*). Here, we have showed that that the pluripotency circuit can be translocated with a one-time uniaxial stretch in the absence of any genetic manipulation or use of exogenously added growth factors or cytokines with effects visible as early as 30 min after stretch. Interestingly, inhibition of translocation of NANOG and OCT4, through blocking of CRM1 inhibited, and delayed differentiation of hESCs. Moreover, our data suggest that mechanotransductive signals through focal adhesions propagate rapidly to phosphorylate FAK and promote LAMIN A/C expression and activity of CRM1 to affect the localization and function of pluripotency-related transcription factors (Figure 2-9). Our result contradicts a report that shows cyclic mechanical strain maintains pluripotency(*26, 27*) while it supports another report that demonstrates mechanical strain inhibits pluripotency gene expression by inhibiting AKT activation(*28*). We do note, that unlike these previous studies that use cyclic strain, we only apply a one-time stretch.

Cell-cell adhesion transmit physical forces and influence the dynamics of tissue formation by enabling cellular processes including tissue remodeling, migration and growth during early development(*46, 58-60*). Interestingly, we found that uniaxial stretch translocated NANOG and OCT4 on matrigel coated substrates, while all the three pluripotency transcription factors were translocated in cytoplasm on e-cadherin coated substrates. These results show that translocation of pluripotency factors is mechanosensitive and is impacted by whether the forces are transduced through cell-

ECM or through cell-cell interactions leading to translocation of different pluripotency-related transcription factors from nucleus to cytoplasm.

Overall, these results in this chapter confirm that biologic responses to mechanical stress may be propagated faster than biochemical cues(*61*). These mechanotransductive processes are dependent on cell-matrix and cell-cell interactions and affect the expression of transcription factors involved in early events of embryo development, such as the translation of CDX2. Understanding how mechanical cues alter stem cell fate will provide us key insights into comprehending developmental biology and advancing regenerative medicine and biotechnology. For example, in stem cell differentiation applications, it is already common protocol to add different activators and inhibitor molecules at different time points to mimic physiological development. Our results suggest that in addition to timed exposure to biochemical factors, timed application of one-time stretch to cells may be a practical and powerful biomimetic cue to guide stem cell differentiation. To drive them the terminal differentiation, biochemical factors may be needed with combination of the timing for further studies. Understanding how mechanical cues alter stem cell fate will provide us key insights into comprehending developmental biology and regenerative medicine therapies.

2.5 References

1. G. Forgács, S. Newman, *Biological physics of the developing embryo*. (Cambridge University Press, Cambridge, UK ; New York, 2005), pp. vi, 337 p.
2. J. Nichols *et al.*, Formation of pluripotent stem cells in the mammalian embryo depends on the POU transcription factor Oct4. *Cell* **95**, 379-391 (1998).
3. H. Niwa, J. Miyazaki, A. G. Smith, Quantitative expression of Oct-3/4 defines differentiation, dedifferentiation or self-renewal of ES cells. *Nat Genet* **24**, 372-376 (2000).
4. K. Takahashi, S. Yamanaka, Induction of pluripotent stem cells from mouse embryonic and adult fibroblast cultures by defined factors. *Cell* **126**, 663-676 (2006).
5. D. E. Parfitt, M. M. Shen, From blastocyst to gastrula: gene regulatory networks of embryonic stem cells and early mouse embryogenesis. *Philos Trans R Soc Lond B Biol Sci* **369**, (2014).
6. I. Chambers *et al.*, Functional expression cloning of Nanog, a pluripotency sustaining factor in embryonic stem cells. *Cell* **113**, 643-655 (2003).
7. K. Mitsui *et al.*, The homeoprotein Nanog is required for maintenance of pluripotency in mouse epiblast and ES cells. *Cell* **113**, 631-642 (2003).
8. J. S. Odorico, D. S. Kaufman, J. A. Thomson, Multilineage differentiation from human embryonic stem cell lines. *Stem Cells* **19**, 193-204 (2001).
9. J. Yu *et al.*, Induced pluripotent stem cell lines derived from human somatic cells. *Science* **318**, 1917-1920 (2007).
10. J. L. Christian, Morphogen gradients in development: from form to function. *Wiley Interdiscip Rev Dev Biol* **1**, 3-15 (2012).
11. L. LeGoff, T. Lecuit, Mechanical Forces and Growth in Animal Tissues. *Cold Spring Harb Perspect Biol* **8**, a019232 (2015).
12. A. Stathopoulos, D. Iber, Studies of morphogens: keep calm and carry on. *Development* **140**, 4119-4124 (2013).
13. T. Lecuit, P. F. Lenne, Cell surface mechanics and the control of cell shape, tissue patterns and morphogenesis. *Nat Rev Mol Cell Biol* **8**, 633-644 (2007).
14. H. Honda, N. Motosugi, T. Nagai, M. Tanemura, T. Hiiragi, Computer simulation of emerging asymmetry in the mouse blastocyst. *Development* **135**, 1407-1414 (2008).
15. D. Bodri *et al.*, Blastocyst collapse is not an independent predictor of reduced live birth: a time-lapse study. *Fertil Steril* **105**, 1476-1483 e1473 (2016).
16. Y. Sun *et al.*, Hippo/YAP-mediated rigidity-dependent motor neuron differentiation of human pluripotent stem cells. *Nat Mater* **13**, 599-604 (2014).
17. W. Chen *et al.*, Nanotopography regulates motor neuron differentiation of human pluripotent stem cells. *Nanoscale* **10**, 3556-3565 (2018).
18. J. Barthes *et al.*, Cell microenvironment engineering and monitoring for tissue engineering and regenerative medicine: the recent advances. *Biomed Res Int* **2014**, 921905 (2014).
19. J. S. Chua *et al.*, Extending neurites sense the depth of the underlying topography during neuronal differentiation and contact guidance. *Biomaterials* **35**, 7750-7761 (2014).

20. G. M. Whitesides, E. Ostuni, S. Takayama, X. Jiang, D. E. Ingber, Soft lithography in biology and biochemistry. *Annu Rev Biomed Eng* **3**, 335-373 (2001).
21. L. G. Villa-Diaz *et al.*, Synthetic polymer coatings for long-term growth of human embryonic stem cells. *Nat Biotechnol* **28**, 581-583 (2010).
22. B. C. Kim *et al.*, Fracture-based fabrication of normally closed, adjustable, and fully reversible microscale fluidic channels. *Small* **10**, 4020-4029 (2014).
23. R. A. McCloy *et al.*, Partial inhibition of Cdk1 in G 2 phase overrides the SAC and decouples mitotic events. *Cell Cycle* **13**, 1400-1412 (2014).
24. A. Burgess *et al.*, Loss of human Greatwall results in G2 arrest and multiple mitotic defects due to deregulation of the cyclin B-Cdc2/PP2A balance. *Proc Natl Acad Sci U S A* **107**, 12564-12569 (2010).
25. T. D. Schmittgen, K. J. Livak, Analyzing real-time PCR data by the comparative C(T) method. *Nat Protoc* **3**, 1101-1108 (2008).
26. S. Saha, L. Ji, J. J. de Pablo, S. P. Palecek, Inhibition of human embryonic stem cell differentiation by mechanical strain. *J Cell Physiol* **206**, 126-137 (2006).
27. S. Saha, L. Ji, J. J. de Pablo, S. P. Palecek, TGFbeta/Activin/Nodal pathway in inhibition of human embryonic stem cell differentiation by mechanical strain. *Biophys J* **94**, 4123-4133 (2008).
28. T. Teramura *et al.*, Mechanical stimulation of cyclic tensile strain induces reduction of pluripotent related gene expressions via activation of Rho/ROCK and subsequent decreasing of AKT phosphorylation in human induced pluripotent stem cells. *Biochem Biophys Res Commun* **417**, 836-841 (2012).
29. F. Chowdhury *et al.*, Material properties of the cell dictate stress-induced spreading and differentiation in embryonic stem cells. *Nat Mater* **9**, 82-88 (2010).
30. D. Dado-Rosenfeld, I. Tzchori, A. Fine, L. Chen-Konak, S. Levenberg, Tensile forces applied on a cell-embedded three-dimensional scaffold can direct early differentiation of embryonic stem cells toward the mesoderm germ layer. *Tissue Eng Part A* **21**, 124-133 (2015).
31. A. Mammoto, T. Mammoto, D. E. Ingber, Mechanosensitive mechanisms in transcriptional regulation. *J Cell Sci* **125**, 3061-3073 (2012).
32. D. Strumpf *et al.*, Cdx2 is required for correct cell fate specification and differentiation of trophectoderm in the mouse blastocyst. *Development* **132**, 2093-2102 (2005).
33. G. Giritharan, D. Ilic, M. Gormley, A. Krtolica, Human embryonic stem cells derived from embryos at different stages of development share similar transcription profiles. *PLoS One* **6**, e26570 (2011).
34. N. K. Dhaliwal, K. Miri, S. Davidson, H. Tamim El Jarkass, J. A. Mitchell, KLF4 Nuclear Export Requires ERK Activation and Initiates Exit from Naive Pluripotency. *Stem Cell Reports* **10**, 1308-1323 (2018).
35. T. Okuyama *et al.*, Structural and mechanistic insights into nuclear transport and delivery of the critical pluripotency factor Oct4 to DNA. *J Biomol Struct Dyn* **36**, 767-778 (2018).
36. G. Pan, B. Qin, N. Liu, H. R. Scholer, D. Pei, Identification of a nuclear localization signal in OCT4 and generation of a dominant negative mutant by its ablation. *J Biol Chem* **279**, 37013-37020 (2004).

37. N. Yasuhara *et al.*, Triggering neural differentiation of ES cells by subtype switching of importin-alpha. *Nat Cell Biol* **9**, 72-79 (2007).
38. S. Osmanagic-Myers, T. Dechat, R. Foisner, Lamins at the crossroads of mechanosignaling. *Genes Dev* **29**, 225-237 (2015).
39. D. Constantinescu, H. L. Gray, P. J. Sammak, G. P. Schatten, A. B. Csoka, Lamin A/C expression is a marker of mouse and human embryonic stem cell differentiation. *Stem Cells* **24**, 177-185 (2006).
40. L. G. Villa-Diaz, J. K. Kim, A. Laperle, S. P. Palecek, P. H. Krebsbach, Inhibition of Focal Adhesion Kinase Signaling by Integrin alpha6beta1 Supports Human Pluripotent Stem Cell Self-Renewal. *Stem Cells* **34**, 1753-1764 (2016).
41. Y. Takao, T. Yokota, H. Koide, Beta-catenin up-regulates Nanog expression through interaction with Oct-3/4 in embryonic stem cells. *Biochem Biophys Res Commun* **353**, 699-705 (2007).
42. K. F. Kelly *et al.*, beta-catenin enhances Oct-4 activity and reinforces pluripotency through a TCF-independent mechanism. *Cell Stem Cell* **8**, 214-227 (2011).
43. K. C. Davidson *et al.*, Wnt/beta-catenin signaling promotes differentiation, not self-renewal, of human embryonic stem cells and is repressed by Oct4. *Proc Natl Acad Sci U S A* **109**, 4485-4490 (2012).
44. R. A. Ridgway *et al.*, Focal adhesion kinase is required for beta-catenin-induced mobilization of epidermal stem cells. *Carcinogenesis* **33**, 2369-2376 (2012).
45. Y. Fonar *et al.*, Focal adhesion kinase protein regulates Wnt3a gene expression to control cell fate specification in the developing neural plate. *Mol Biol Cell* **22**, 2409-2421 (2011).
46. G. F. Weber, M. A. Bjerke, D. W. DeSimone, A mechanoresponsive cadherin-keratin complex directs polarized protrusive behavior and collective cell migration. *Dev Cell* **22**, 104-115 (2012).
47. M. Simoes Sde, A. Mainieri, J. A. Zallen, Rho GTPase and Shroom direct planar polarized actomyosin contractility during convergent extension. *J Cell Biol* **204**, 575-589 (2014).
48. M. Pines *et al.*, Mechanical force regulates integrin turnover in Drosophila in vivo. *Nat Cell Biol* **14**, 935-943 (2012).
49. B. D. Crawford, C. A. Henry, T. A. Clason, A. L. Becker, M. B. Hille, Activity and distribution of paxillin, focal adhesion kinase, and cadherin indicate cooperative roles during zebrafish morphogenesis. *Mol Biol Cell* **14**, 3065-3081 (2003).
50. K. A. Rosowski, A. F. Mertz, S. Norcross, E. R. Dufresne, V. Horsley, Edges of human embryonic stem cell colonies display distinct mechanical properties and differentiation potential. *Sci Rep* **5**, 14218 (2015).
51. S. W. Moore, P. Roca-Cusachs, M. P. Sheetz, Stretchy proteins on stretchy substrates: the important elements of integrin-mediated rigidity sensing. *Dev Cell* **19**, 194-206 (2010).
52. M. A. Schwartz, D. W. DeSimone, Cell adhesion receptors in mechanotransduction. *Curr Opin Cell Biol* **20**, 551-556 (2008).
53. M. F. Pera, B. Reubinoff, A. Trounson, Human embryonic stem cells. *J Cell Sci* **113 (Pt 1)**, 5-10 (2000).

54. P. J. Donovan, J. Gearhart, The end of the beginning for pluripotent stem cells. *Nature* **414**, 92-97 (2001).
55. J. L. Kopp, B. D. Ormsbee, M. Desler, A. Rizzino, Small increases in the level of Sox2 trigger the differentiation of mouse embryonic stem cells. *Stem Cells* **26**, 903-911 (2008).
56. Y. H. Loh *et al.*, The Oct4 and Nanog transcription network regulates pluripotency in mouse embryonic stem cells. *Nat Genet* **38**, 431-440 (2006).
57. M. Oka, T. Moriyama, M. Asally, K. Kawakami, Y. Yoneda, Differential role for transcription factor Oct4 nucleocytoplasmic dynamics in somatic cell reprogramming and self-renewal of embryonic stem cells. *J Biol Chem* **288**, 15085-15097 (2013).
58. C. P. Heisenberg, Y. Bellaiche, Forces in tissue morphogenesis and patterning. *Cell* **153**, 948-962 (2013).
59. D. E. Leckband, Q. le Duc, N. Wang, J. de Rooij, Mechanotransduction at cadherin-mediated adhesions. *Curr Opin Cell Biol* **23**, 523-530 (2011).
60. S. Budnar, A. S. Yap, A mechanobiological perspective on cadherins and the actin-myosin cytoskeleton. *F1000Prime Rep* **5**, 35 (2013).
61. J. L. Maitre *et al.*, Asymmetric division of contractile domains couples cell positioning and fate specification. *Nature* **536**, 344-348 (2016).

CHAPTER III

Acoustic Tweezing Cytometry Induces Rapid Initiation of Human Embryonic Stem Cells Differentiation

3.1 Introduction

Human embryonic stem cells (hESCs) derived from blastocyst stage embryos can be maintained in an undifferentiated state *in vitro*(*1*). Better understanding of the factors that control hESC differentiation may help understand the processes of human development and facilitate future clinical applications for hESCs including disease modeling (*2*), drug screening (*3*), and regenerative medicine (*4*).

While the significance of soluble factors has been well recognized, the mechanobiology of hESCs has only recently gained interest to reveal the significant roles of the insoluble solid-state signals of the cell microenvironment. These microenvironmental cues include variations in the rigidity and composition of the extracellular matrix (ECM), and external mechanical forces that regulate cellular behaviors in human development and diseases (*5-8*). In most *in vitro* studies of mechanoresponsiveness of hESCs, mechanical factors such as matrix rigidity, fluid shear stress, and stretching forces are globally applied and generally presented as a uniform and relatively stable long-term condition for all cells in a monolayer (*9, 10*).

Under such conditions, cytoskeleton (CSK) tension and cell-ECM interactions reach a balanced state, and it is difficult to disentangle the integrated roles of external mechanical stimuli and cell-cell interaction in mechanoresponses of hESCs. Uniform culture conditions also hinder the investigation of intrinsic mechanosensitivity of hESCs to local and acute mechanical signals. Since embryonic development occurs through a dynamic process of spatiotemporally changing physical environments, it is possible that local and dynamic mechanical signals provide potent signaling cues capable of initiating important processes in hESCs such as differentiation and epithelial-mesenchymal transition (EMT), a developmental milestone by which the pluripotent epiblast commits towards differentiated paths through extensive morphogenetic changes (*11, 12*).

Here we employed a recently developed ultrasound (US)-based technique, acoustic tweezing cytometry (ATC) (*13-15*) to investigate how hESCs respond to spatiotemporally non-uniform mechanical forces. Since ATC only exerts cyclic forces to a cell via one or several integrin-bound MBs on cell surface, the technique provided a unique opportunity to investigate mechanoresponses of the hESCs that were directly subjected to the integrin-targeted forces and other cells in a colony that were not.[†]

[†] The results presented in this chapter are adapted from my recent publication: Topal *et al.*, Nature Scientific Reports, DOI: 10.1038/s41598-018-30939-z. The research presented in this chapter has received technical assistance from Dr. Adeline Hong, Dr. Zhenzhen Fan, Mr. Xufeng Xue, Mr. Ninad Kanetkar, and Mr. Joe Nguyen. I would like to thank Dr. Jianping Fu, Dr. Cheri Deng, and Dr. Paul H. Krebsbach for their comments on the research presented in this chapter.

3.2 Materials and Methods

3.2.1 Matrigel preparation

Matrigel® (hESC-Qualified Matrix, *LDEV-Free, cat# #354277) was diluted to a concentration of 0.1 mg/ml in cold Dulbecco's modified Eagle's medium/F12 (DMEM/F12; GIBCO) and then applied to glass bottom tissue culture polystyrene (TCPS) dishes (35 mm; 10mm glass diameter, MatTek Corporation cat# P35G- 1.5- 10-C). The coating was allowed to polymerize for 2 hours incubation at room temperature. Excess Matrigel-DMEM/F12 solution was aspirated before plating cells, and then dishes were washed with sterilized Dulbecco's phosphate buffered saline (D-PBS).

3.2.2 hESC culture

hESCs (H9 and H1, WiCell Research Institute, Madison, WI) were cultured on the synthetic surface PMEDSAH as described previously (*16*) with human-cell-conditioned medium (HCCM, MTI-Global Stem, Gaithersburg, MD, http://www.mti-globalstem.com) supplemented with 5 ng/mL of human recombinant basic fibroblast growth factor (FGF2; InvitrogenTM, Carlsbad, CA, http://www.invitrogen.com), and 1%antibiotic-antimycotic (Gibco). The hPSC culture medium was replaced every other day and all cell culture was performed in designated incubators at 37^{0}C in 5% CO_2 and high humidity. Differentiated cells were mechanically removed using a sterile pulled-glass pipet under a stereomicroscope (LeicaMZ9.5, Leica Microsystems Inc., Buffalo Grove, IL).

For single cells: Undifferentiated colonies were washed with PBS and a non-enzymatic cell attachment passaging solution (Lonza L7 hPSC) was added for gentle disassociation of colonies and incubated at 37^0C for 5 min. L7 was removed and 2 ml of HCCM was added, and then cells were scraped and collected into conical tube for brief centrifugation. The cell pellet was dispersed in HCCM supplemented with 5 ng/mL bFGF and 10 mM of ROCK inhibitor (Sigma) (26) and passed through a 40 mm nylon mesh cell strainer (BD Biosciences, Bedford, MA) to remove large cell aggregates. Single hESCs were counted and 100K/ ml cells were plated on Matrigel coated glass dishes cultured for overnight for attachment

For colonies: Undifferentiated colonies were cut into small pieces and transferred them onto matrigel coated glass dishes (~5-6 as small cell clusters for each plate), and let them to attach for overnight.

3.2.3 Attachment of targeted lipid microbubble to cells

Visistar^{TM}-Integrin lipid microbubbles (MBs) with high affinity for α5β3 integrin (mean ± SE of bubble radius: 2.11 ± 0.07 μm, n = 119; Targeson) were diluted to a final concentration of $2*10^7$ MBs mL^{-1} in HCCM. Cell culture in Matrigel-coated petri dish was gently washed with D-PBS, and loaded with 100 μL diluted MBs in culture media. The petri dish was flipped upside down and incubated at 37°C for 10 min to enable attachment of MBs to hESCs via RGD-integrin binding, followed by another gentle wash with culture media to remove unbound MBs.

3.2.4 Ultrasound stimulation

A planar ultrasound (US) transducer with 1 MHz center frequency (-6 dB beam width of 3.54 mm at a Rayleigh distance of 9 mm; Advanced Devices) was used for ATC application. The US transducer was positioned at an angle of 45° relative to the horizontal direction facing downward, and at 9 mm from the cells seeded at the bottom of the petri dish. The petri dish was filled with culture media to submerge the active surface of the transducer and allow acoustic coupling. The US transducer was driven by two waveform generators (Agilent Technologies) and a 75 W power amplifier (Amplifier Research) to generate cyclic pulses with 1 Hz pulse repetition frequency (PRF) and 50% duty cycle. The US transducer was calibrated in free field in water using a needle hydrophone (HNR-0500, Onda). The cells were exposed to 30 min ultrasound treatment at an acoustic pressure level ramping from 0.03 to 0.04 and 0.05 MPa, 10 min at each level.

The primary acoustic radiation force was estimated as:

$$F = 2\pi P_A^2 D R_0/\delta_{tot}\rho_0 c\omega_0 T$$

where P_A is the acoustic pressure, D is the pulse duration (50 ms), R_0 is the bubble radius, δ_{tot} is the total damping constant ($\delta_{tot} = 0.16$), ρ_0 is the medium density (1000 kg m^{-3}), and c is the sound speed in media (1500 m s^{-1}), ω_0 is the resonance frequency (1.25 MHz), and T is the pulse repetition period (1 s) *(17).*

To observe the MB dynamics, images of the MBs exposed to ultrasound stimulation were captured with a high-speed camera (FASTCAM SA1, Photron) at a frame rate of 2000 frame/s. MB radius and location in each frame were quantified and tracked over time using an automated MATLAB script.

3.2.5 Contractile force quantification using PDMS micropost array

Contractile force measurements were performed as described before *(18)*. Briefly, hESCs were seeded on PDMS micropost array (PMA) either as single cells or colonies, and incubated overnight to allow attachment. The PMA top surface was coated with fibronectin (Sigma-Aldrich) to promote cell adhesion. Microposts with 1.83 µm diameter, 7.1 µm height, and a spring constant of 7.22 nM/µm were used in this study. Fluorescence images of the PMA top surface were captured throughout the ultrasound treatment using an inverted epi-fluorescence microscope enclosed in a cage incubator (Carl Zeiss MicroImaging) maintaining the temperature at 37°C and the CO_2 at 5%. Using a custom-written MATLAB script, micropost deflections were detected, quantified, and multiplied by the micropost spring constant to produce the horizontal contractile force.

3.2.6 Drug Inhibition Assays

PF-562271 (Sigma-Aldrich) was added to the culture media at 1 µM an hour before ultrasound treatment to inhibit focal adhesion kinase phosphorylation. To inhibit the Rock pathway and the myosin-II heavy chain, Y27632 and blebbistatin (Sigma-Aldrich) was added to the media respectively at 10 µM 30 min before applying ultrasound stimulation.

3.2.7 Fluorescence Ratiometric calcium imaging

The cells were loaded with Fura2-AM by incubating in the culture medium dissolved with 10µM Fura2-AM (Invitrogen) and 0.05%vol/vol of 10% wt/vol Pluronic

F-127 (Invitrogen) for 60 minutes. After incubation, excess dye was removed by washing three times. Fast speed fluorescence imaging was performed using a cooled CCD camera (Photometrics QuantEM), a monochromator with 5-nm bandpass (DeltaRAM X^{TM}, PTI), and a polychroic filter (73000v2, Chroma). The samples were excited at 340nm and 380nm alternatively, and emission fluorescence was collected at 520nm. The pseudocolored ratio images of $[Ca^{2+}]_i$ based on two excitation channels were generated using Matlab (Mathworks).

3.2.8 Immunoblot analysis

Cells were collected and lysed in NP40 lysis buffer (NaCl at 150 mM, NP-40 at 1.0%, and TrisCl at 50 mM, pH 8.0). Supernatant was quantified using Bio-Rad Protein Assay (Bio-Rad; cat# 5000006) with the Biotek Nova Spectrophotometer at 595 nm wavelength. 10 μg of protein lysate was mixed with 3x Laemmli loading buffer (4% SDS, 10% 2-mercaptoethanol, 20% glycerol, 0.004% bromophenol blue, 0.125 M Tris-HCl, brought to pH 6.8). Novex® Tris-Glycine SDS Running Buffer 10X (TFS: cat# LC2675-4) was diluted to 1X with milliQ filtered deionized water. We used Novex™ WedgeWell™ 4-20% Tris-Glycine Gels (TFS; cat# XP04205BOX) and XCell SureLock® Mini-Cell (TFS; cat# EI0001). For optimal separation of proteins ranging 50 to 75 kDa for S6K2 phosphorylation immunoprecipitation analysis, we used the Novex™ WedgeWell™ 10% Tris-Glycine Gels (TFS; cat# XP00105BOX). Precision Plus Protein™ Dual Color Standards (Bio-Rad; cat# 1610374) to approximate molecular weights from 10 kDa to 250 kDa. Gels are run at 150V for 85 min. For transfer of proteins, we use Trans-Blot® SD Semi-Dry Transfer Cell (Bio-Rad; cat# 170-3940) and

PVDF membranes dipped in methanol briefly and rinsed in 1X Transfer Buffer (25 mM Tris, 192 mM glycine, 20% methanol (v/v), 0.5% SDS at pH 8.3) (Bio-Rad; cat# 162-0177 R) to transfer 24V for 60 min. After the transfer, membranes were blocked for 30 min in a 2.5% blocking solution (Bio-Rad; cat# 1706404) in 50 mL 1X TBST (50 mM Tris-Cl, pH 7.5, 150 mM NaCl, Tween-20 (FS; cat# BP337-100) for 30 min, followed by 1x wash for 30 min in 1X TBST. Prior to antibody incubation, membranes were cut between the 75 kDa and 100 kDa bands to optimize for proteins above 100 kDa in size, above 75 kDa and above the 37 kDa membrane for proteins within those ranges, and between 20 – 25 kDa for proteins above and below those ranges. This allows for optimal antibody incubation with the proper membranes. After incubating membranes in primary antibodies overnight at 4°C, they were washed for 30 min in 1X TBST at room temperature (RT), shaking. Next, membranes were incubated in the appropriate secondary antibody for one hour and washed for 30 min in 1X TBST at RT. For film capture, membranes were incubated with SuperSignal™ West Pico Chemiluminescent Substrate (TFS; cat# 34078) for 3 min at RT. We used HyBlot CL autoradiography film (Denville Scientific: cat# e3018). Primary antibodies for immunoblot analysis: E-cadherin, p-FAK (Tyr^{397}), p-YAP (S127), Ki-67, Vimentin, and Oct4 were used at 1:1,000 dilution in 5% BSA in 1X TBST buffer with 0.04% sodium azide. Almost all antibodies from Cell Signaling Technologies (CST) are rabbit: Oct4 (Cell Signaling Technologies (CST): cat# #2750S), p-FAK(Y397) (CST: cat#13008S), Vimentin (D21H3)(CST: cat# 57419), p-YAP(S127) (CST: cat# 13008S), E-cadherin (CST:mouse, cat#14472), Ki-67 (CST: mouse cat #9449). Secondary antibodies for immunoblot analysis: 1:4,000 dilution for α-mouse IgG (H+L) HRP conjugate (Promega; cat#

W4021). 1:7,500 dilution for α-rabbit IgG (H+L) HRP conjugate (Promega; cat# W4011).

3.2.9 Cell immunofluorescence analysis

hESCs on MatTek Corporation glass bottom dishes were washed with PBS for 5 min and aspirated out the supernant and addded 1 ml of Z-Fix solution (Anatech LTD: cat# 170) for 10 min at RT shaking. Next, we washed 3x with 1 mL of PBS for 10 min at RT. Next, we added unmasking solution (PBS, 2N HCL, 0.5% TritonX) for 10 min, removed it, added quenching solution (TBS, 0.1% Sodium Borohydride) for 10 min, removed it, added permeabilization solution (PBS, 0.02% TritonX) for 10 min. Then, we blocked with 1 mL of 5% BSA in 1X PBS for 30 min. Next, glass bottom dishes were incubated in primary antibodies overnight at 4˚C shaking. Slides were then washed with 1X PBS 3 times for 10 min at RT while shaking. We then incubated in secondary antibodies covered in foil for at least one hour at RT while shaking. Afterwards, we washed twice in PBS for 10 min, incubated in DAPI solution for 10 min and washed in 1X PBS for 10 min. Finally, we added 1 drop of ProLong® Gold Antifade Mountant onto each well, placed a glass cover slip, and sealed with acrylic nail polish. We used Nikon Ti Eclipse Confocal Microscope, 20x and 60x magnification lenses, with water to capture images. We captured images with or without 3x digital zoom, ¼ frames per second, 512x512 image capture, 1.2 Airy Units, 2x line averaging, appropriate voltage and power settings optimized per antibody. No modification was done, except image sizing reduction, rotation, or gray scale change for figure preparation. All original and unaltered blots are found in the supplementary figures. Primary antibodies for immunofluorescence: All antibodies were used as following with a working volume of 1 mL in 5% BSA in PBS, unless noted otherwise:

Oct4 (SantaCruz: goat, 1:500, cat# sc8629), Nanog (Abcam: mouse, 1:100 cat#ab62734), Sox2 (Millipore: rabbit, 1:500, cat# ab5603), E-cadherin (R&D Systems: mouse, 1:100, cat# AF648), pFAK (Invitrogen: Tyr 397, 31H5L17; rabbit, 1:500, cat# 700255), b-catenin (CST: rabbit, 1:100, cat#8480), N-cadherin (CST: mouse, 1:100, cat# 13116), YAP (SantaCruz: mouse, 1:500, cat#sc101199), Snai1 (SantaCruz: mouse, 1:500, cat# sc271977), Slug (CST: rabbit, 1:400, cat# 9585), and T (brachyury) (SantaCruz: rabbit, 1:500, cat# sc20109). Secondary antibodies for immunofluorescence: All antibodies were used at a concentration of 1:1,500 with a working volume of 1.5 mL in 5% BSA in PBS. DAPI stain was used for DNA. Donkey anti-Mouse IgG Secondary Antibody, Alexa Fluor® 488 (TFS: cat# R37114) Donkey anti-Rabbit IgG Secondary Antibody, Alexa Fluor® 594 (TFS: cat# A-21207)

3.2.10 Image Analysis

Image J was used to quantify fluorescent intensity (*19, 20*). Briefly, after selecting the cell of interest using any of the polygon drawing/selection tools, “set measurement” was selected from the Analyze menu by selecting area, integrated density and mean gray value. Then, "Measure" was selected from the analyze menu, and a region next to the cell that has no fluorescence was selected for background. This step was repeated for each single cell in the field and then the all data were analyzed on excel, and this formula was followed for the corrected total cell fluorescence (CTCF).

CTCF = Integrated Density - (Area of selected cell X Mean fluorescence
of background readings)

3.2.11 Extraction and purification of total RNA

Plates were washed with PBS and 1000µl of Trizol Reagent (Invitrogen, Carlsbad, CA) was added to the plates, and RNAs were collected after vigorous pipetting. 200 µl Chloroform was added to this solution followed by centrifugation (13,000 g-15 min). Aqueous phase containing RNA was separated and 500-µl isopropanol was added and stored at 20^0C at least overnight. Then, the manufacturer's RNA Clean-up protocol, RNeasy Mini-Kit (Qiagen, Valencia, CA), with the optional On-column DNAse treatment was followed. RNA quality and concentration were checked using a Synergy NEO HTS Multi-Mode Microplate Reader (BioTek Instruments, Winooski, VT).

3.2.12 Reverse-transcription PCR (RT-PCR) analysis

Reverse transcription from 2.5 µg of total RNA in a 20-µL reaction into cDNA was performed using SuperScript™ VILO™ Master Mix (ThermoFisher Cat#11755050). The synthesis of first-stranded cDNA was carried out in the PCR tube after combining SuperScript VILO, RNA, and DEPC-treated water, in the first cycle at 25ºC for 10 min, incubating at 42ºC for 60 min, and terminating the reaction at 85ºC for 5 min. Quantitative PCR was performed triplicate for for each sample using TaqMan probes (Applied Biosystems) and TaqMan Universal PCR Master Mix (Applied Biosystems) on 7900 HT Fast Real Time PCR system (Applied Biosystems). Relative quantification of Nanog, Oct4, Sox2, FAK, Snai1, T, ITGAV, and Pax6 gene expression data were normalized to the GAPDH expression and calculated using the $2^{-\Delta\Delta CT}$ expression level(*21*).

All primers for qRT-PCR were purchased from ThermoFisher Life Technologies: NANOG (Assay ID: Hs02387400_g1 (FAM-MGB), UniGeneID: Hs.635882), POU5F1 (OCT 3/4) (Assay ID: Hs03005111_g1 (FAM-MGB), UniGeneID: Hs.249184), SOX2 (Assay ID: Hs01053049 (FAM-MGB) (FAM-MGB), UniGeneID: Hs.518438), FAK (PTK2) (Assay ID: Hs03657683 (FAM-MGB), UniGeneID: Hs. 395482), SNAI1 (Assay ID: Hs00195591_m1 (FAM-MGB), UniGeneID: Hs. 48029), T (BRACHURY) (Assay ID: Hs00610080_m1 (FAM-MGB), UniGeneID: Hs. 389457), ITGAV (Assay ID: Hs00233808_m1 (FAM-MGB), UniGeneID: Hs. 436873), PAX6 (Assay ID: Hs00240871_m1 (FAM-MGB), UniGeneID: Hs.446336), GAPDH (Assay ID: Hs02786624_g1 (FAM-MGB), UniGeneID: Hs.544577).

3.2.13 Statistical Analysis

Results are presented as Mean ± SEM. Unpaired two-tailed student's t test was performed for comparisons, and a p-value < 0.05 was considered statistically significant.

3.3 Results and Discussion

3.3.1 ATC-mediated cyclic strains *via* integrin increased cellular contractility of hESCs

To use ATC to apply cyclic forces to hESCs via integrin, we attached lipid-shelled targeted microbubbles (MBs) coated with RGD peptides targeting $\alpha_V\beta_3$ integrin receptors (Visistar^{TM}-Integrin MBs, Targeson) (radius 2.11 ± 0.07 µm, *n* = 119) to hESCs (Figure 3-1A). Application of US pulses (Figure 3-1 B, C) exerted directional forces (17.0 ~ 25.0 nN) on the integrin-anchored MBs (*15*), displacing them from their original positions during the US pulses (Figure 3-1D). The displacement and retraction of the integrin-bound MBs after each US pulse reveal the characteristic viscoelastic behaviors reflecting properties of the MB-integrin-CSK linkage (Figure 3-1D). Essentially, displacements of the integrin-bound MBs away from their pre-US location reflected strains applied to the molecular RGD-integrin-CSK linkage by ATC application, leading to stretching/distortion of the molecular assembly. Such stretching/distortion could lead to modification of adhesion and cytoskeletal proteins, key factors in conversion of mechanical forces into biological signals (*22, 23*). Interestingly, after each US pulse, these integrin-anchored MBs often retracted only partially from the peak displacement (Figure 3-1D), (Figure 3-2, A- C), resulting in a gradual shift in the "resting" position of MBs (~ 0.6 µm after 7 pulses, (Figure 3-1D), (Figure 3-2D). Partial retraction of MB displacements suggested partial recovery of the stretching/distortion of the adhesion and CSK proteins associated with the bubble-integrin linkage after the force was removed, while the shift in the MB resting location represented more permanent changes in the adhesion and/or CSK proteins due to application of US pulses.

Because cell contractility is an important morphogenetic trait responsive to external forces (*24*), we measured cellular contractile forces of hESCs during ATC application using poly-(dimethylsiloxane) (PDMS) micropost arrays as real-time force sensors (*13*). To examine the direct effect of cyclic force/strain to the cells and exclude the contribution of cell-cell contacts, we conducted experiments using single adherent hESCs, which were viable and maintained pluripotency 24 h after plating before our experiments. For single hESCs that had MBs attached, the cellular contractility increased immediately after ATC application (Figure 3-3), suggesting robust cellular responses to integrin-targeted external forces/strains. The single hESCs without attached MBs did not show any changes in cellular contractility even with the application of US pulses, underscoring the role of acoustic actuation of integrin-anchored MB. Because ROCK signaling is crucial for the activation of cell contractility, we hypothesized that blockage of ROCK signaling would result in a decrease in cell contractility (*25*). Indeed, when cells were treated with Y27632, ROCK pathway specific inhibitor (*26*) (*27*), increase of cell contractility was dramatically abated (Figure 3-3B) suggesting that increased contractility of single hESCs subjected to integrin-targeted forces requires tension in an intact CSK.

Interestingly, ATC application also increased cellular contractility in hESCs throughout a colony even though not all of the hESCs in the colony has attached MBs (Figure 3-1E), and the effect was again abolished by Y27632 (Figure 3-1H). In our experiments, MBs preferentially attached to the hESCs near the colony periphery (Figure 3-1, F and G), with 1.44 ± 0.14 MBs/cell (456 ± 80 MBs, $n = 7$) in the peripheral zone (defined as the region occupying the outer 30% of colony radius) and 0.17 ± 0.03

MBs/cell (61 ± 13 MBs, $n = 7$) in the central zone (region within the inner 70% of colony radius), respectively. Thus, many cells in the colony's central zone did not have MBs attached to them, thus were not directly subjected to forces via integrin-bound MBs during ATC application. Despite the fact that only some cells were directly subjected to integrin-targeted strain/force, ATC application increased cellular contractility globally throughout the colony (Figure 3-1, E and H), highlighting the critical role of cell-cell communication in generating mechanoresponses in other hESCs in a colony. Interestingly, while the cells in the central zone exhibited lower contractile forces than those in the peripheral zone before ATC application (Figure 3-1, E and H) (*28*), they sustained greater increases in contractility as shown by the larger slope of force increase (center panel in Figure 3-1H) for these cells to match the level in the periphery during ATC application (Figure 3-1H), resulting in mechanical homogenization of a hESC colony. Particularly, since only a subpopulation of the hESCs in the colony were subjected directly to the ATC-mediated forces, this global response suggests an important role of cell-cell communication in the mechanoresponsiveness of hESC colony to integrin-targeted cyclic forces.

In addition to global changes in cellular contractility, we also observed that ATC application induced intracellular calcium activities throughout entire hESC colonies, despite that MBs were mostly attached to cells in the periphery (Figure 3-4) . Since spontaneous calcium activities do not occur in undifferentiated hESCs (*29*), these ATC-induced calcium transients suggested an aspect of collective mechanoresponse of hESCs in a colony to external forces via integrin.

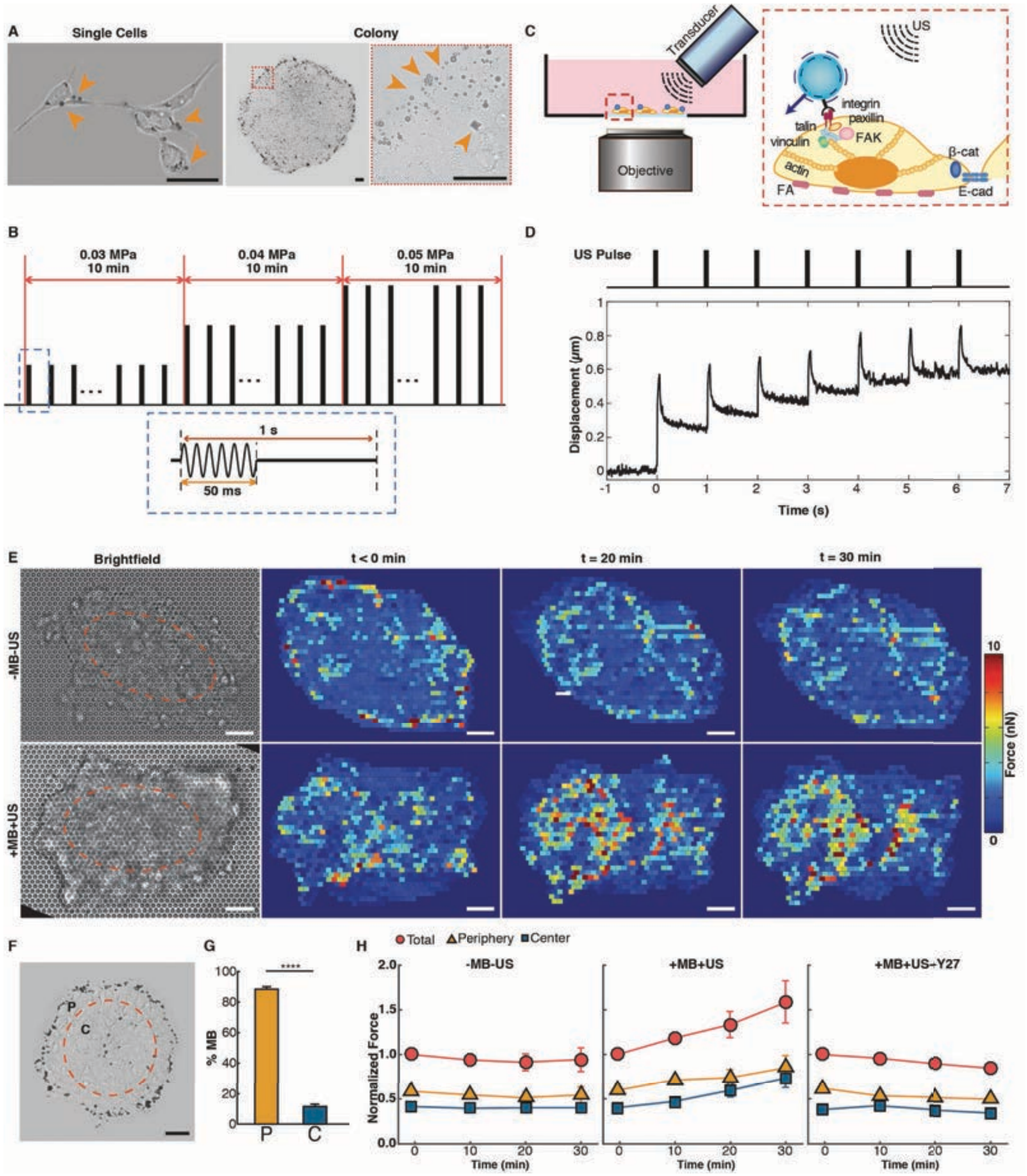

Figure 3-1. ATC application using ultrasound (US) excitation of integrin-anchored microbubbles (MBs) and increased cellular contractile forces of hESCs. (A) Bright field images of single hESCs and colony with integrin-bound MBs (arrow heads). Scale bar 40 µm. (B) US pulses used in ATC. (C) Experimental setup for ATC. (D) Cyclic MB displacement vs. time subjected to pulsed US application during ATC application. (E) Bright field images of hESCs seeded on PDMS micropost force sensor array and subcellular contractile force distributions in control hESC colony (-MB-US) (top) and hESC colony treated by ATC (+MB+US) (bottom) at t = 0, 20 and 30 min. ATC was applied at t = 0 for 30 min. 'P' denotes periphery zone and 'C' central zone. Scale bar 20 µm. (F) Bright field image showing distribution of MBs attached to hESCs in a colony. Colony area is divided into two equal regions marked by the orange circle: periphery (P) (outer 30% radius) and central zone (C) (center 70% radius). (G) Percentage of MBs attached to hESCs in colonies (*n* = 7) in the periphery (P, 88.53% ± 1.63%) and in the center (C, 11.47% ± 1.63%) (Mean ± SEM). **** denotes $p < 0.0001$. (H) Normalized contractile force in the entire colony, in the periphery zone, and in the center zone *vs*. time for control (-MB-US), ATC-treated (+MB+US), and Y27632 (Y27) (10 µM) treated hESC colonies (Mean ± SEM, *n* = 10).

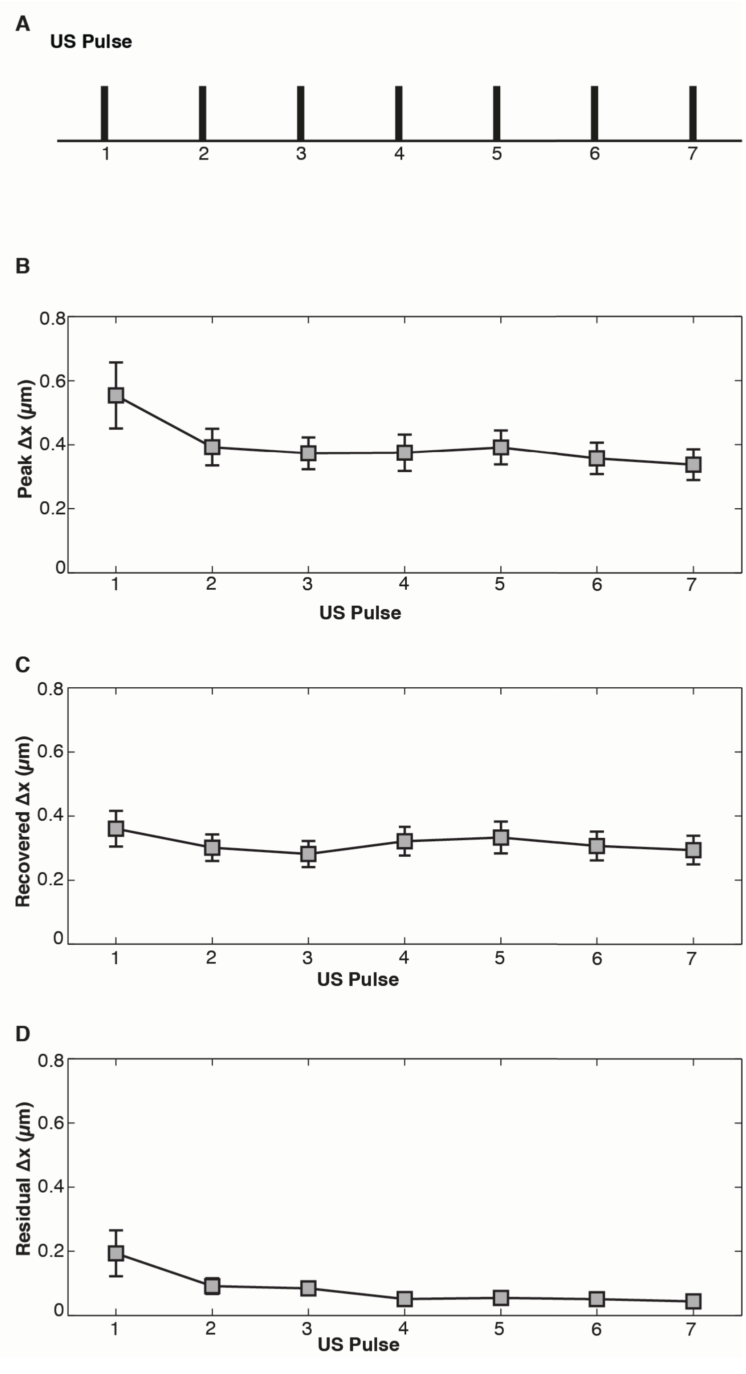

Figure 3-2. MB displacements driven by pulsed US exhibit characteristic viscoelastic properties. (A) Schematic of US pulses with a pulse repetition frequency (PRF) of 1 Hz, duration of each pulse 50 ms, and acoustic pressure amplitude 0.03 MPa. (B) Peak displacements (Δx) of MBs during the first 7 US pulses (Mean ± SEM, *n* = 118). (C) Values of displacement recovery after

each US pulse for the first 7 pulses (Mean ± SEM, *n* = 118). (D) Residual displacements of MBs after each US pulses for the first 7 pulses (Mean ± SEM, *n* = 118).

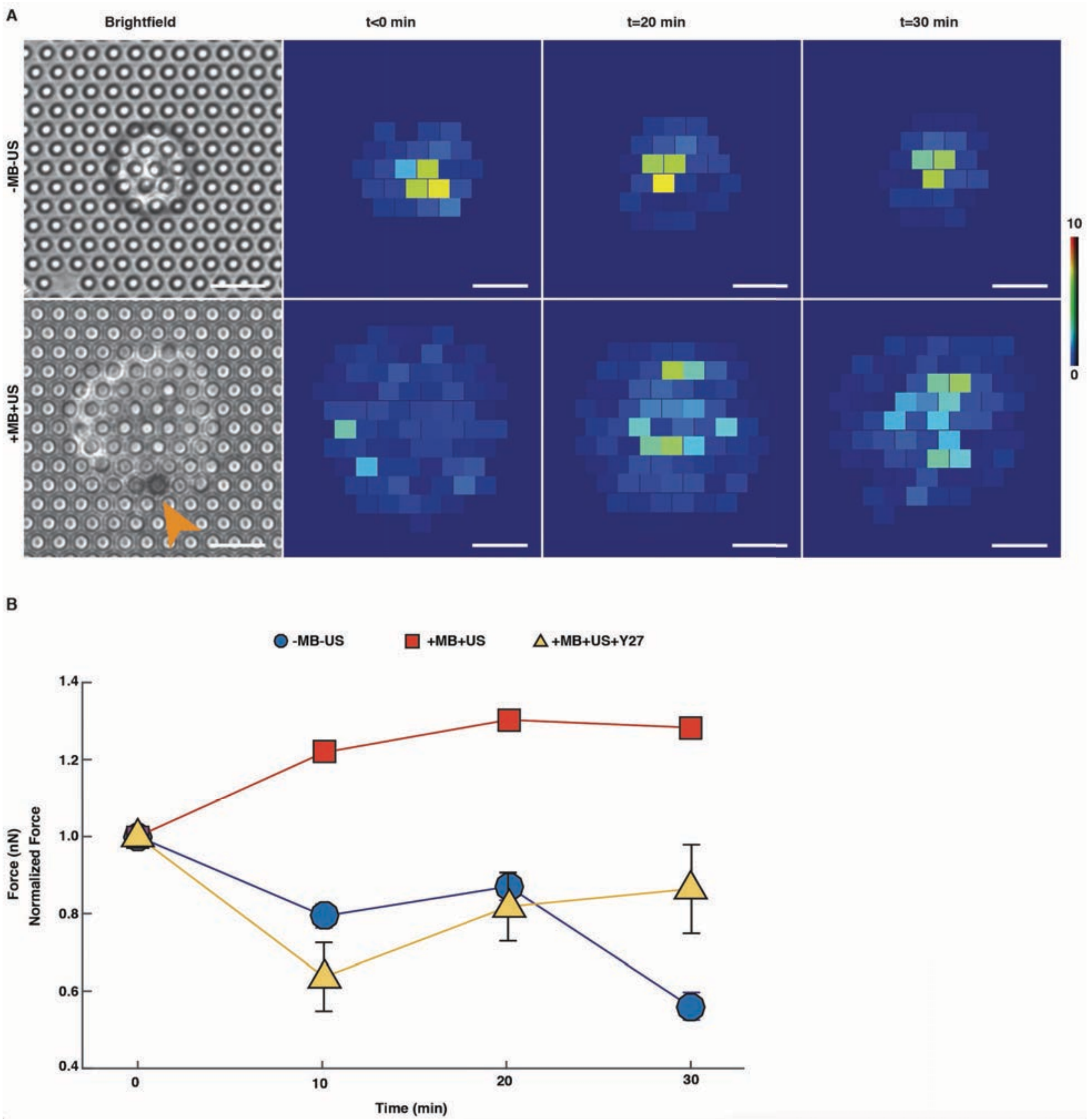

Figure 3-3 ATC application using pulsed US excitation of integrin-bound MBs increased cellular contractile forces in single hESCs. (A) Bright field images and subcellular contractile force distributions in single hESCs at t = 0, 20 and 30 min in control group (-MB-US; top) and ATC treated group (+MB+US; bottom). ATC was applied at t = 0 for 30 min. Scale bars 10 µm. (B) Normalized contractile force of single hESCs cells in control group (-MB-US), ATC-treated group (+MB+US), and (+MB+US + Y27632 group (Y27) (10 µM) treated groups (Mean ± SEM, n = 8). Contractile force was normalized to pre-ATC treatment values.

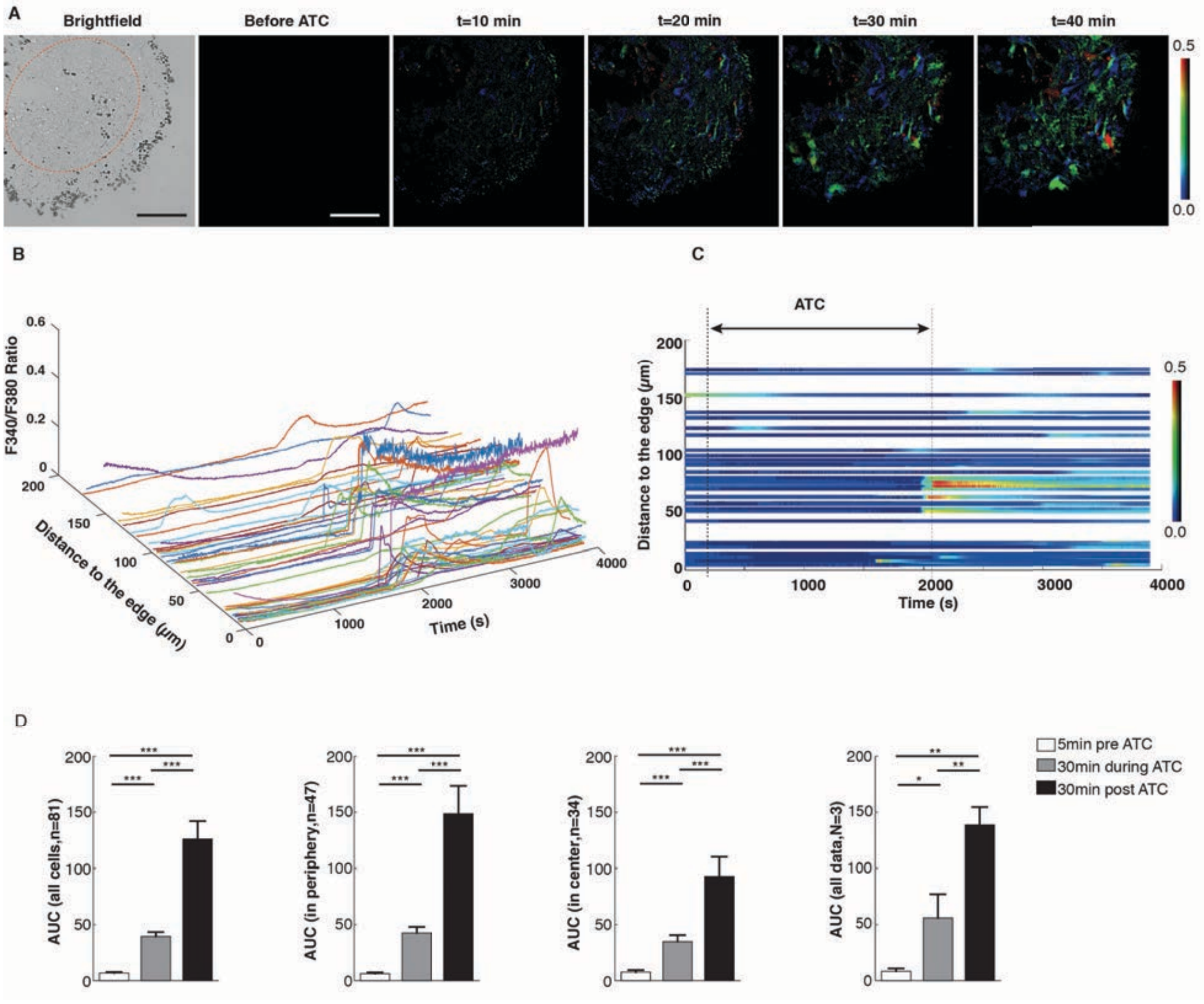

Figure 3-4. ATC application generated calcium transients in ESC colony. (A) Bright field image showing microbubble preferentially attached to cells near the periphery with the number of bubbles in the central zone (within 70% of colony radius) and periphery zone (outside central zone) being 35 and 410 respectively; pseudo-color ratiometric calcium images (background subtracted) at t = - 5 min, 10 min, 20 min, 30 min, and 40 min. ATC was applied at t = 0 min for 30 min. Scale bars 100 µm. (B) Time-course of F340/380 ratio in cells in (A) (49 cells out of 190 cells). The ratio of fluorescence intensity excited at 340 nm and 380 nm (F340/380 Ratio) is linearly proportional to the intracellular calcium concentration. The y axis is the distance between a cell and the edge of the colony. Scale bars 100 µm. (C) 2D plot of F340/F380 in (B). (D) Area under curve (AUC) of F340/380 before, during, and after ATC application, n = 81 cells from N = 3 experiments. There were 34 cells in the central zone (70% of radius of colony) and 47 cells in periphery zone (region outside central zone) that exhibited calcium activities. t test p values < 0.05 (*), < 0.01(**), and < 0.001 (***).

3.3.2 Cyclic forces to integrin induced rapid decrease of Nanog and Oct4

We next examined transcriptional response of hESCs to ATC application. For single hESCs targeted by MBs (arrow), rapid decease in Oct4 and Nanog was clearly evident after just 30 min application of US pulses, while Sox2 was not significantly affected (Figure 3-5, A and B). In contrast, single hESCs without attached MBs, although exposed to the same US pulses, exhibited no change in Oct4 or Nanog (arrow in Figure 3-5A), suggesting that these transcription factors responded directly to integrin-targeted cyclic forces for single hESCs. Interestingly, for hESC colonies, even though MBs were mostly attached to the cells near the colony periphery (Figure 3-5C), ATC application for 30 min also decreased Oct4 and Nanog in the entire colony (Figure 3-5, C and D), suggesting a collective mechanoresponse of hESC colony to locally applied external forces. These effects were not observed in hESC colonies without attached MBs or without US application (Figure 3-6 A, B, D). In addition, the ATC-induced decreases in Oct4 and Nanog were irreversible, as shown by immunostaining results after 48 hours of culture after ATC treatment (Figure 3-7). Mirroring the global increases in cellular contractility and calcium activities in hESC colonies (Figure 3-1E and Figure 3-4), these ATC-induced global transcription responses within the entire colony demonstrate the community characteristics of hESC mechanoresponses and initiation of differentiation induced by local integrin-targeted cyclic forces.

Immunoblot analysis confirmed decreased expression of Oct4 and Nanog following ATC treatment (Figure 3-5E), while in other control groups (-MB +US and +MB -US), no change was observed (Figure 3-6C). Gene expression analysis showed no change in Nanog, Oct4, and Sox2, while a decrease was observed in neuroepitelial (NE) marker, Pax6 in microbubble attached and ultrasound treated group (Figure 3-6E). Comparable effects of ATC-mediated forces were observed in another hESC line (H1) (Figure 3-8). Taken together, these results highlight a remarkable mechnosensitivity and community characteristics of hESCs to locally applied integrin-targeted cyclic forces/strains, which initiated hESC differentiation in the entire colony only after 30 min of ATC treatment, an observation in distinct contrast to the multiple-day differentiation process induced by soluble factors or regulated by uniform matrix rigidity (*9*).

Although direct cyclic forces via integrin-anchored MBs were only applied to a fraction of the cells in the colony with attached MBs, the changes in OCT4, Nanog, and Sox2 expression were global and throughout the colony (Figure 3-5). These results highlight the involvement of cell-cell communication of the cells in the colony in their response the integrin-targeted cyclic forces.

Immunoblot analysis confirmed decreased expression of Oct4 and Nanog following ATC treatment (Figure 3-5). Comparable effects of ATC-mediated forces were observed in another hESC line (H1) (Figure 3-8) Taken together, these results highlight a remarkable sensitivity and community characteristics of hESCs to localized, integrin-targeted cyclic forces, which initiated hESC differentiation evident 30 min after ATC treatment, an observation in distinct contrast to the multiple-day differentiation process with transcription changes in the presence of soluble factors or regulated by uniform matrix rigidity (*9*).

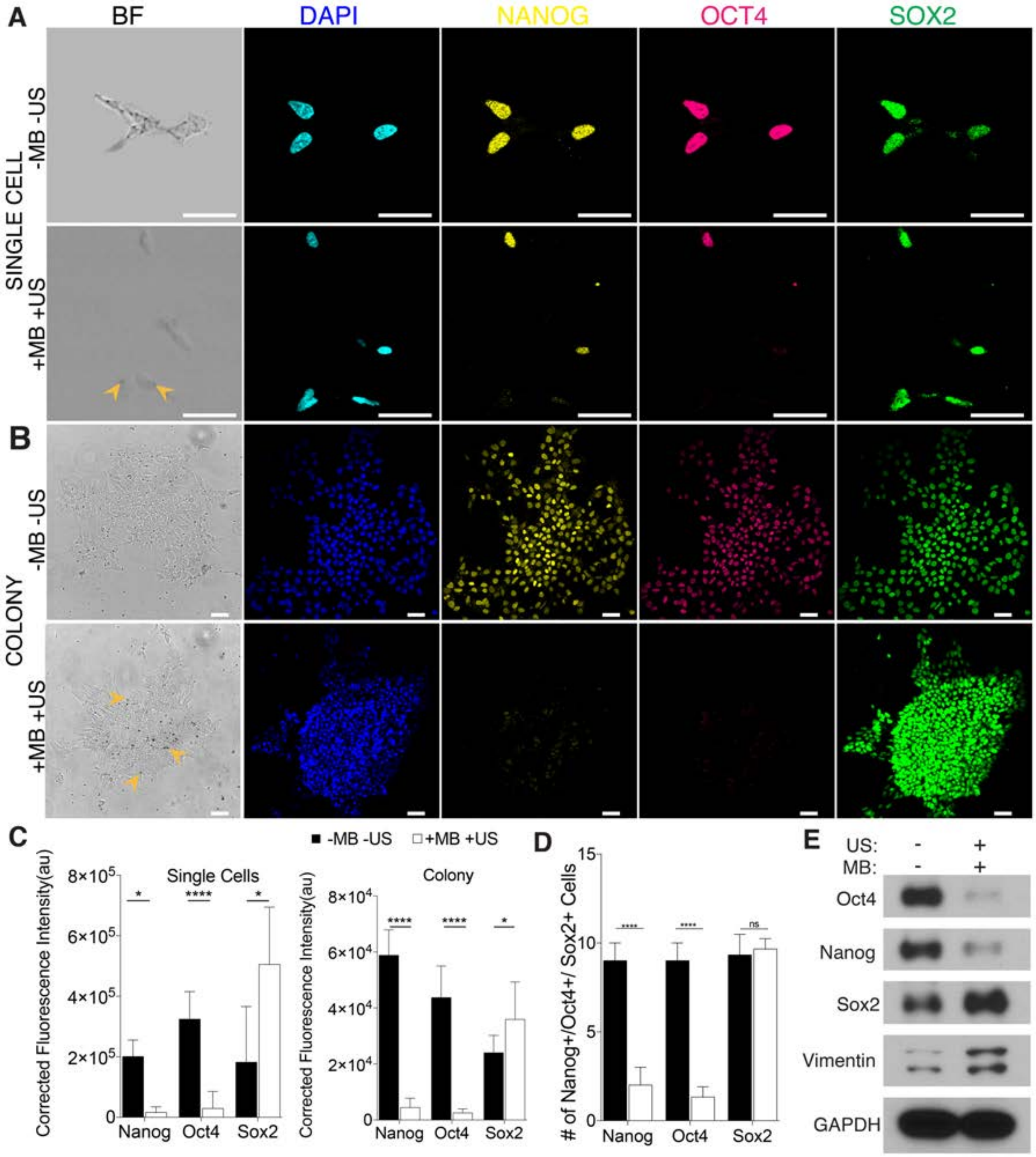

Figure 3-5. ATC application downregulated pluripotency markers in hESCs. (A) Bright field images of single ESCs and integrin-bound MBs (arrows). Confocal fluorescence images of single hESCs stained with DAPI (blue), Oct4 (magenta), Nanog (yellow), and Sox2 (green) with and without ATC application (30 min). Scale bars: 50 µm. (B) Percentages of hESCs with Oct4, Nanog, and Sox2 after ATC treatment compared with control. (C) Bright field images of a hESC colony and integrin-bound MBs (arrows). Confocal fluorescence images showing hESCs stained with DAPI (blue), Oct4 (magenta), Nanog (yellow), and Sox2 (green) with and without ATC application. Scale bars: 50 µm. (D) Corrected fluorescence intensity measurement of hESCs with Nanog, Oct4, and Sox2 after ATC treatment. (E) Immunoblot analysis of protein expression in hESCs. All quantifications were from at least 3 independent experiments with two replicates per experiment. Unpaired *t* test p values < 0.05 (*), < 0.01(**), and < 0.001 (***); n.s, not significant

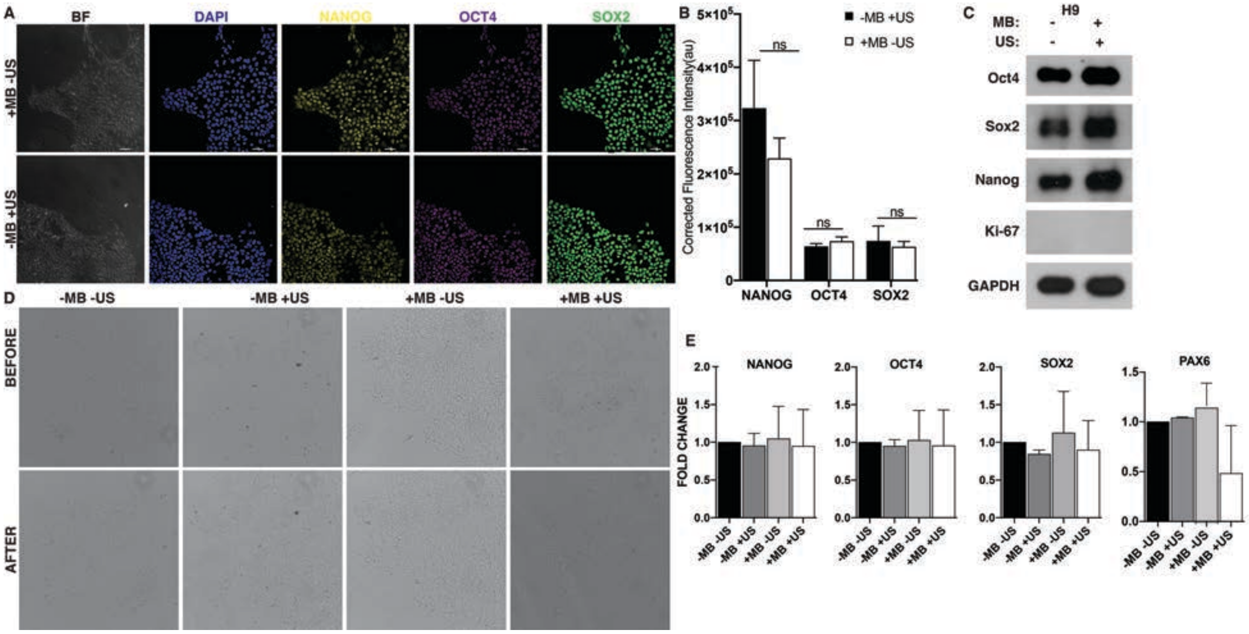

Figure 3-6. A-B) Confocal micrographs of colonies of hESCs in control groups (+MB-US, -MB+US) exhibit no changes in expression of transcription factors. Scale bars 50 µm. C) Immunoblot analysis of control groups (+MB-US, -MB+US) exhibits no changes in expression of transcription factors. D) Bright field images of hESC colonies before and after ATC treatment E) qRT-PCR analysis of Nanog, Oct4, Sox2, and Pax6.

Although direct cyclic forces via integrin-anchored MBs were only applied to a fraction of the cells in the colony with attached MBs, the changes in OCT4, Nanog, and Sox2 expression were global and throughout the colony (Figure 1-1). These results highlight the involvement of cell-cell communication of the cells in the colony in their response the integrin-targeted cyclic forces.

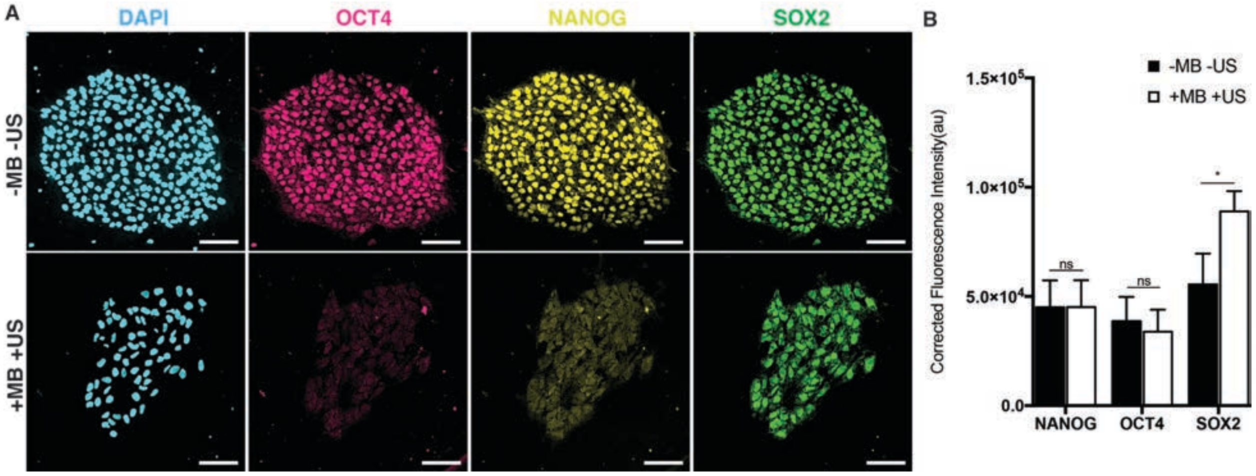

Figure 3-7. ATC-induced decreases of nuclear Oct4 and Nanog in hESCs persisted for 48 hours. (A) Confocal fluorescence images of hESC colony stained with DAPI (blue), Oct4 (magenta), Nanog (yellow), and Sox2 (green) with and without ATC application after 48 hours culture. (B) Percentages of ATC applied hESCs with nuclear Oct4, Nanog, and Sox2 after 48 hours culture. Scale bars 50 µm. Quantifications were from 3 independent experiments with two replicates per experiment. Quantifications were mean ± SEM; unpaired t test p values < 0.001 (***).

Taken together, these results highlight a remarkable mechnosensitivity and community characteristics of hESCs to locally applied integrin-targeted cyclic forces/strains, which induced rapid loss of pluripotency and initiation of hESC differentiation in the entire colony immediately after 30 min of ATC treatment, an observation in distinct contrast to the multiple-day process needed for transcriptional changes in differentiation induced by soluble factors or regulated by uniform matrix rigidity (*9*).

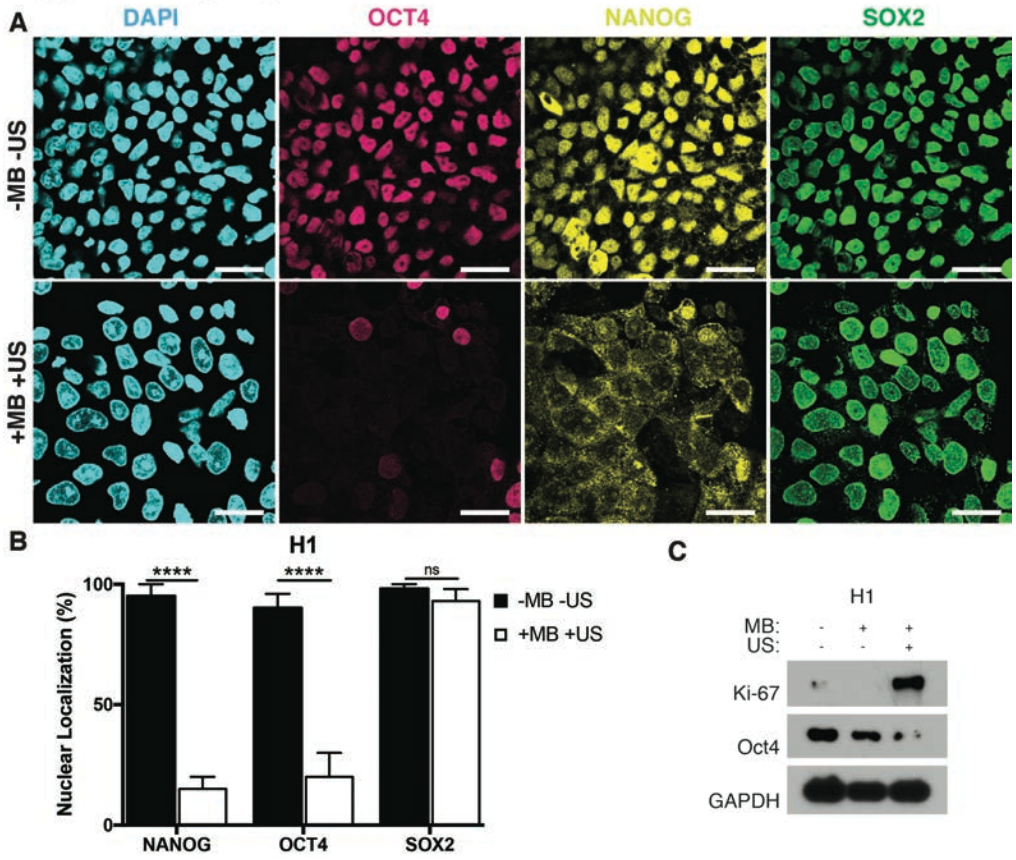

Figure 3-8. ATC-induced changes in another hESC line H1. (A) Confocal fluorescence images of hESCs stained with DAPI (blue), Oct4 (magenta), Nanog (yellow), and Sox2 (green) with and without ATC application (30 min). (B) Percentages of hESCs with nuclear Nanog, Oct4, and Sox2 after ATC treatment compared with control. (C) Immunoblot analysis of protein expression in hESCs. Scale bars: 50 μm. All quantifications were from at least 3 independent experiments with two replicates per experiment. Unpaired t test p values < 0.05 (*), < 0.01(**), and < 0.001 (***); n.s, not significant.

3.3.3 Cyclic forces to hESCs activated focal adhesion kinase (FAK) and a switch from E- to N-cadherin

Since FAK is an important mechanotransductive component downstream of force-activated integrin (*30*), we examined whether ATC application influenced changes of FAK in hESCs. We detected phosphorylated FAK (pFAK) in the cytoplasm of hESCs subjected to ATC stimulation, and the percentage of cells with cytoplasmic pFAK increased significantly compared with untreated controls (Figure 3-9B). These results are consistent with a recent result of pFAK in differentiated hESCs (*31*). No change was observed in the cells without attached microbubbles with ultrasound (-MB +US) and with attached microbubble and without ultrasound (+MB -US) treatment groups (Figure 3-10A, B). In addition, a decrease was observed in integrin alpha V (ITGAV) and FAK (PTK2) gene expression in microbubble attached and ultrasound treated group while no change was observed in control groups (Figure 3-10C). In addition, we also found that loss of Oct4 and Nanog in hESCs due to ATC application was accompanied with decreased E-cadherin expression (Figure 3- 9A and B) (*32, 33*). These results support the role of E-cadherin in maintenance of hESC pluripotency (*26, 33, 34*), further suggesting loss of pluripotency and initiation of differentiation of hESCs differentiation induced by ATC application.

Unlike E-cadherin, N-cadherin is not expressed in undifferentiated hESCs, and cadherin switching from E- to N-cadherin is crucial for morphogenetic movement in embryonic development (*26, 34*). Interestingly, ATC treatment elevated N-cadherin expression hESCs, accompanied by significantly decreased Oct4 and β-catenin expression (Figure 3-11A and B). No change was observed in the group without attached microbubbles with ultrasound (-MB +US) and the group with attached microbubble and without ultrasound application (+MB -US) (Figure 3-12). When hESCs were pre-treated with PF562271 (10 mM) to inhibit FAK activity, minimal changes in N-cadherin, pFAK or Oct4 expression were observed with ATC stimulation (Figure 3- 13A and B). Treatment with blebbistatin (100 μM) also abrogated expression changes in β-catenin, E-cadherin and Oct4 due to ATC application (Figure 3- 13C and D). Taken together, these results demonstrate that cyclic force-mediated loss of pluripotency and initiation of hESCs differentiation in a colony required FAK activation and myosin II activity.

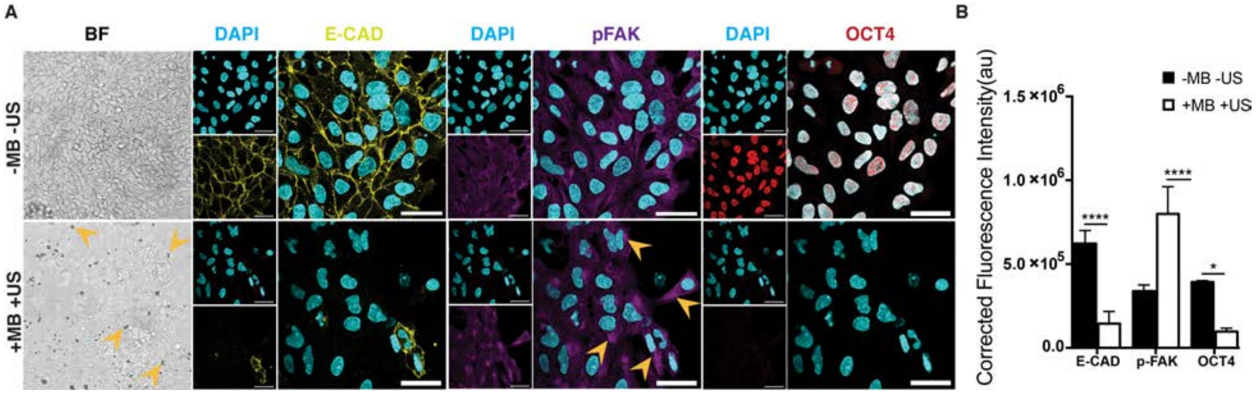

Figure 3-9 ATC application activated FAK signaling and induced differentiation of hESCs. (A) Adherent colony of hESCs stained with DAPI (blue), E-cadherin (yellow) and pFAK (purple) with and without ATC stimulation (30 min). (B) Corrected fluorescence intensity of E-cadherin, pFAK activation and Oct4 after 30 min ATC stimulation compared with control group. Scale bars 50 µm. All quantifications were from at least 3 independent experiments with two replicates per experiment. Unpaired *t* test *p* values < 0.05 (*), < 0.01(**), and < 0.001 (***). n.s. not significant.

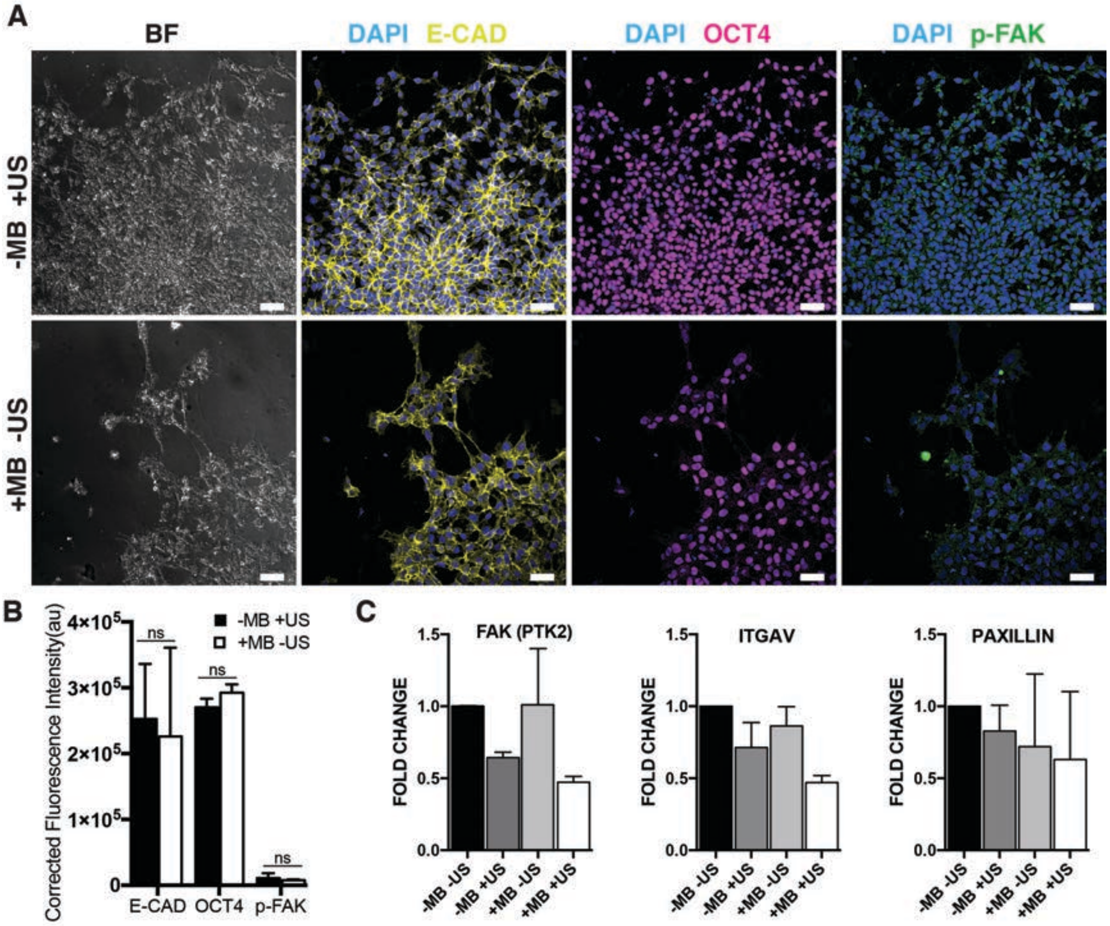

Figure 3-10. A, b) Colonies of hESCs in control groups (+MB-US, -MB+US) exhibit no changes in expression of transcription factors. C) qRT-PCR analysis of FAK, ITGAV, and Paxillin. Scale bars 50 µm. All quantifications were from at least 3 independent experiments with two replicates per experiment. Unpaired *t* test *p* values < 0.05 (*), < 0.01(**), and < 0.001 (***). n.s. not significant

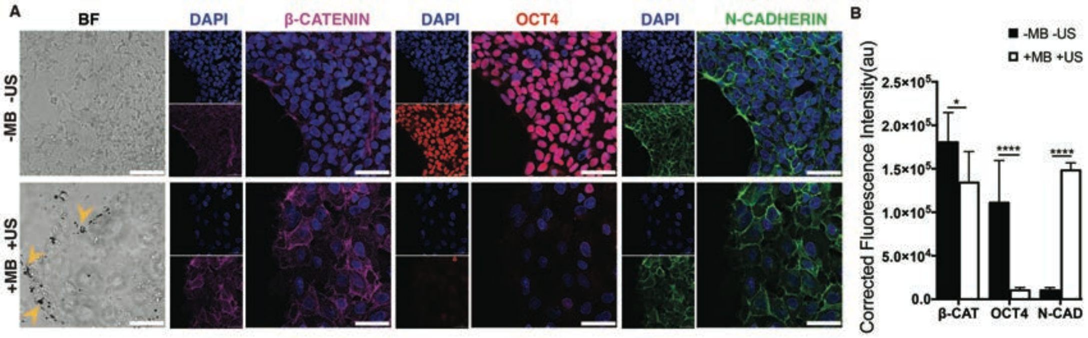

Figure 3-11 ATC application induced differentiation of hESCs by elevated levels of N-cadherin and decreased β-Catenin expression (A) Adherent colony of hESCs stained with DAPI (blue), β-Catenin (yellow), and N-Cadherin (green) after 30 min of ATC stimulation vs. control. (B) Corrected fluorescence intensity of β-catenin, N-cadherin, and Oct4 expression in hESCs after 30 min of ATC stimulation compared control. Scale bars 50 µm. All quantifications were from at least 3 independent experiments with two replicates per experiment. Unpaired *t* test *p* values < 0.05 (*), < 0.01(**), and < 0.001 (***). n.s. not significant.

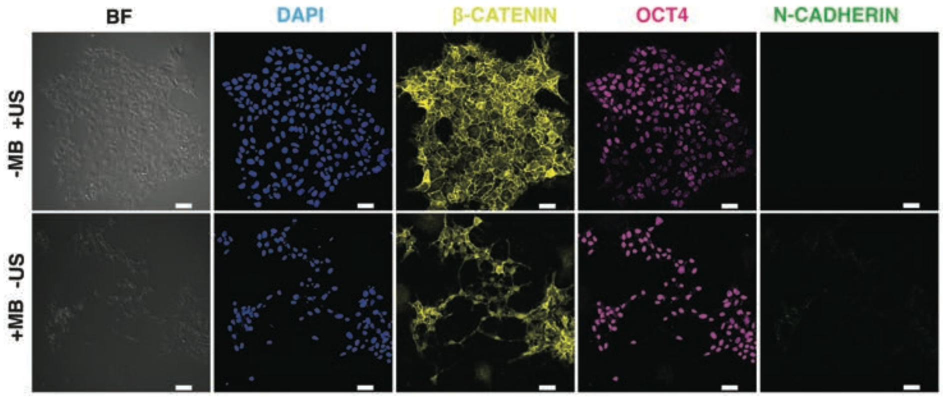

Figure 3-12: Colonies of hESCs in control groups (+MB-US, -MB+US) exhibit no changes in expression of β-catenin, Oct4 and N-cadherin. Scale bars 50 µm. All quantifications were from at least 3 independent experiments with two replicates per experiment. Unpaired *t* test *p* values < 0.05 (*), < 0.01(**), and < 0.001 (***). n.s. not significant

3.3.4 Cyclic forces applied to integrin induced rapid epithelial-mesenchymal transition (EMT) in hESCs

As the ATC-induced loss of pluripotency and initiation of differentiation of hESCs in monolayer culture is associated with characteristic EMT events such as an E- to N-cadherin switch (Figure 3-9), we examined the extent of ATC induced up-regulation of E-cadherin repressor molecules in hESC colonies (*33, 34*). Indeed, ATC application significantly upregulated the transcription factors Snail and Slug, while decreasing Oct4 in hESCs (Figure 14, A and B). No change was observed in the group without attached microbubbles with ultrasound (-MB +US) and the group with attached microbubble and without ultrasound (+MB -US) (Figure 3-15, A and B). In addition, hESCs subjected to ATC treatment exhibited a significant increase in T (brachyury) expression (Figure 3-16, A and B). No change was observed in the group without attached microbubbles with ultrasound (-MB +US) and the group with attached microbubble and without ultrasound (+MB -US) (Figure 3-15, C and D). No change was observed in T and Snai1 gene expression (Figure 3-16C). These results demonstrated that 30 min application of ATC-mediated cyclic forces/strains to integrin induced rapid initiation of differentiation and EMT in hESC colonies, in stark contrast with the multiple-day process of differentiation and EMT in hESCs in the presence of morphogenic factors or regulated by matrix rigidity (*33-35*).

3.3.5 ATC-mediated cyclic forces inhibit YAP nuclear localization in hESCs

Yes-associated protein (YAP) is critically involved in mechanotransduction (*36*). We conducted experiments to examine YAP activity due to ATC application. We found that 30 min ATC treatment induced translocation of YAP from the nucleus to the cytoplasm of hESCs (fig. S12 A and B), and treatment with blebbistatin abolished this effect (Figure 3-17, C and D), suggesting a possible role of YAP and CSK tension in ATC-induced hESC phenotypic change. These results are consistent with the notion that force-mediated Hippo/YAP activities and CSK contractility are involved in mechanotransductive processes in hESCs (*9*). It has been shown that stiff surfaces promote nuclear localization of YAP to facilitate hESC expansion (*37*), and compliant substrates inhibit nuclear localization of YAP, promoting efficient differentiation of hPSCs into postmitotic neurons (*9, 38*). However, ATC-mediated cyclic forces increased cell contractility while promoting cytoplasmic YAP localization in differentiating hESCs. This result suggests that ATC induced initiation of hESC differentiation in a different manner from substrate rigidity, highlighting the unique mode of integrin-targeted cyclic forces in directing hESC fate.

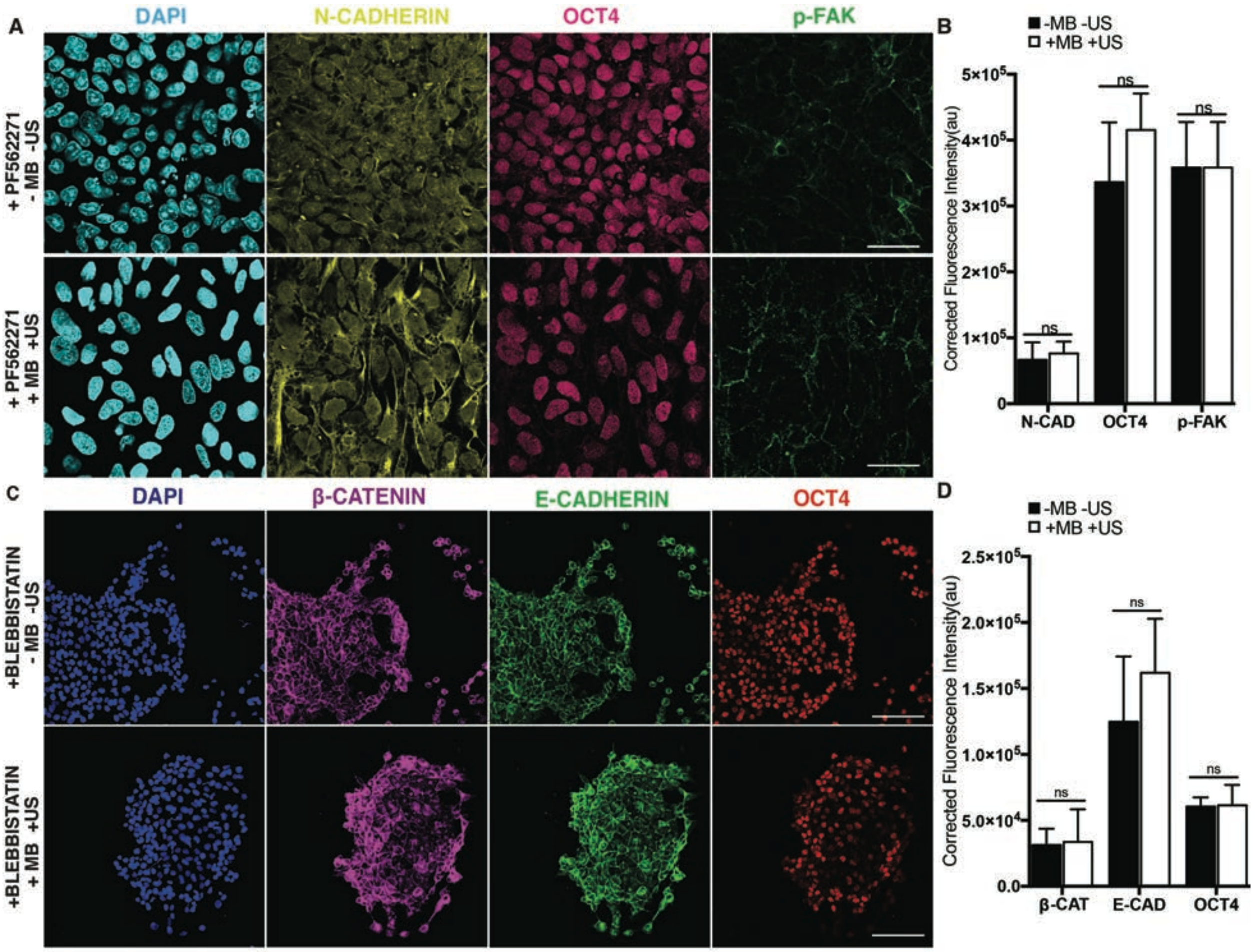

Figure 3-13: FAK inhibition abolished ATC-induced changes in hESCs. (A) hESCs treated with FAK inhibitor PF562271 showing DAPI (blue), N-cadherin (yellow), Oct4 (magenta), and pFAK (green) stain with and without ATC application. (B) Fluorescent intensity of N-cadherin expression and percentages of hESCs with Oct4 and pFAK expression in hESCs treated by PF562271 with and without ATC stimulation. (C) hESCs treated with blebbistatin stained with DAPI (blue), β-Catenin (pink), E-Cadherin (yellow), and Oct4 (red) with and without 30 min application of ATC. (D) Fluorescent intensities of β-catenin and E-cadherin expressions, and percentage of hESCs with Oct4 localization with and without ATC stimulation. Scale bars 50 μm. All quantifications were from at least 3 independent experiments with two replicates per experiment. Quantifications were mean ± SEM; unpaired t test p values < 0.05 (*), < 0.01(**), and < 0.001 (***); n.s. not significant.

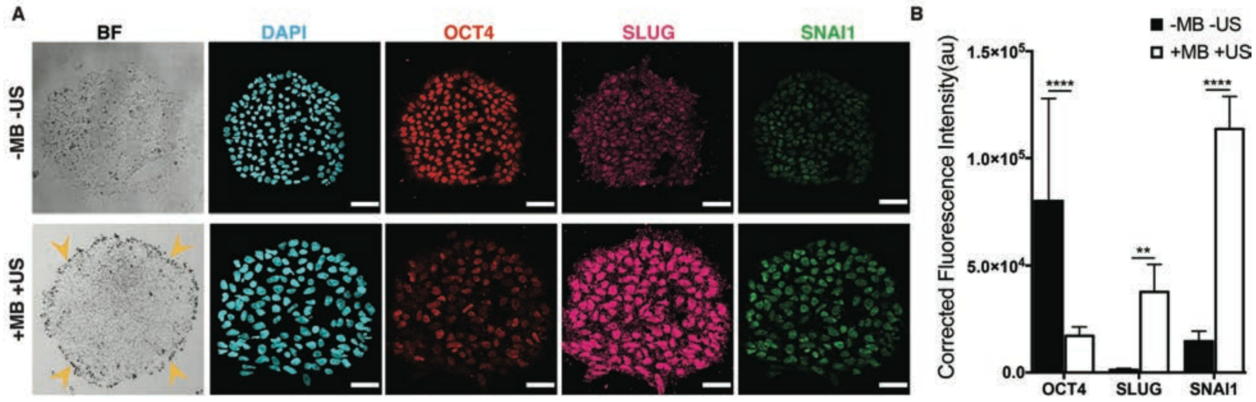

Figure 3-14. ATC application induced differentiation and EMT events in hESC colonies. (A) Colony of hESCs stained with DAPI (blue), Oct4 (magenta), Slug (yellow), and Snai1 (green) with and without ATC stimulation (30 min). (B) Corrected fluorescence intensity of Oct4, Snail, and Slug expression in the cells after 30 min of ATC stimulation compared with control. Scale bars 50 µm. All quantifications were from at least 3 independent experiments with two replicate monolayers per experiment. Unpaired *t* test *p* values < 0.05 (*), < 0.01(**), and < 0.001 (***). n.s. not significant.

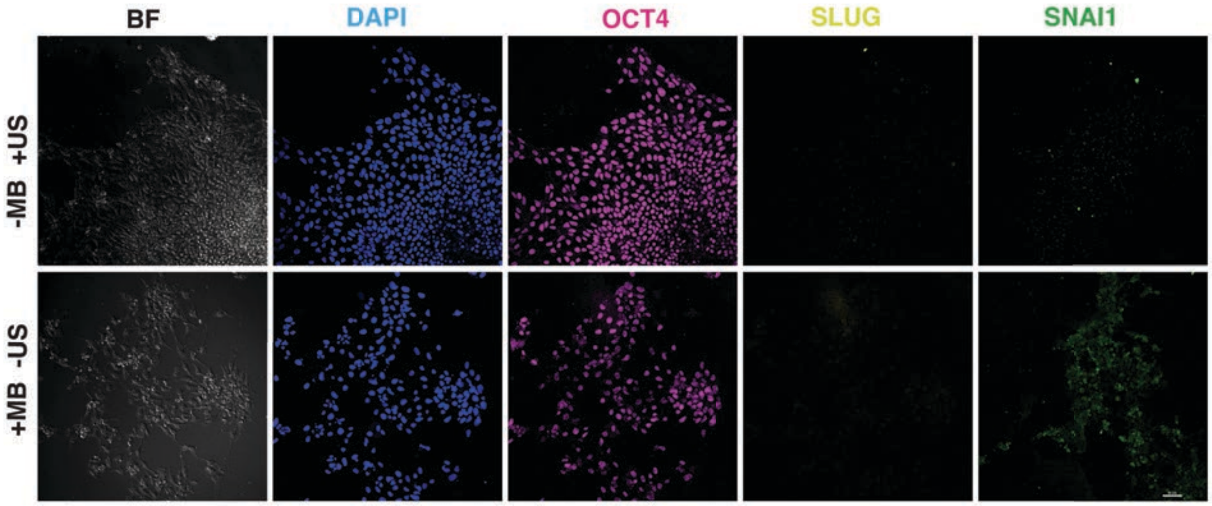

Figure 3-15: Colonies of hESCs in control groups (+MB-US, -MB+US) exhibit no changes in expression of Slug and Snai1. Scale bars 50 µm

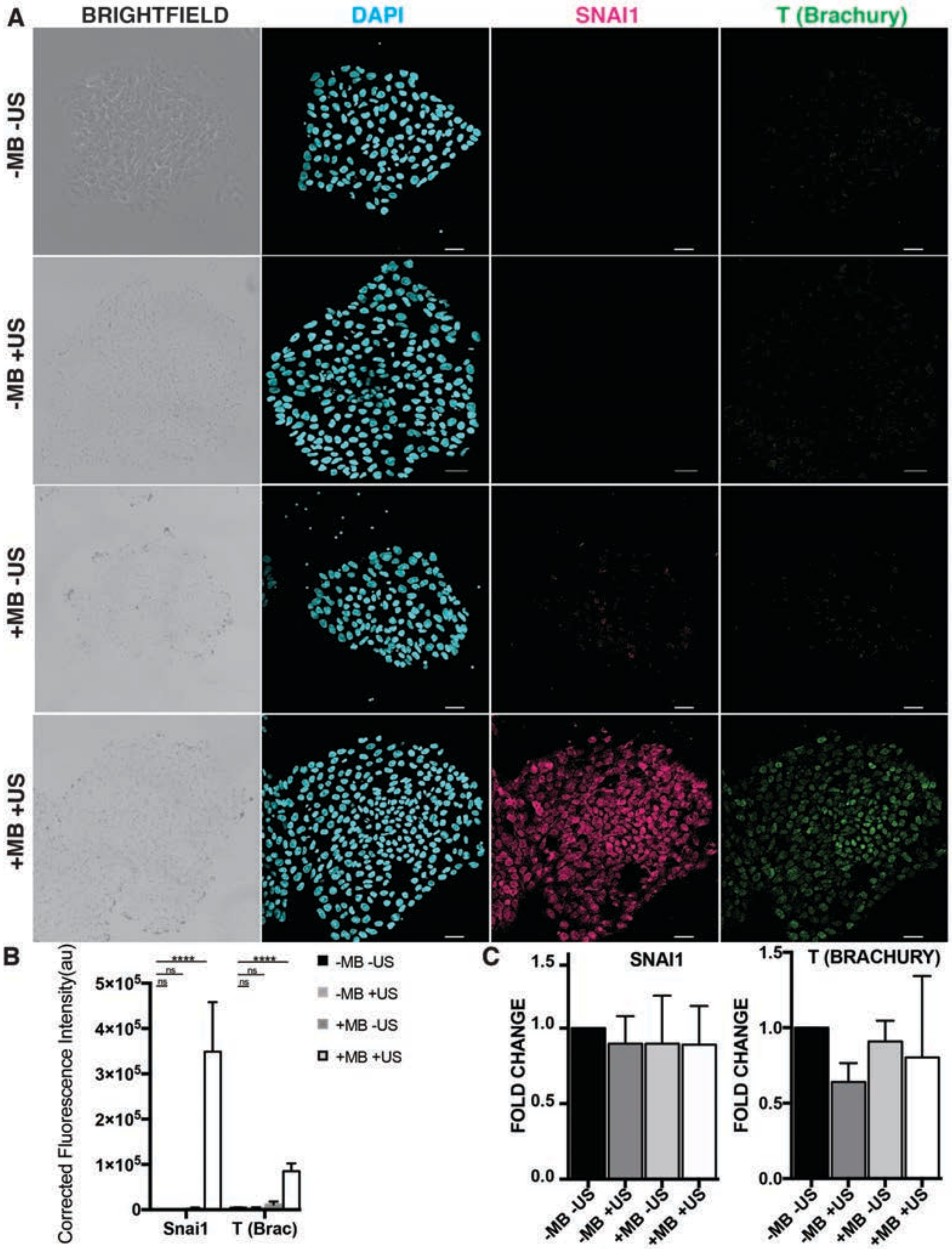

Figure 3-16: ATC application increased expression of Snail and T in hESC colonies. (A) hESCs were stained with DAPI (blue), Snail (purple), and T (Brachury) (yellow) with and without 30 min of ATC stimulation. Scale bars 50 µm. (B) Quantification of Snai1 and T expression after 30 min of ATC application compared with control group. Data from 3 independent experiments with two replicates per experiment. Unpaired t test p values < 0.05 (*), < 0.01(**), and < 0.001 (***). n.s. not significant.

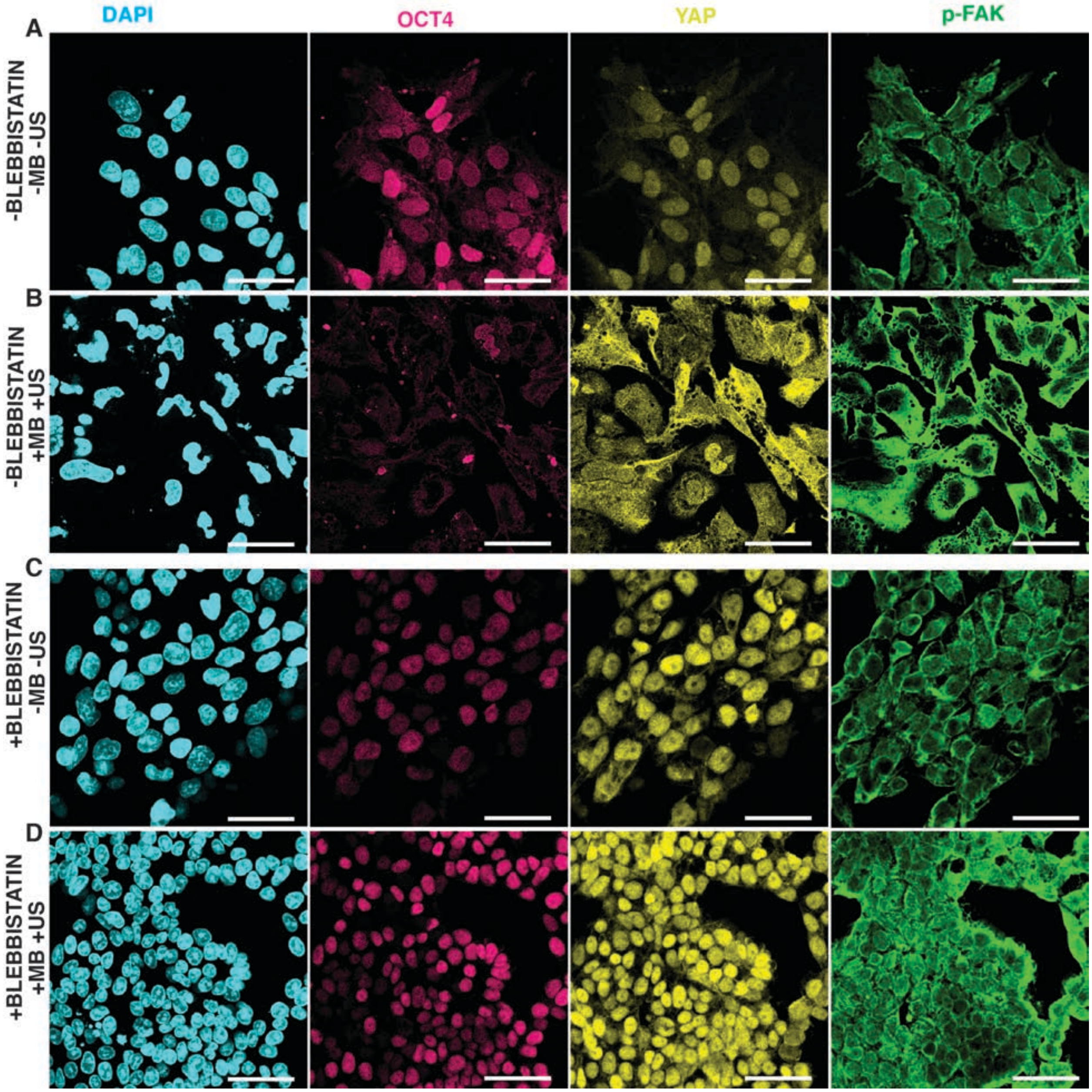

Figure 3-17: ATC-induced hESC differentiation required activation of FAK and NMII activity. hESCs with (A and B) and without (C and D) Blebbistatin treatment were stained with DAPI (blue), Oct4 (magenta), pFAK (yellow), and YAP (green), with and without 30 min of ATC stimulation. Scale bars 50 µm.

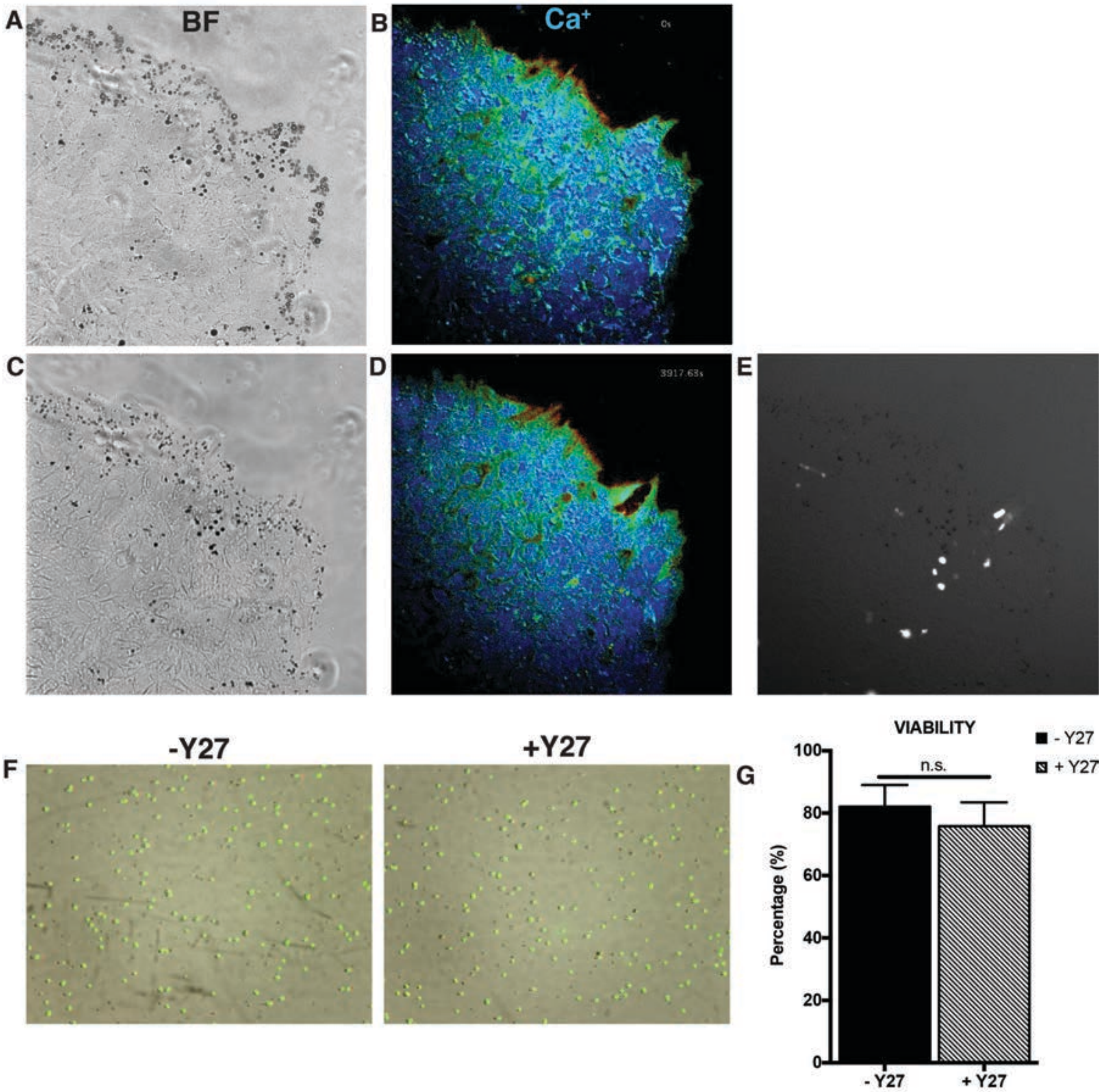

Figure 3-18 ATC-induced hESC differentiation does not lead cell death. Bright field images and pseudo color ratio matric calcium image (A, B) before ATC, and C,D) post entire fluorescent recording (5mins pre ATC, 30mins ATC and 30 mins post ATC). (E) PI image after the entire fluorescent recording. PI was added after the entire fluorescent recording. Cells treated with and without rock inhibitor (y27) to check viability using Acridine Orange/Propidium Iodide, green (live) cells (AO^+), red (dead) cells (PI^+) (F and G).

3.4 Conclusion

It is well known in other organisms that the embryo will experience tension and compression forces before and after gastrulation, i.e. attachment of to the uterine wall and beginning the development processes, with many cells enacting their forces on the embryo to facilitate development. However, as the magnitude and duration of the actual forces experienced by earlier embryos encountered during implantation is difficult to obtain, it is difficult to make direct comparison between the ATC induced forces and that in *in vivo* environment. Nevertheless, ATC application exerted cyclic forces with a repetition frequency and amplitude that can be readily adjusted. In this work, we chose 1 Hz for the cyclic force application and about 15 nN for the magnitude, which is generally in the same order of that of typical physiological biomechanical rhythms. The short duration of ATC application in our study makes it likely to represent an acute, dynamic mechanical cue that initiated subsequent changes.

Our results demonstrate that direct cyclic force and strain applied to integrin of hESCs for 30 min generated rapid mechanoresponses in single hESCs and hESC colonies, inducing enhancement of cellular contractility, calcium activity, decrease in expression of Oct4 and Nanog, as well as events associated with EMT. For single cells and colonies, the cyclic forces not only induced changes in the cells with attached MBs, but also the cells throughout the colony. As not all the cells in the colony had attached MBs, our results reveal the orchestration of mechanoresponses in hESC colony through integrin and cell-to-cell contacts. As a result, hESCs in a colony subjected to locally applied cyclic forces/strains via integrin by ATC application progress as a homogeneous population from a pluripotent state with downregulation of transcription factors of Oct4 and Nanog, exhibiting EMT with a loss of E-cadherin and gain of migratory properties by N-cadherin expression, which were accompanied by Snail, Slug, as well as Ki-67 expression. It is possible that such responses to ATC induced cyclic forces are amplitude- and duration dependent. Whether a threshold of ATC application exists for these phenomena remains to be examined in further study.

In this study, we demonstrate that ATC application, by displacing integrin-bound microbubbles to hESCs, applied targeted forces to generate cyclic strains to individual cells with a subcellular resolution. Since US pulses used in ATC can be broadly applied to actuate integrin-bound MBs, our technique provides a high throughput strategy that can be used to study a large number of hESCs in situ simultaneously. This provides a distinct advantage over other established biophysical techniques such as optical tweezer and atomic force microscopy (AFM), which are limited to single cell analysis. Furthermore, our results show that this technique does not lead cell death based on our cell viability assay results (Figure 3-18). Our results demonstrate the potential of ATC as a new biomechanical technique that could be used for mechanobiology studies and for potentially improving the differentiation efficiency of existing protocols using growth factors for differentiation of hESCs.

3.5 References:

1. C. E. Murry, G. Keller, Differentiation of embryonic stem cells to clinically relevant populations: lessons from embryonic development. *Cell* **132**, 661-680 (2008).
2. A. Colman, O. Dreesen, Pluripotent stem cells and disease modeling. *Cell Stem Cell* **5**, 244-247 (2009).
3. C. W. Pouton, J. M. Haynes, Embryonic stem cells as a source of models for drug discovery. *Nat Rev Drug Discov* **6**, 605-616 (2007).
4. G. Q. Daley, D. T. Scadden, Prospects for stem cell-based therapy. *Cell* **132**, 544-548 (2008).
5. D. E. Discher, D. J. Mooney, P. W. Zandstra, Growth factors, matrices, and forces combine and control stem cells. *Science* **324**, 1673-1677 (2009).
6. D. E. Discher, P. Janmey, Y. L. Wang, Tissue cells feel and respond to the stiffness of their substrate. *Science* **310**, 1139-1143 (2005).
7. D. E. Ingber, Mechanical control of tissue morphogenesis during embryological development. *Int J Dev Biol* **50**, 255-266 (2006).
8. P. A. Janmey, R. T. Miller, Mechanisms of mechanical signaling in development and disease. *J Cell Sci* **124**, 9-18 (2011).
9. Y. Sun *et al.*, Hippo/YAP-mediated rigidity-dependent motor neuron differentiation of human pluripotent stem cells. *Nat Mater* **13**, 599-604 (2014).
10. S. Saha, L. Ji, J. J. de Pablo, S. P. Palecek, Inhibition of human embryonic stem cell differentiation by mechanical strain. *J Cell Physiol* **206**, 126-137 (2006).
11. D. Shook, R. Keller, Mechanisms, mechanics and function of epithelial-mesenchymal transitions in early development. *Mech Dev* **120**, 1351-1383 (2003).
12. L. Przybyla, J. M. Muncie, V. M. Weaver, Mechanical Control of Epithelial-to-Mesenchymal Transitions in Development and Cancer. *Annu Rev Cell Dev Biol* **32**, 527-554 (2016).
13. Z. Fan *et al.*, Acoustic tweezing cytometry for live-cell subcellular modulation of intracellular cytoskeleton contractility. *Sci Rep* **3**, 2176 (2013).
14. D. Chen, Y. Sun, C. X. Deng, J. Fu, Improving survival of disassociated human embryonic stem cells by mechanical stimulation using acoustic tweezing cytometry. *Biophys J* **108**, 1315-1317 (2015).
15. D. Chen *et al.*, Two-bubble acoustic tweezing cytometry for biomechanical probing and stimulation of cells. *Biophys J* **108**, 32-42 (2015).
16. L. G. Villa-Diaz *et al.*, Synthetic polymer coatings for long-term growth of human embryonic stem cells. *Nat Biotechnol* **28**, 581-583 (2010).
17. P. A. Dayton *et al.*, A preliminary evaluation of the effects of primary and secondary radiation forces on acoustic contrast agents. *Ieee T Ultrason Ferr* **44**, 1264-1277 (1997).
18. X. Xue, X. Hong, Z. Li, C. X. Deng, J. Fu, Acoustic tweezing cytometry enhances osteogenesis of human mesenchymal stem cells through cytoskeletal contractility and YAP activation. *Biomaterials* **134**, 22-30 (2017).
19. A. Burgess *et al.*, Loss of human Greatwall results in G2 arrest and multiple mitotic defects due to deregulation of the cyclin B-Cdc2/PP2A balance.

Proceedings of the National Academy of Sciences of the United States of America **107**, 12564-12569 (2010).

20. R. A. McCloy *et al.*, Partial inhibition of Cdk1 in G 2 phase overrides the SAC and decouples mitotic events. *Cell cycle* **13**, 1400-1412 (2014).
21. T. D. Schmittgen, K. J. Livak, Analyzing real-time PCR data by the comparative C(T) method. *Nat Protoc* **3**, 1101-1108 (2008).
22. A. del Rio *et al.*, Stretching single talin rod molecules activates vinculin binding. *Science* **323**, 638-641 (2009).
23. X. Hu, F. M. Margadant, M. Yao, M. P. Sheetz, Molecular stretching modulates mechanosensing pathways. *Protein Sci* **26**, 1337-1351 (2017).
24. M. A. Wozniak, C. S. Chen, Mechanotransduction in development: a growing role for contractility. *Nat Rev Mol Cell Biol* **10**, 34-43 (2009).
25. M. Amano, M. Nakayama, K. Kaibuchi, Rho-kinase/ROCK: A key regulator of the cytoskeleton and cell polarity. *Cytoskeleton (Hoboken)* **67**, 545-554 (2010).
26. K. Watanabe *et al.*, A ROCK inhibitor permits survival of dissociated human embryonic stem cells. *Nat Biotechnol* **25**, 681-686 (2007).
27. J. K. Liao, M. Seto, K. Noma, Rho kinase (ROCK) inhibitors. *J Cardiovasc Pharmacol* **50**, 17-24 (2007).
28. K. A. Rosowski, A. F. Mertz, S. Norcross, E. R. Dufresne, V. Horsley, Edges of human embryonic stem cell colonies display distinct mechanical properties and differentiation potential. *Sci Rep* **5**, 14218 (2015).
29. J. J. Huang *et al.*, Functional expression of the Ca2+ signaling machinery in human embryonic stem cells. *Acta Pharmacol Sin*, (2017).
30. S. K. Mitra, D. A. Hanson, D. D. Schlaepfer, Focal adhesion kinase: in command and control of cell motility. *Nat Rev Mol Cell Biol* **6**, 56-68 (2005).
31. L. G. Villa-Diaz, J. K. Kim, A. Laperle, S. P. Palecek, P. H. Krebsbach, Inhibition of Focal Adhesion Kinase Signaling by Integrin alpha6beta1 Supports Human Pluripotent Stem Cell Self-Renewal. *Stem Cells* **34**, 1753-1764 (2016).
32. J. Lim, J. P. Thiery, Epithelial-mesenchymal transitions: insights from development. *Development* **139**, 3471-3486 (2012).
33. K. A. D'Amour *et al.*, Efficient differentiation of human embryonic stem cells to definitive endoderm. *Nat Biotechnol* **23**, 1534-1541 (2005).
34. A. M. Eastham *et al.*, Epithelial-mesenchymal transition events during human embryonic stem cell differentiation. *Cancer Res* **67**, 11254-11262 (2007).
35. C. Y. Yu, H. C. Kuo, The Trans-Spliced Long Noncoding RNA tsRMST Impedes Human Embryonic Stem Cell Differentiation Through WNT5A-Mediated Inhibition of the Epithelial-to-Mesenchymal Transition. *Stem Cells* **34**, 2052-2062 (2016).
36. S. Dupont *et al.*, Role of YAP/TAZ in mechanotransduction. *Nature* **474**, 179-183 (2011).
37. S. Musah *et al.*, Glycosaminoglycan-binding hydrogels enable mechanical control of human pluripotent stem cell self-renewal. *ACS Nano* **6**, 10168-10177 (2012).
38. S. Musah *et al.*, Substratum-induced differentiation of human pluripotent stem cells reveals the coactivator YAP is a potent regulator of neuronal specification. *Proc Natl Acad Sci U S A* **111**, 13805-13810 (2014).

CHAPTER IV

Rapid Induction of Neural Rosettes Differentiation of Human Embryonic Stem Cells

4.1 Introduction

Human embryonic stem cells (hESCs) are pluripotent cells, which derived from the inner cell mass of pre-implementation embryos, and they are capable to differentiate into all three germ layers and tissues in vitro and vivo (*1*). The isolation and culture of hESCs has opened up new opportunities for the understanding of basic stem cells biology and early human embryonic development, and to study regenerative medicine. Further, the stem cell research field was revolutionized by the development of induced pluripotent stem cells (iPSC) which are generated from fibroblasts (*2*). These cells can potentially provide unlimited numbers of neural cells for cells therapy and drug discovery due to their unique ability to produce any type of somatic cells. Since these cells provide a novel model system to elucidate the molecular signals for the development of various lineages, they are considered a useful source of somatic cells to be used in injured tissues of human diseases due their ability to differentiate into neurons, liver cells, cardiac cells that function in animal models of different diseases (*3*). During development, ectoderm develops into the polarized cells that form the neuroepithelium and neural tube arises from folding of a neuroepithelium to form central nervous system (CNS) neural cells in all vertebrates (*4*). The neural rosettes are the developmental signature of neuroprogenitors which derived from hESCs *in vitro* to recapitulate the molecular and morphogenetic sequence of events from gastrulation (*5*).

Forces are generated and transmitted across multiple scales and alter cell fate during early embryonic development (*6*). hPSCs are sensitive to their microenvironment properties, including biomechanical, and topographical cues during differentiation since they communicate with their microenvironment and this alter their cell fate including differentiation and self-renewal (*7*). Most differentiation methods developed primarily depending on soluble growth factors and small molecules that inhibit and/or stimulate particular intracellular pathway in defined culture conditions and this process takes weeks (*8-10*). For neural differentiation, most protocols accessible up to now are based on the initial embryoid bodies (EBs) formation, which initially hESCs were differentiated in free floating aggregates in the presence of serum and serum replacement, often contain cells of all 3-germ layers (*11*). However, using this method arises a complexity of multicellular aggregates, therefore it is difficult to use this system to study signaling pathways essential for the neural differentiation (*12*). Moreover, different protocols have been reported for the generation of neural stem cell cultures to enhance neural induction by using small inhibitors (SMAD inhibitor), and sonic hedgehog (SHH) pathway to yield efficient neurons (*13-15*). However, using an adherent monolayer culture system to visualize the process of direct differentiation of hESC to neural lineage is costly due to utilizing chemically defined medium for days (>10 days) and time consuming (*16*).

Patterning and differentiation protocols with many new engineering tools and methods have been developed to generate neural progeny from human pluripotent stem cells by altering their microenvironment properties and growth factors (*17, 18*). These topographical surfaces control the proliferation and differentiation of hESCs by interacting with focal adhesions through cell membrane and consequently alter intracellular signaling and transcriptional activity. Different sized-micropatterns of circular geometry was shown a self-organization ability of hESCs in the presence of BMP4 and these cells underwent to radially symmetric differentiation of 3-germ layers after 48 hours (*19*). Further, the advances in biomechanical techniques enable the studies to disentangle, investigate and elucidate the role of mechanical forces in influencing stem cell development, for example, local cyclic stress via magnetic twist cytometry (MTC) induced mouse embryonic stem cell spreading and Oct4 gene downregulation (*20*).

In our previous chapter, we reported an immediate effect of cyclic forces on hESC (*21*)and observed an upregulation of Sox2, one of the neuroectoderm markers, expression after ATC application. Here, we investigated the effects of cyclic forces combined with biochemical cues on differentiation of hESCs. Herein, using biochemical cues following ATC application, we explicitly demonstrate how extrinsic- cyclic forces mediated intracellular biochemical and transcriptional responses, ultimately inducing hESCs into neural-like rosettes in a very short time.[5]

---

[5] The research presented in this chapter has received technical assistance from Dr. Zhenzhen Fan. I would like to thank Dr. Paul H. Krebsbach and Dr. Cheri Deng for their comments on the research presented in this chapter.

4.2 Materials and Methods

4.2.1 Matrigel preparation

Matrigel® (hESC-Qualified Matrix, *LDEV-Free, cat# #354277) was diluted to a concentration of 0.1 mg/ml in cold Dulbecco's modified Eagle's medium/F12 (DMEM/F12; GIBCO) and then applied to glass bottom tissue culture polystyrene (TCPS) dishes (35 mm; 10mm glass diameter, MatTek Corporation cat# P35G- 1.5- 10-C). The coating was allowed to polymerize for 2 hours incubation at room temperature. Excess Matrigel-DMEM/F12 solution was aspirated before plating cells, and then dishes were washed with sterilized Dulbecco's phosphate buffered saline (D-PBS).

4.2.2 hESC culture

hESCs were maintained in a feeder free system- the synthetic surface PMEDSAH as described previously (*22*) and lactate dehydrogenase-elevating virus *LDEV-Free hESC-qualified Matrigel® hESC-Qualified Matrix, (Fisher Scientific, Formulation: Dulbecco's Modified Eagle's Medium with 50µg/ml gentamycin, Cat# #354277) with human-cell- conditioned medium (HCCM, MTI-Global Stem, Gaithersburg, MD, http://www.mti-globalstem.com) supplemented with 5 ng/mL of human recombinant basic fibroblast growth factor (FGF2; InvitrogenTM, Carlsbad, CA, http://www.invitrogen.com), and 1%antibiotic-antimycotic (Gibco). The hPSC culture medium was replaced every other day and all cell culture was performed in designated incubators at 37^0C in 5% CO2 and high humidity. All cultures were visually examined during every passage to ensure the absence of spontaneously differentiated cell. Differentiated cells were mechanically removed using a sterile pulled-glass pipet under a stereomicroscope (LeicaMZ9.5, Leica Microsystems Inc., Buffalo Grove, IL). All hESC were used before reaching P60.

Undifferentiated colonies were washed with PBS and a non-enzymatic cell attachment passaging solution (Lonza L7 hPSC) was added for gentle disassociation of colonies and incubated at 37^0C for 5 min. L7 was removed and 2 ml of HCCM was added, and then cells were scraped and collected into conical tube for brief centrifugation. The cell pellet was dispersed in HCCM supplemented with 5 ng/mL bFGF and 10 mM of ROCK inhibitor (Sigma) (26) and passed through a 40 mm nylon mesh cell strainer (BD Biosciences, Bedford, MA) to remove large cell aggregates. Single hESCs were counted and 100K/ ml cells were plated on Matrigel coated glass dishes cultured for overnight for attachment

4.2.3 Attachment of targeted lipid microbubble to cells

Size-isolated monodisperse functionalized ultrasound contrast agent microbubbles, SIMB4-5 (Advanced Microbubble Laboratories, Boulder, CO), was used in this study. Biotin-tagged SIMB4-5 microbubbles are biotin-tagged lipid-coated gas-filled microbubbles with the monodisperse size distribution with the peak between 4 and 5 microns. Bio-tagged SIMB4-5 microbubbles were first mixed with streptavidin solution (ThermoFisher, at the concentration of 10mg/ml) for 20mins at room temperature, at a volume ratio of 20:1 to form streptavidin-linked microbubbles. Then biotinylated Arg-Gly-Asp (RGD) peptides (Peptides International, at concentration of 2mg/ml) was added to the streptavidin microbubble mixture at the volume ratio of 2:21 and incubated for 20mins at room temperature to generate RGD linked microbubbles. To conjugated RGD-microbubbles to the cell surface, the culture medium was removed, followed by immediate addition of 50µl of microbubble solution. Then the cell culture dishes was flipped over and sit in the incubator for 10 mins to allow binding between the microbubble and the cells. Finally, the dish was flipped back, and gentle washing was performed to remove the unbound microbubbles before experiments.

4.2.4 Experimental Set up for Ultrasound

As shown in Figure 4-1, two experimental setups were employed in this study. One has the ultrasound application from the top, with the microscopic imaging ability (Figure 4-1A). Another is for large scale ATC application (Figure 4-1B). In first setup, a single element ultrasound transducer (1.25Mhz, Advanced Devices, Wakefield, MA) was mounted from the top 45 degree oblique, with its active surface submerged in the medium and 9mm (Rayleigh distance) away from the cells. The glass-bottom culture dish was placed on an inverted microscope (Nikon Eclipse Ti-U, Melville, NY), equipped with a high-speed camera (Photron FASTCAM Mini Ax200, San Diego, CA). In the second setup, a home-made single element ultrasound transducer with central frequency at 1Mhz was fixed in a programmable 3D manipulator. This setup was used for large scale ATC application. A 6-well plate was positioned in water tank, with the bottom emerged in the water. The ultrasound application was 45-degree oblique from the bottom, at 54mm (Rayleigh distance) away from the cells. The ultrasound transducer scans the whole well while sending out acoustic signal, staying at each point for 30second, and move with step size of 5mm (half of the -6db band width). Both ultrasound transducers were calibrated in free field using a 40µm calibrated needle hydrophone (Precision

Acoustics HPM04/1, UK). During the ultrasound treatment, both transducers were driven by a waveform generator (Agilent Technologies 33250A, Palo Alto, CA) and a 75W power amplifier (Amplifier Research 75A250, Souderton, PA). The total ultrasound exposure was 30 mins, including three 10mins sections with 0.035MPa, 0.045MPa, 0.055MPa pressure respectively. The PRF was 1Hz, and duty cycle was 5%.

4.2.5 Differentiation Protocol

After 30 min of with and without microbubbles and ultrasound treatment, Stemdif^{TM} SMADi neural Induction Kit (Stem Cell Tech # 08581) were added to each conditions and cultured for 6, 24, and 48 hours. After each time points, supernatant was aspirated out and plates were washed with PBS. After washing step, 1ml of Z-Fix solution was added to the plates (Anatech LTD: cat# 170), added more PBS and parafilmed to store at 4 degrees till it is used. For RNA, 1 ml of Trizol and 20ul of Glycogen were added to collect RNA after vigorous pipetting, collected in 1.5ml tubes and store at -80 degrees till it is used.

4.2.6 Drug Inhibition Assays

PF-562271 (Sigma-Aldrich) was added to the culture media at 1 µM an hour before ultrasound treatment to inhibit focal adhesion kinase phosphorylation. To inhibit the Rock pathway and the myosin-II heavy chain, Y27632 and blebbistatin (Sigma-Aldrich) was added to the media respectively at 10 µM 30 min before applying ultrasound stimulation.

4.3.7 Cell immunocytochemistry analysis

hESCs in microchannel were washed with PBS for 5 min and aspirated out the supernant and addded 1 ml of Z-Fix solution (Anatech LTD: cat# 170) for 10 min at RT shaking. Next, cells were washed 3x with 1 mL of PBS for 15 min each at RT. This was followed by sequential incubation with unmasking solution (PBS, 2N HCL, 0.5% TritonX) for 15 min, its removal, quenching solution (TBS, 0.1% Sodium Borohydride) for 15 min, its removal, and permeabilization solution (PBS, 0.02% TritonX) for 15 min. Then, blocking solution (5% BSA in 1X PBS) was added for 1hour. Microchannels were then incubated in primary antibodies overnight at 4˚C shaking. Channels were then washed with 1X PBS 3 times for 15 min at RT while shaking. We then incubated in secondary antibodies covered in foil for at least one hour at RT while shaking. Afterwards, channels were washed twice in PBS for 20 min, incubated in DAPI solution for 20 min and washed in 1X PBS for 20 min.

All antibodies, their resources, and dilutions are listed in Table B-1, and Table C-1.

All antibodies were used at a concentration of 1:1,500 with a working volume of 1.5 mL in 5% BSA in PBS. DAPI stain was used for DNA.

4.3.8 Confocal Microscopy and Image Analysis

Images were acquired on a Nikon Ti Eclipse Confocal Microscope, 20x and 60x magnification lenses, with water to capture images with or without 3x digital zoom, ¼ frames per second, 512x512 image capture, 1.2 Airy Units, 2x line averaging, appropriate voltage and power settings optimized per antibody. No modification was done, except image sizing reduction, rotation, or gray scale change for figure preparation.

Fluorescence images acquired from confocal microscopy were reconstructed in 3D using Imaris8.2 (Bitplane).

Image J was used to quantify fluorescent intensity(*23, 24*). Briefly, after selecting the cell of interest using any of the polygon drawing/selection tools, “set measurement” was selected from the Analyze menu by selecting area, integrated density and mean gray value. Then, "Measure" was selected from the analyze menu, and a region next to the cell that has no fluorescence was selected for background. This step was repeated for each single cells in the field and then the all data were analyzed on excel, and this formula was followed for the corrected total cell fluorescence (CTCF).

CTCF = Integrated Density - (Area of selected cell X Mean fluorescence
of background readings)

4.3.9 Extraction and Purification of Total RNA

Samples were washed with PBS and 1000µl of Trizol Reagent (Invitrogen, Carlsbad, CA) including 50µl Glycogen, RNA grade (TheormoFisher, R0551) was added to the plates, and RNAs were collected after vigorous pipetting. 200 µl Chloroform was added to this solution followed by centrifugation (13,000 g-15 min). Aqueous phase containing RNA was separated and 500 µl isopropanol was added and stored at 200C at least overnight. Then, the manufacturer’s RNA Clean-up protocol, RNeasy Mini-Kit (Qiagen, Valencia, CA), with the optional On-column DNAse treatment was followed. RNA quality and concentration were checked using a Synergy NEO HTS Multi-Mode Microplate Reader (BioTek Instruments, Winooski, VT).

4.3.10 Reverse-transcription PCR (RT-PCR) analysis

Reverse transcription from 2.5 µg of total RNA in a 20 µL reaction into cDNA was performed using SuperScript™ VILO™ Master Mix (ThermoFisher Cat#11755050). The synthesis of first-stranded cDNA was carried out in the PCR tube after combining SuperScript VILO, RNA, and DEPC-treated water, in the first cycle at 25ºC for 10 min, incubating at 42ºC for 60 min, and terminating the reaction at 85ºC for 5 min. Quantitative PCR was performed triplicate for for each sample using TaqMan probes (Applied Biosystems) and TaqMan Universal PCR Master Mix (Applied Biosystems) on 7900 HT Fast Real Time PCR system (Applied Biosystems). Relative quantification of gene expression data were normalized to the GAPDH expression and calculated using the 2-ΔΔCT expression level(*25*) .

All primers for RT-qPCR were purchased from ThermoFisher Life Technologies: NANOG (Assay ID: Hs02387400_g1 (FAM-MGB), UniGeneID: Hs.635882), POU5F1 (OCT 3/4) (Assay ID: Hs03005111_g1 (FAM-MGB), UniGeneID: Hs.249184), SOX2 (Assay ID: Hs01053049 (FAM-MGB), UniGeneID: Hs.518438), PAX6 (Assay ID: Hs00240871_m1 (FAM-MGB), UniGeneID: Hs.446336), SOX1 (Assay ID: Hs01057642_s1(FAM-MGB) , UniGeneID: Hs.202526), NESTIN (Assay ID: Hs04187831g1(FAM-MGB), UniGeneID: Hs.527971), BETA III TUBULIN (TUBB#3) (Assay ID: Hs00801390_s1(FAM-MGB), UniGeneID: Hs.511743), AP2A1 (Assay ID: Hs00900330_m1(FAM-MGB), UniGeneID: Hs.467125), AP2A2 (Assay ID: Hs00392195_m1(FAM-MGB) , UniGeneID: Hs.19121,), GAPDH(Assay ID: Hs02786624_g1(FAM-MGB) , UniGeneID: Hs.544577).

4.3.11 Statistical Analysis

Results are presented as Mean ± SEM. Unpaired two-tailed student's t test was performed for comparisons, and a p-value < 0.05 was considered statistically significant.

4.3 Results and Discussion

4.3.1 Upregulation of Pax6 and Sox1 expression by ATC-mediated cyclic strains in 6 hours

To use ATC to apply cyclic forces to hESCs via integrin, lipid-shelled targeted microbubbles (MBs) SIMB4-5 (Advanced Microbubble Laboratories) coated with RGD peptides targeting α5β3 integrin receptors were attached to the cells (Figure 4-1, A-C), as previously reported(*21*). Application of ultrasound (US) pulses (Figure 4-2A) exerted directional forces (17.0~25 nN) on the integrin-anchored and displacing them from their original equilibrium (Figure 4-2A). The time dependent displacement and retraction curves of the integrin-bound MBs after each pulse reveal he characteristic viscoelastic behaviors reflecting properties of he MB-integrin CSK linkage (Figure 4-2C) (Figure 4-2B). MBs Neural induction medium (NIM) was added to ATC treated and un-treated hESCs (Figure 4-1D) and we examined transcriptional response of hESCs.

hESCs undergo morphogenetic events characterized by the formation of radially organized cells termed as "neural tube-like rosettes" during neural differentiation (*11*). Cells in these structures express early neuroectoderm markers including Pax6 and Sox1 (*26, 27*). Cells in this stage are capable of differentiating into various region specific neural cell types in response appropriate cue, such as SMAD inhibitor(*28*). Pax6 is an early neuroectodermal differentiation marker and is used to monitor neural induction

(*29*), and its expression was observed as early as day 4 (*17*). We conducted experiments to examine Pax6 expression following application of ATC and neural induction. We found that hESCs without attached MBs, and US pulses in the presence of neural induction medium (NIM) exhibited no change in Oct4 and Pax6^+ expression (Figure 4-3, A and C), while Pax6^+ expression was observed as early as 6 hours (14.8%) in the presence of neural induction medium following 30 min of ATC application (Figure 4-3). Upon formation of neuroectoderm, Sox1 is expressed upon formation of neuroectoderm, while Pax6 is expressed after the formation of neural plate in the developing mouse brain (*30, 31*). We further examined Sox1 expression, another early neuro-ectodermal differentiation marker, in 30-min ATC treated and 6 hours NIM supplemented cells.

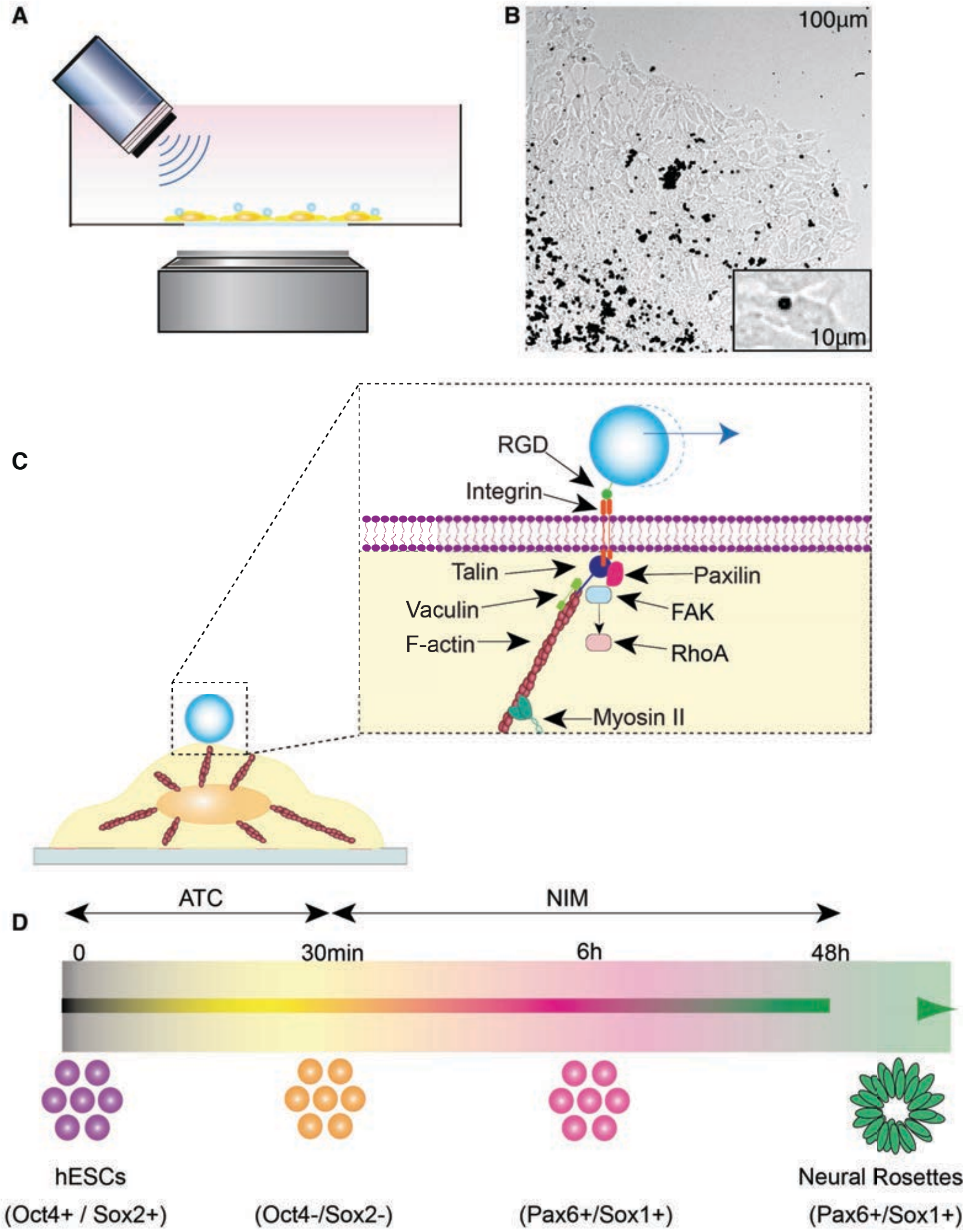

Figure 4-1. ATC application using ultrasound (US) excitation of integrin-anchored microbubbles (MBs) on hESCs and the schematic showing the hESCs differentiation protocol (A) Schematic showing ultrasound (US) excitation used in ATC (B) Bright Field images showing localization/distribution of MBs on hESC Scale bars:100 µm and 10 µm. (C) Schematic showing ultrasound (US) excitation of functionalized microbubbles (MBs) attached to a hESC via RGD-integrin binding US pulses used in ATC, resulting in mechanical stimulation via BM-integrin-CKS linage upon lateral displacement of MBs (D) Experimental setup for ATC and differentiation protocol.

We found that Sox1 started to express upon application of ATC and NIM after 6 hours (29.9%) (Figure 4-3, B and C). Although the role of cytoplasmic beta-catenin is currently unknown in controlling stem cell fate, it is documented in regulation gene expression in the nucleus as a transcriptional co-activator (*32*). In this study, beta-catenin is localized in the cytoplasm in +MB and +US group, while it is located in the nucleus in the –MB and US (Figure 4-3). In contrast, there is no change was observed in Pax6 and Sox1 expression and localization of beta-catenin without attached bubbles although exposed to the same pulses (-MB +US) and with bubbles in the absence of US pulses (+MB –US) (Figure 4-4), suggesting that expression of transcription factors started once to integrin-targeted cyclic forces applied to hESC and cultured with NIM for 6 hours suggesting that expression of transcription. Together, these results demonstrated that 30 min applications of ATC-mediated cyclic forces were accelerated Pax6 and Sox1 expression in the presence of neural induction medium as early as 6 hours.

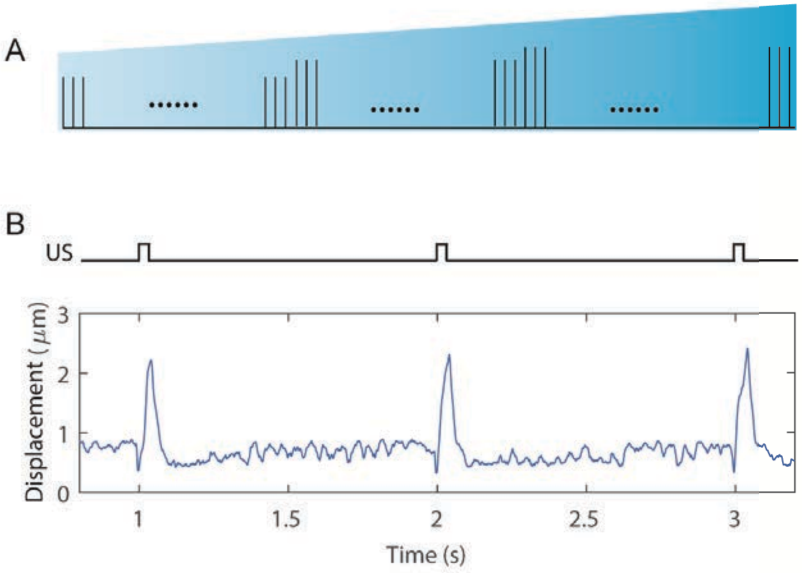

Figure 4-2. Microbubbles activity and displacement induced by ATC (A) Ultrasound pulses used in ATC (B) Cyclic MB displacement vs. time subjected to US application during ATC application.

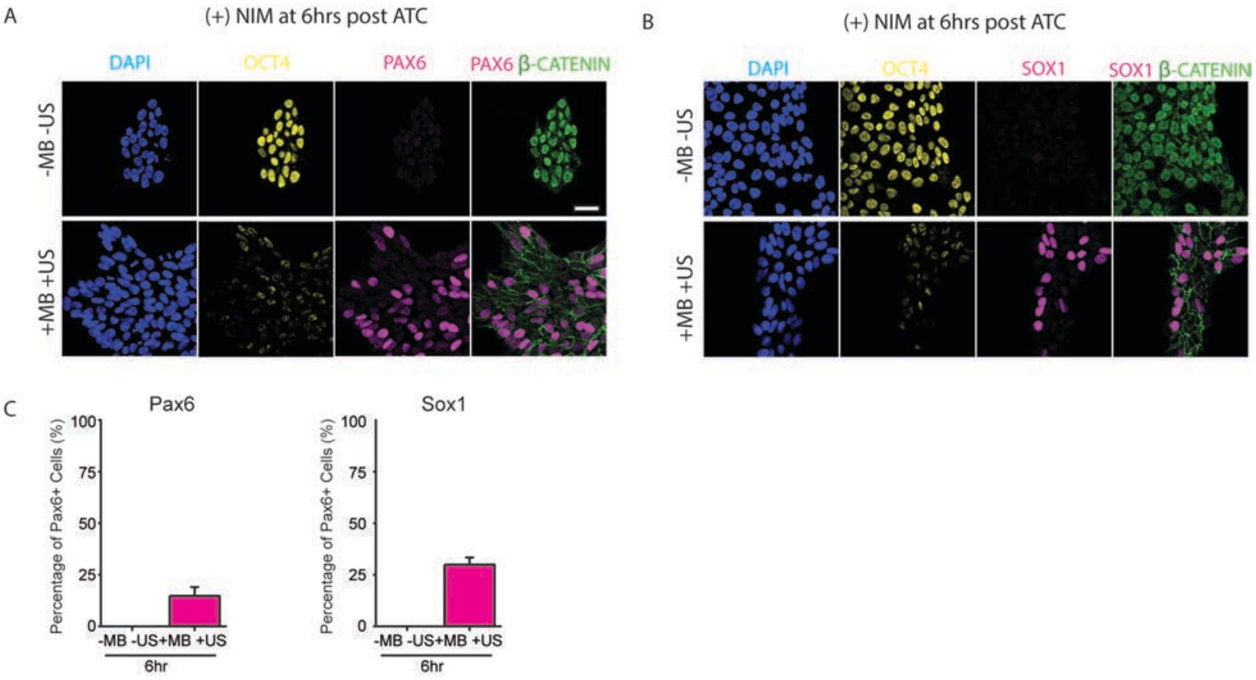

Figure 4-3. ATC application elevated Pax6 and Sox1 Expression in 6 hours. (A) Confocal fluorescence images of hESC colonies stained with DAPI (Blue), Oct4 (Yellow), Pax6 (Magenta) and Beta-catenin (Green). (B) Confocal fluorescence images of hESC colonies stained with DAPI (Blue), Oct4 (Yellow), Sox1 (Magenta), and Beta-catenin (Green). (C) Bar plots showing percentages of nuclear Pax6$^+$ and Sox1$^+$ at 6 hours. Scale bar: 50 µm

4.3.2 ATC mediated cyclic strains induce rosette formation in 48 hours

A previous report indicated that Pax6 uniformly expressed in neural rosettes at day 10, but not Sox1 in the presence of growth factors and inhibitors (*33*). Another study showed that chemically defined media supplemented with noggin resulted in Pax6$^+$/ Sox1$^-$ neural rosettes, and Pax6$^+$/ Sox1$^+$ was observed once fibroblast growth factors (FGF2, FGF8) was supplemented (*34*). On the contrary, it has shown that Pax6 expression occurs after sox1 expression during mouse brain development (*31*). We conducted experiments to examine both Pax6/ Sox1 expressions due to ATC application (Figure 4-5). Pax6$^+$/ Sox1$^+$ was not expressed in the absence of MBs and US (Figure 4-5, A and B). We found that Pax6$^+$ homogenously expressed in 48 hours in the presence of

NIM after 30 min of US pulses applied, while Oct4 expression down-regulated (Figure 4-5, C and E). We also observed catenin occurs with biochemical stimulation in 48 hours in the absence of MBs and US, while it localizes in the cytoplasm in 6 hours upon ATC treatment.

Further, qRT-PCR was performed to quantify the temporal expression of pluripotency (Nanog, Oct4, and Sox2) and neuro-ectodermal related genes (Pax6, Sox1, Nestin, Zo-1, and βIII-Tubulin) during neural induction. Pluripotency transcription factors circuitry was disrupted in MB attached and US treated cells (+MB +US) (Figure 4-7), while instantaneously stimulating neuro-ectodermal gene expression (Pax6$^+$, Sox1$^+$, and βIII-Tubulin$^+$) (Figure 4-5F) and (Figure 4-7), while there is no significant change was observed in control groups, without MB and US (-MB –US), with MB without US (+MB –US), and without MB and with US (-MB +US) (Figure 4-7). Consistent with the results reported previously that Pax$^-$ cells co-express neural crest (NC) markers, APA1A and AP2A2(*17*), no change was observed in temporal mRNA expression of AP1A and AP2A, while Pax6$^+$ expression was increased in qRT-PCR in +MB +US group (Figure 4-7).

Taken together these data demonstrate that external cyclic strain alters transcriptional activity in hESC and initiates of Pax6 and Sox1 expression in the presence of biochemical cues. This method could be leveraged to achieve substantial improvement in the neuroectoderm differentiation of hESC.

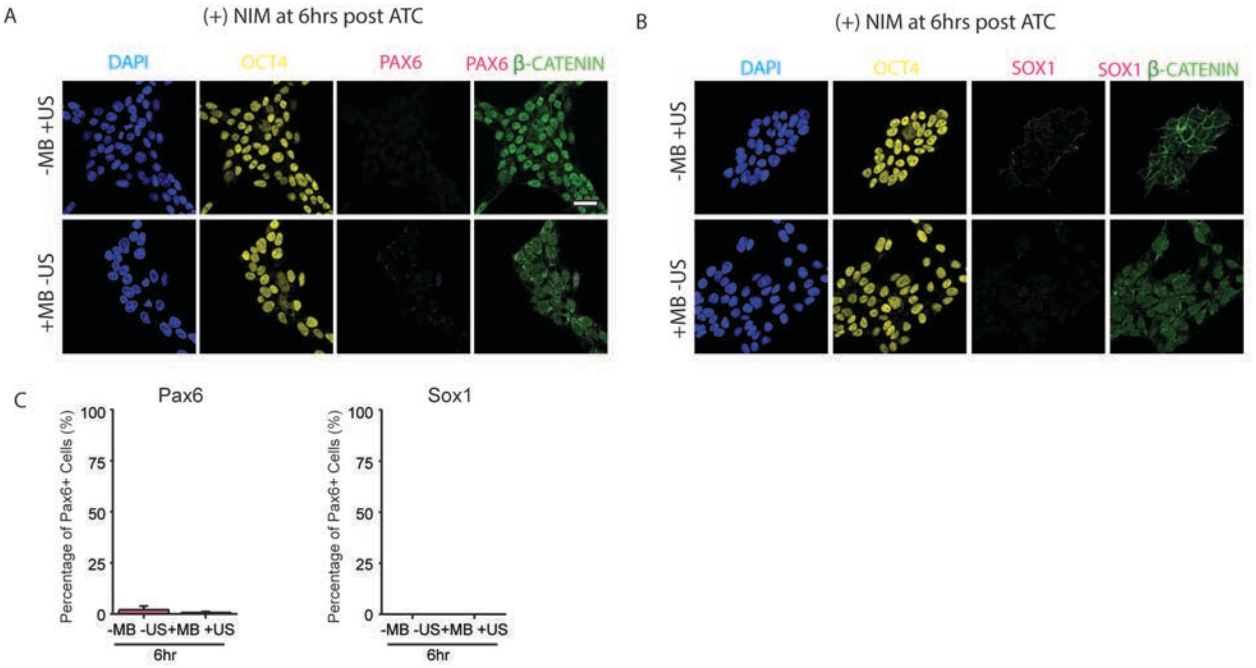

Figure 4-4. Pax6 and Sox1 Expression in 6 hours in control groups (A) Confocal fluorescence images of hESC colonies stained with DAPI (Blue), Oct4 (Yellow), Pax6 (Magenta) and Beta-catenin (Green). (B) Confocal fluorescence images of hESC colonies stained with DAPI (Blue), Oct4 (Yellow), Sox1 (Magenta), and Beta-catenin (Green). (C) Bar plots showing percentages of nuclear Pax6$^+$ and Sox1$^+$ at 6 hours. Scale bar: 50 µm

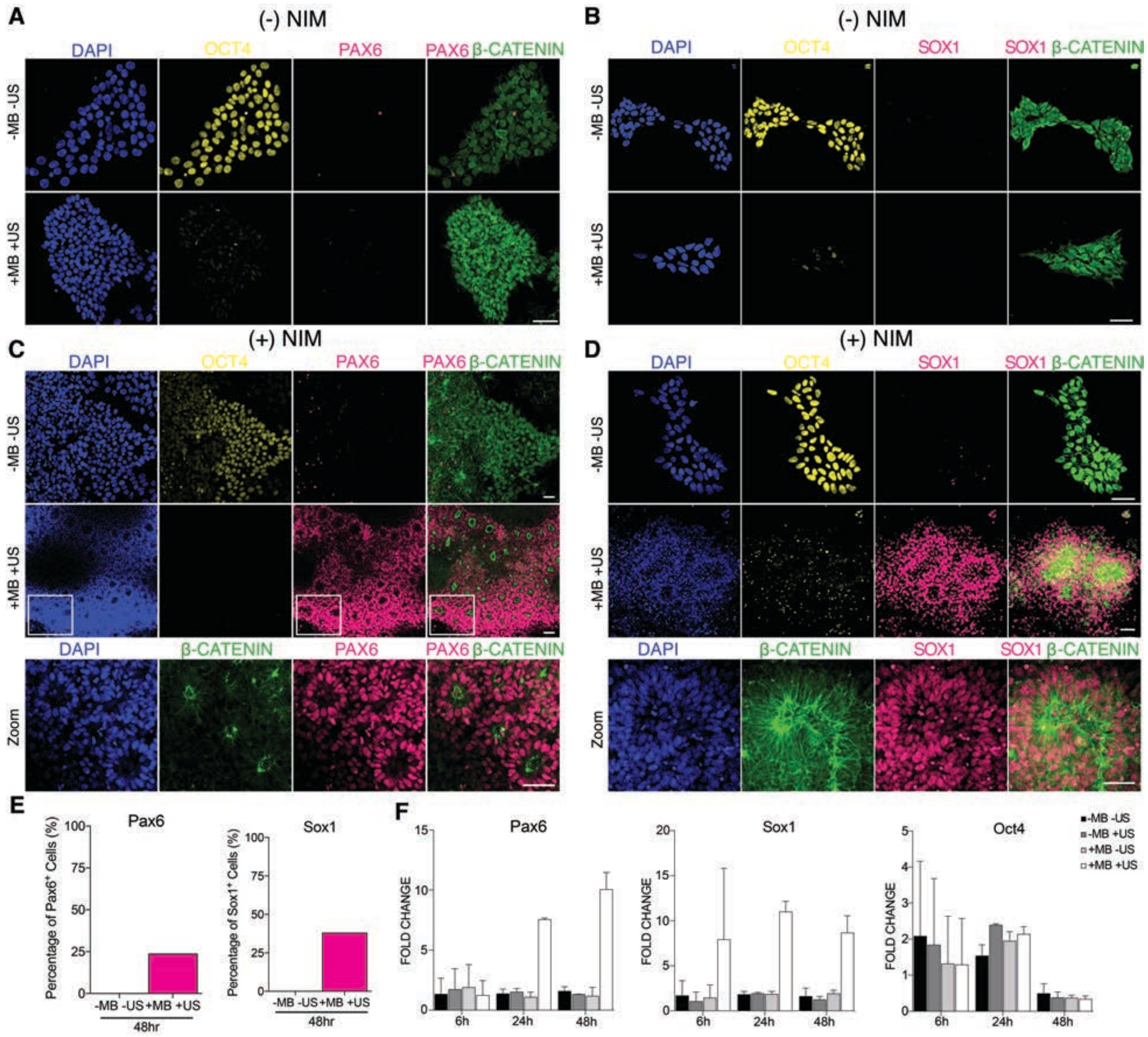

Figure 4-5. Neural-Rosette formation after 48 hours upon application of ATC (A-B) Representative immunoflurorensce images showing colony hESC stained with DAPI (Blue), Oct4 (Yellow), Pax6 and Sox1 (Magenta) and Beta-catenin (Green) in human conditioned medium (-NIM): no neural induction medium was added) (C-D) Confocal fluorescence images of hESC colonies stained with DAPI (Blue), Oct4 (Yellow), Sox1 (Magenta), and Beta-catenin (Green). After ATC application, cells were cultured in neural induction medium for 48 hours and neural rosettes formed (Zoom images) (E) Bar plots showing percentages of nuclear Pax6$^+$ and Sox1$^+$ at 48 hours. (F) Bar plots showing the fold change in qRT-PCR of Pax6, Sox1, and Oct4. Scale bar: 50 µm.

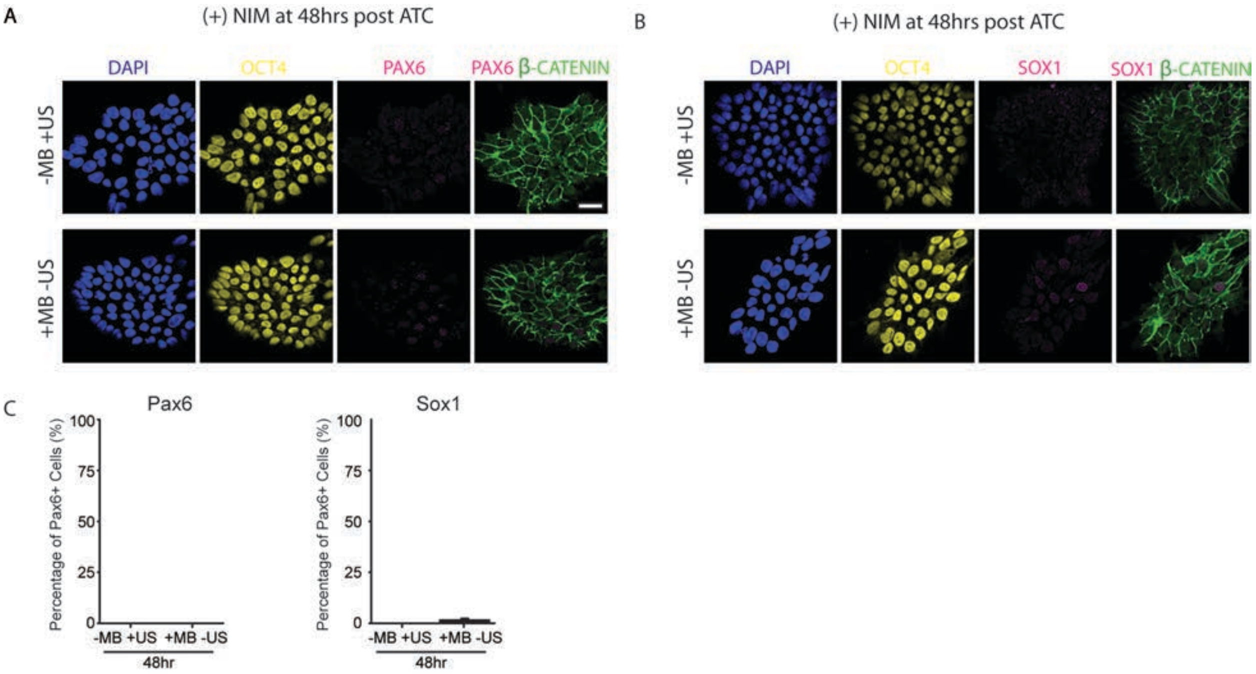

Figure 4-6. Pax6 and Sox1 expression in 48 hours in control groups (-MB +US, +MB – US) (A) Confocal fluorescence images of hESC colonies stained with DAPI (Blue), Oct4 (Yellow), Pax6 (Magenta) and Beta-catenin (Green). (B) Confocal fluorescence images of hESC colonies stained with DAPI (Blue), Oct4 (Yellow), Sox1 (Magenta), and Beta-catenin (Green). (C) Bar plots showing percentages of nuclear Pax6$^+$ and Sox1$^+$ at 48 hours. Scale bar: 50 µm

4.3.3 FAK, myosin II and Rho/ROCK signaling is required for ATC-mediated Neural Rosette Formation

The ability of cells to sense and response to intrinsic and extrinsic mechanical signal and biomechanical properties is critical in development for transduction of the information which triggers signaling pathways and this sensing occurs in cell-ECM, mainly integrin associated extracellular matrix, and cell-cell interaction, i.e. cadherins (*35, 36*). In our previous report, we have shown that inhibiting focal adhesion components by utilizing from blebbistatin, Rock Inhibitor, and FAK inhibitor, abolished

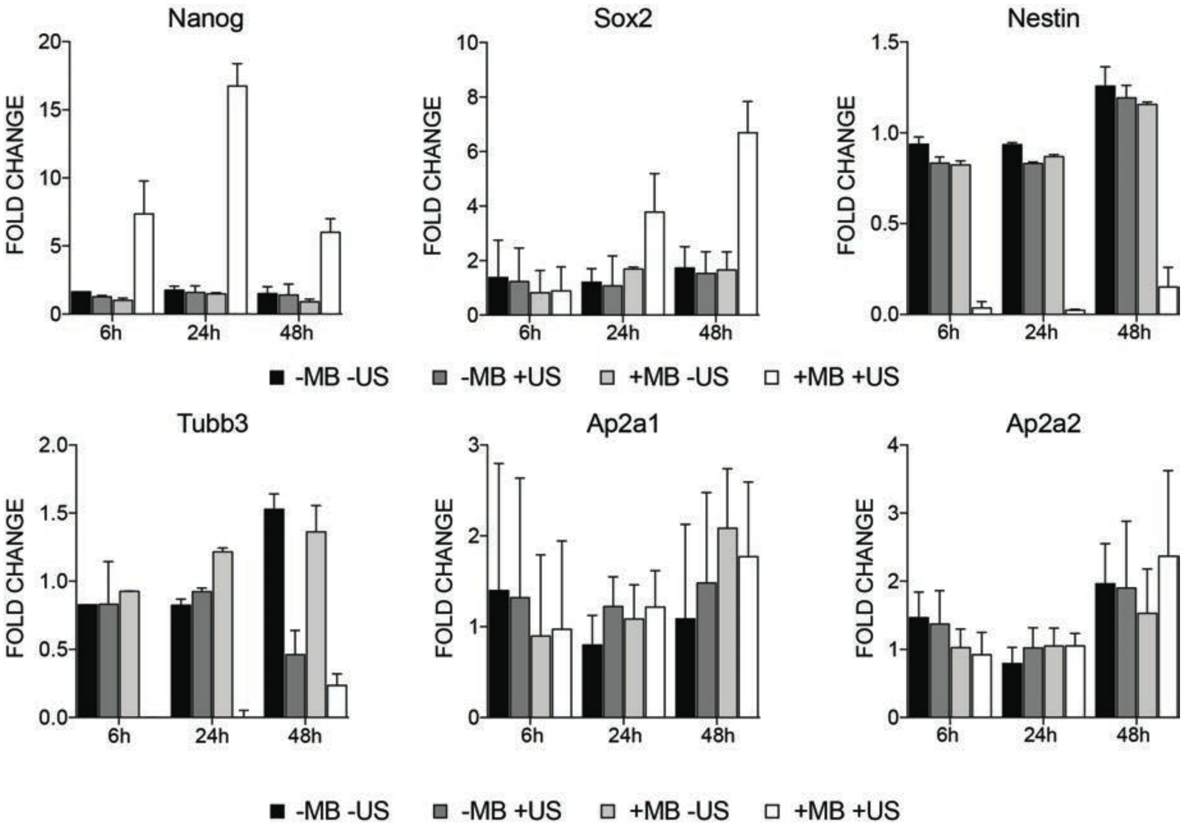

Figure 4-7. Gene expression of neural and pluripotency markers upon application of ATC and neural induction medium. Bar plots of Pluripotency markers: Nanog expression started to express at 6 hour, while Sox2 expression increased at 48 hours; -Neural markers: Nestin and Tubb3 decreased at as early as 6 hours, and no change was observed in AP2 gene expression based on the qRT PCR analysis.

the force-mediated differentiation of hESCs(*21*). Here, again we showed that inhibiting focal adhesion components by using these inhibitors during ATC treatment eliminated the effect of external mechanical forces on differentiation of hESC in the presence of neural induction medium. To prove that, we examined the expression of Pax6, Sox1, and Oct4 in all four groups (-MB –US, -MB +US, +MB –US, and +MB +US) and no expression was observed in Pax6 and Sox1 transcription factors, while Oct4 remained in the nucleus (Figure 4-8) (Figure 4-9). Taken these results together validate that cyclic force-mediated differentiation is required the activation of integrin mediated focal adhesion sites and actomyosin contractility including myosin II and Rho/ROCK pathway. Our resutsl further supports the notion that phosphorylation of FAK and Rho GTPases function in controlling ATC-mediated neuroectoderm differentiation.

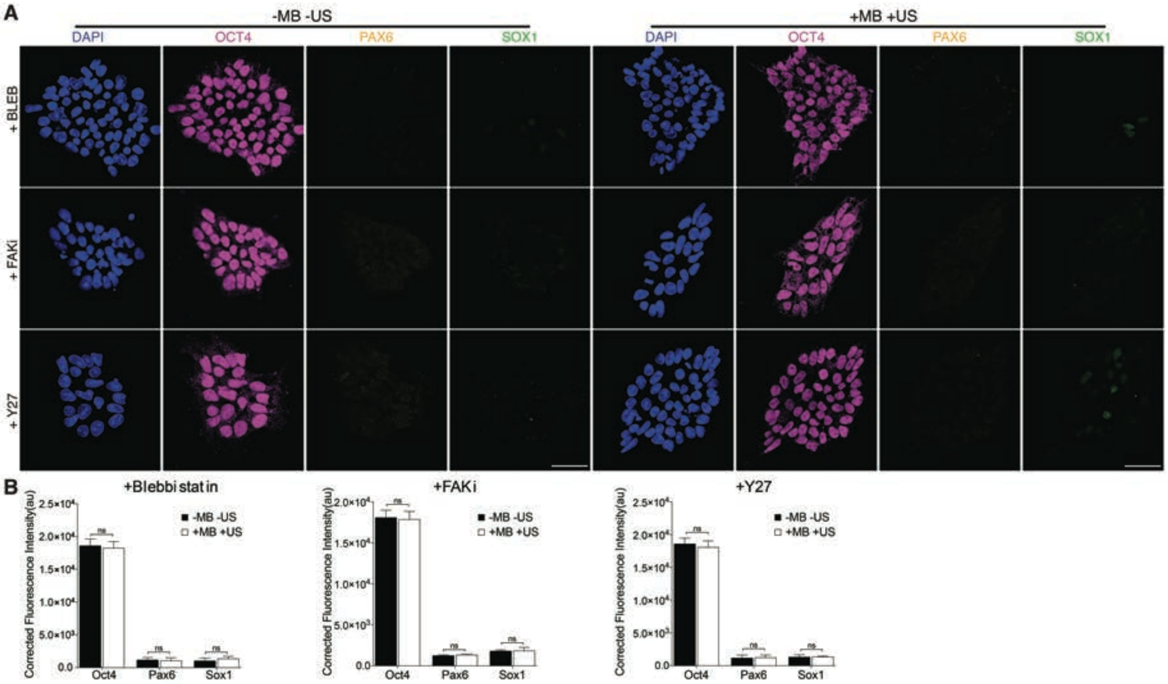

Figure 4-8. FAK, myosin II and Rho/ROCK signaling is required for ATC-mediated Neural Rosette Formation (A &B) Representative immunoflurorensce images (A) and bar plot (B) showing localization of Pax6 and Sox1 under different drug treatments. Colonies were treated with pharmacological drugs for 1 hour before ATC application (+MB +US). Negative controls (-MB –US) were included for comparison. Blebbistatin (+Bleb), FAK inhibitor (+FAK*i*), and Y-27632 (+Y27). hESC Colonies were stained for DAPI (Blue), Oct4 (Magenta), Pax6 (Yellow) and Sox1 (Green) in the presence of NIM. All quantifications were from at least 3 independent experiments with two replicates per experiment. Unpaired *t* test *p* values < 0.05 (*), < 0.01(**), and < 0.001 (***); n.s, not significant

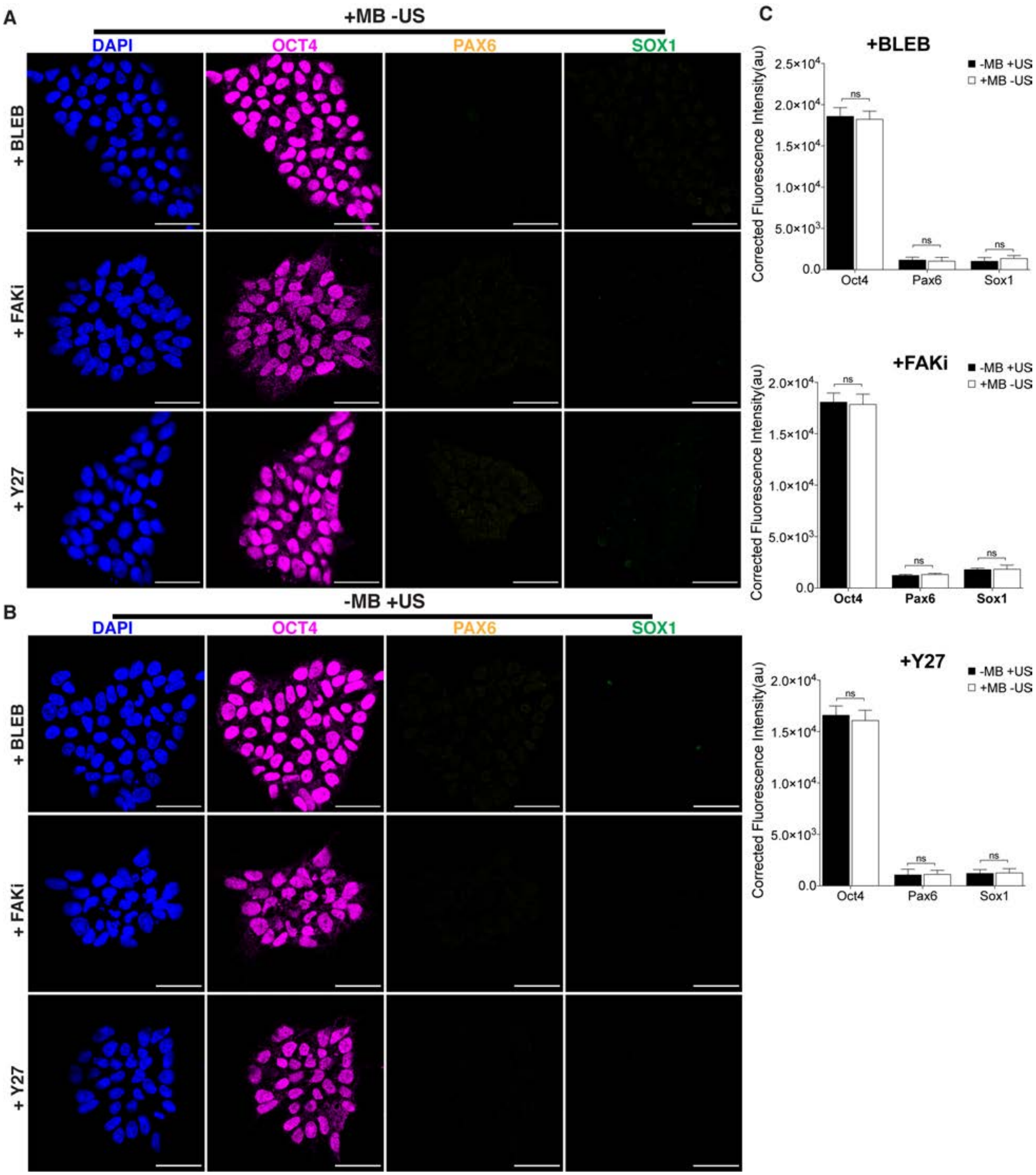

Figure 4-9. Confocal micrographs of colonies of hESC in control groups under Blebbistatin (+Bleb), FAK inhibitor (+FAK*i*), and Y-27632 (+Y27) drugs in 48 hours. (A &B) Representative immunoflurorensce images and bar plot (C) showing localization of Pax6 and Sox1 under different drug treatments. Colonies were treated with pharmacological drugs for 1 hour before ATC application (-MB +US) and MB added group was used as comparison (+MB –US). Blebbistatin (+Bleb), FAK inhibitor (+FAK*i*), and Y-27632 (+Y27). hESC Colonies were stained for DAPI (Blue), Oct4

(Magenta), Pax6 (Yellow) and Sox1 (Green) in the presence of NIM. Scale bar: 50 μm. All quantifications were from at least 3 independent experiments with two replicates per experiment. Unpaired *t* test *p* values < 0.05 (*), < 0.01(**), and < 0.001 (***); n.s, not significant

4.4 Conclusion

Recently established *in vitro* implantation protocols utilizing mouse and human embryonic stem cells have expanded our knowledge about post-implantation during early development (*37-39*). Interactions between embryonic tissue (epiblasts) and extra embryonic tissues (trophectoderm and primitive endoderm) require intricate interactions to coordinate morphogenesis during early development (*40*). During these physical interactions and cell rearrangements, epiblasts polarize and implement a rosette-like configuration (*41*). Despite the differences to form neural rosettes in different species, many contexts such as extracellular cues, physical forces regulate shaping cell polarization and rosette formation during morphogenesis at post-implantation stage of the early embryo development (*39*).

Our seminal observations that application of ATC on hESCs can elicit changes in biochemical signaling within cells. We demonstrated that ATC treated hESCs formed neural-tube like rosettes in 48 hours upon supplementing these cells with neural induction medium. Our method has accelerated neural rosette formation, which it usually takes more than 10 days *in vitro* with conventional methods. Since ATC stimulate acto-myosin contractility via MBs-integrin-CSK linkage as discussed in Chapter 3, these acto- myosin cables at cell junctions cause cell rearrangements under tension and spontaneously produce an anisotropic state in the presence of neural induction medium and form rosettes. Our approach indicates acute local mechanical stimulation has profound, long-term impact for hESC differentiation since the effect of external cues were disrupted in the presence of inhibitors even neural induction medium was supplemented. With appropriate growth factors and inhibitors cues, these cells in the neural rosettes could be used to further differentiate into various neuronal and glial cells types, such as astrocytes and dopaminergic neurons.

Our results also demonstrate the potential of ATC as a new tool for biomechanical technique to be able to use in mechanobiology of hESC to understand early development, also to utilize a high throughput setting by using a large number of hESC colonies for regenerative medicine and tissue engineering.

Beyond this feasibility study, further work is required to discover the dose-effect of magnitude and duration of ATC, and consequently the biological response of the cells to these factors. In addition, the definitive signaling pathways are needed to explore to understand molecular mechanism how integrin-bound MBs hESCs induce rapid mechanochemical conversion as detected by at local sites in the hESC cell surface.

4.5 References:

1. J. A. Thomson *et al.*, Embryonic stem cell lines derived from human blastocysts. *Science* **282**, 1145-1147 (1998).
2. K. Takahashi *et al.*, Induction of pluripotent stem cells from adult human fibroblasts by defined factors. *Cell* **131**, 861-872 (2007).
3. R. Passier, V. Orlova, C. Mummery, Complex Tissue and Disease Modeling using hiPSCs. *Cell Stem Cell* **18**, 309-321 (2016).
4. P. G. Wilson, S. S. Stice, Development and differentiation of neural rosettes derived from human embryonic stem cells. *Stem Cell Rev* **2**, 67-77 (2006).
5. Y. Elkabetz *et al.*, Human ES cell-derived neural rosettes reveal a functionally distinct early neural stem cell stage. *Genes Dev* **22**, 152-165 (2008).
6. C. J. Chan, C. P. Heisenberg, T. Hiiragi, Coordination of Morphogenesis and Cell-Fate Specification in Development. *Curr Biol* **27**, R1024-R1035 (2017).
7. Y. Sun *et al.*, Hippo/YAP-mediated rigidity-dependent motor neuron differentiation of human pluripotent stem cells. *Nature materials* **13**, 599-604 (2014).
8. M. E. Hester *et al.*, Rapid and efficient generation of functional motor neurons from human pluripotent stem cells using gene delivered transcription factor codes. *Mol Ther* **19**, 1905-1912 (2011).
9. B. Y. Hu, S. C. Zhang, Differentiation of spinal motor neurons from pluripotent human stem cells. *Nat Protoc* **4**, 1295-1304 (2009).
10. S. M. Chambers *et al.*, Highly efficient neural conversion of human ES and iPS cells by dual inhibition of SMAD signaling. *Nat Biotechnol* **27**, 275-280 (2009).
11. S. C. Zhang, M. Wernig, I. D. Duncan, O. Brustle, J. A. Thomson, In vitro differentiation of transplantable neural precursors from human embryonic stem cells. *Nat Biotechnol* **19**, 1129-1133 (2001).
12. M. K. Carpenter *et al.*, Enrichment of neurons and neural precursors from human embryonic stem cells. *Exp Neurol* **172**, 383-397 (2001).
13. P. Reinhardt *et al.*, Derivation and expansion using only small molecules of human neural progenitors for neurodegenerative disease modeling. *PLoS One* **8**, e59252 (2013).
14. D. S. Kim *et al.*, Robust enhancement of neural differentiation from human ES and iPS cells regardless of their innate difference in differentiation propensity. *Stem Cell Rev* **6**, 270-281 (2010).
15. M. Komada, Sonic hedgehog signaling coordinates the proliferation and differentiation of neural stem/progenitor cells by regulating cell cycle kinetics during development of the neocortex. *Congenit Anom (Kyoto)* **52**, 72-77 (2012).
16. L. Gerrard, L. Rodgers, W. Cui, Differentiation of human embryonic stem cells to neural lineages in adherent culture by blocking bone morphogenetic protein signaling. *Stem Cells* **23**, 1234-1241 (2005).
17. Y. Sun *et al.*, Hippo/YAP-mediated rigidity-dependent motor neuron differentiation of human pluripotent stem cells. *Nat Mater* **13**, 599-604 (2014).
18. W. Chen *et al.*, Nanotopography regulates motor neuron differentiation of human pluripotent stem cells. *Nanoscale* **10**, 3556-3565 (2018).

19. A. Warmflash, B. Sorre, F. Etoc, E. D. Siggia, A. H. Brivanlou, A method to recapitulate early embryonic spatial patterning in human embryonic stem cells. *Nat Methods* **11**, 847-854 (2014).
20. F. Chowdhury *et al.*, Soft substrates promote homogeneous self-renewal of embryonic stem cells via downregulating cell-matrix tractions. *PLoS One* **5**, e15655 (2010).
21. T. Topal *et al.*, Acoustic Tweezing Cytometry Induces Rapid Initiation of Human Embryonic Stem Cell Differentiation. *Scientific Reports* **8**, (2018).
22. L. G. Villa-Diaz *et al.*, Synthetic polymer coatings for long-term growth of human embryonic stem cells. *Nat Biotechnol* **28**, 581-583 (2010).
23. R. A. McCloy *et al.*, Partial inhibition of Cdk1 in G 2 phase overrides the SAC and decouples mitotic events. *Cell Cycle* **13**, 1400-1412 (2014).
24. A. Burgess *et al.*, Loss of human Greatwall results in G2 arrest and multiple mitotic defects due to deregulation of the cyclin B-Cdc2/PP2A balance. *Proc Natl Acad Sci U S A* **107**, 12564-12569 (2010).
25. T. D. Schmittgen, K. J. Livak, Analyzing real-time PCR data by the comparative C(T) method. *Nat Protoc* **3**, 1101-1108 (2008).
26. A. L. Perrier *et al.*, Derivation of midbrain dopamine neurons from human embryonic stem cells. *Proc Natl Acad Sci U S A* **101**, 12543-12548 (2004).
27. D. M. Suter, D. Tirefort, S. Julien, K. H. Krause, A Sox1 to Pax6 switch drives neuroectoderm to radial glia progression during differentiation of mouse embryonic stem cells. *Stem Cells* **27**, 49-58 (2009).
28. S. Shin *et al.*, Long-term proliferation of human embryonic stem cell-derived neuroepithelial cells using defined adherent culture conditions. *Stem Cells* **24**, 125-138 (2006).
29. X. Zhang *et al.*, Pax6 is a human neuroectoderm cell fate determinant. *Cell Stem Cell* **7**, 90-100 (2010).
30. L. Kan *et al.*, Sox1 acts through multiple independent pathways to promote neurogenesis. *Dev Biol* **269**, 580-594 (2004).
31. T. Mori, A. Buffo, M. Gotz, The novel roles of glial cells revisited: the contribution of radial glia and astrocytes to neurogenesis. *Curr Top Dev Biol* **69**, 67-99 (2005).
32. X. Zhou, J. P. Chadarevian, B. Ruiz, Q. L. Ying, Cytoplasmic and Nuclear TAZ Exert Distinct Functions in Regulating Primed Pluripotency. *Stem Cell Reports* **9**, 732-741 (2017).
33. B. Y. Hu *et al.*, Neural differentiation of human induced pluripotent stem cells follows developmental principles but with variable potency. *Proc Natl Acad Sci U S A* **107**, 4335-4340 (2010).
34. S. Yao *et al.*, Long-term self-renewal and directed differentiation of human embryonic stem cells in chemically defined conditions. *Proc Natl Acad Sci U S A* **103**, 6907-6912 (2006).
35. S. Cho, J. Irianto, D. E. Discher, Mechanosensing by the nucleus: From pathways to scaling relationships. *J Cell Biol* **216**, 305-315 (2017).
36. D. E. Jaalouk, J. Lammerding, Mechanotransduction gone awry. *Nat Rev Mol Cell Biol* **10**, 63-73 (2009).

37. I. Bedzhov, M. Zernicka-Goetz, Self-organizing properties of mouse pluripotent cells initiate morphogenesis upon implantation. *Cell* **156**, 1032-1044 (2014).
38. A. Deglincerti *et al.*, Self-organization of the in vitro attached human embryo. *Nature* **533**, 251-254 (2016).
39. S. E. Harrison, B. Sozen, N. Christodoulou, C. Kyprianou, M. Zernicka-Goetz, Assembly of embryonic and extraembryonic stem cells to mimic embryogenesis in vitro. *Science* **356**, (2017).
40. G. Reig *et al.*, Extra-embryonic tissue spreading directs early embryo morphogenesis in killifish. *Nat Commun* **8**, 15431 (2017).
41. J. D. Axelrod, D. C. Bergmann, Coordinating cell polarity: heading in the right direction? *Development* **141**, 3298-3302 (2014).

CHAPTER V

Summary, Conclusions and Future Directions

5.1 Rapid Nuclear Export of Oct4 and Nanog by External Uniaxial Forces

Summary and Conclusion

Embryonic stem cells are pluripotent cells that derived from the inner cell mass of the mammalian blastocyst, and they are capable of self-renewal in vitro under certain conditions (*1, 2*). The precise balance of transcription factors, Nanog, Oct4, and Sox2, plays essential roles in regulation hESC pluripotency, and down-regulation and/or over-expression of any of these factors leads a loss of maintenance of pluripotency and initiates differentiation, such as overexpression of Sox2 prompts neuroectodermal specification (*3*), while overexpression/ downregulation of Oct4 and Nanog leads mesodermal differentiation (*4, 5*).

The delicate interactions between these transcription factors suggest that not only the transcription factor levels but subcellular localization changes may also play key roles(*6*, *7*), particularly in the early stages of differentiation. Studies of pluripotency-related transcription factor translocation, however, is limited to a few reports such as a recent report that an ERK phosphorylation mutant leads to KLF4 and NANOG translocation from the nucleus to the cytoplasm and subsequent differentiation in mouse ESCs (*6*). Here, we have showed that that the pluripotency circuit can be translocated with a one-time uniaxial stretch in the absence of any genetic manipulation or use of exogenously added growth factors or cytokines with effects visible as early as 30 min after stretch. Interestingly, inhibition of translocation of NANOG and OCT4, through blocking of CRM1 inhibited, and delayed differentiation of hESCs. Moreover, our data suggest that mechanotransductive signals through focal adhesions propagate rapidly to phosphorylate FAK and promote LAMIN A/C expression and activity of CRM1 to affect the localization and function of pluripotency-related transcription factors (Figure 2-9). Our result contradicts a report that shows cyclic mechanical strain maintains pluripotency(*8, 9*) while it supports another report that demonstrates mechanical strain inhibits pluripotency gene expression by inhibiting AKT activation(*10*). We do note, that unlike these previous studies that use cyclic strain, we only apply a one-time stretch.

Cell-cell adhesion transmits physical forces and influences the dynamics of tissue formation by enabling cellular processes including tissue remodeling, migration and growth during early development(*11-14*). Interestingly, we found that uniaxial stretch translocated NANOG and OCT4 on matrigel coated substrates, while all the three-pluripotency transcription factors were translocated in cytoplasm on e-cadherin coated substrates. These results show that translocation of pluripotency factors is mechanosensitive and is impacted by whether the forces are transduced through cell-ECM or through cell-cell interactions leading to translocation of different pluripotency-related transcription factors from nucleus to cytoplasm. In this dissertation, we clearly demonstrated that external mechanical cues on pre-implantation stage of embryo development- namely uniaxial stretching and cyclic forces. Our mechanistic study indicates that pluripotency circuit can be disrupted as early as 30 min in the absence of any growth factors or mutations once uniaxial stretch was applied in an irreversible manner. This pluripotency-related transcription factor translocation is directed by intracellular transmission of biophysical signals from cell surface integrins to nuclear CRM1 and is not reliant on exogenous soluble factors (Figure 5-1).

Overall, these results in this chapter confirm that biologic responses to mechanical stress may be propagated faster than biochemical cues(*15*). These mechanotransductive processes are dependent on cell-matrix and cell-cell interactions and affect the expression of transcription factors involved in early events of embryo development, such as the translation of CDX2. Understanding how mechanical cues alter stem cell fate will provide us key insights into comprehending developmental biology and advancing regenerative medicine and biotechnology. For example, in stem cell differentiation applications, it is already common protocol to add different activators and inhibitor molecules at different time points to mimic physiological development. Our results suggest that in addition to timed exposure to biochemical factors, timed application of one-time stretch to cells may be a practical and powerful biomimetic cue to guide stem cell differentiation.

Future Directions

Translocation of pluripotency markers (KLF4 and NANOG) initiates the differentiation in mouse embryonic stem cells via mutation of ERK phosphorylation differentiation via mutating ERK phosphorylation (*6*). Here we were able to show translocation of pluripotency related factors in a short period of time by utilizing external stimuli. It is imperative to acknowledge that mechanotransduction is more physiologically relevant and an integrated cellular regulation process alter hESC fate toward specific lineages in more controllable manner. Hence, a deeper study on the role of mechanosensitive focal adhesion-cytoskeleton in relation with transcription factors signaling pathway is needed in the future to be able answer the role of biophysical cues in pre-implantation development. To drive stretched-applied cells into the terminal differentiation, biochemical factors may be needed with combination of the timing and different magnitude forces for further studies. These findings may provide new insights into the field of mechanobiology and mechanotransdcution with the help of engineering tools. Further, understanding how mechanical cues alter stem cell fate will provide us key insights into comprehending developmental biology and regenerative medicine therapies.

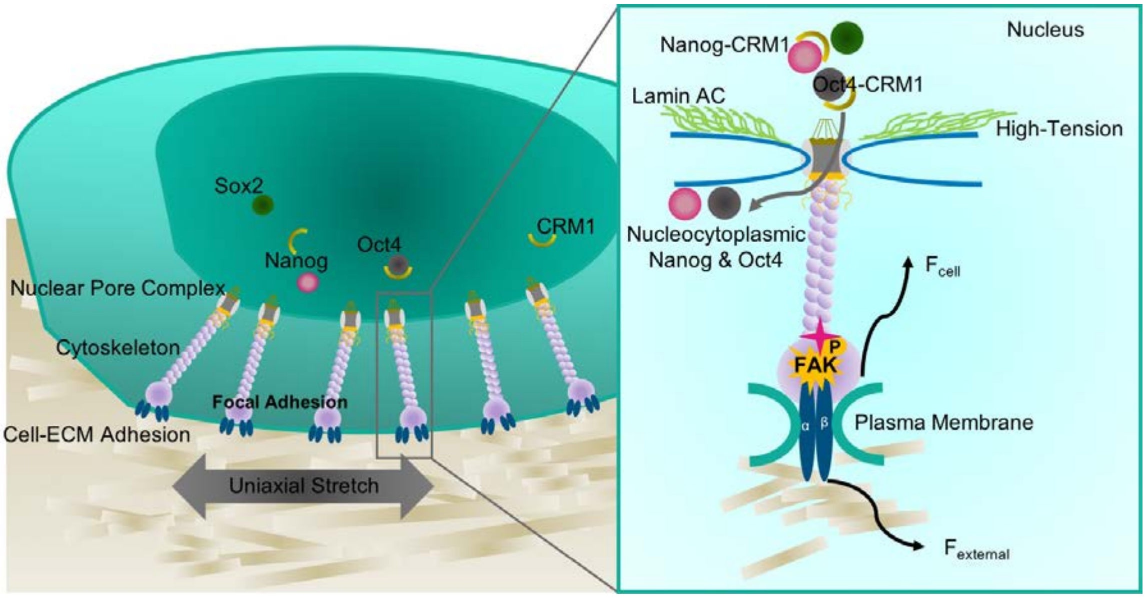

Figure 5-1 Schematic illustrations of mechanotransductive signals activated in hESCs by uniaxial mechanical strain.

5.2 Acoustic Tweezing Cytometry Induces Rapid Differentiation of Human Embryonic Stem Cells

Summary and Conclusion

It is well known in other organisms that the embryo will experience tension and compression forces before and after gastrulation, i.e. attachment of to the uterine wall and beginning the development processes, with many cells enacting their forces on the embryo to facilitate development. However, as the magnitude and duration of the actual forces experienced by earlier embryos encountered during implantation is difficult to obtain, it is difficult to make direct comparison between the ATC induced forces and that in *in vivo* environment. Nevertheless, ATC application exerted cyclic forces with a repetition frequency and amplitude that can be readily adjusted. In this work, we chose 1 Hz for the cyclic force application and about 15 nN for the magnitude, which is generally in the same order of that of typical physiological biomechanical rhythms. The short duration of ATC application in our study makes it likely to represent an acute, dynamic mechanical cue that initiated subsequent changes.

Our results demonstrated that direct cyclic force and strain applied to integrin of hESCs for 30 min generated rapid mechanoresponses in single hESCs and hESC colonies, inducing enhancement of cellular contractility, calcium activity, decrease in expression of Oct4 and Nanog, as well as events associated with EMT. For single cells and colonies, the cyclic forces not only induced changes in the cells with attached MBs, but also the cells throughout the colony. As not all the cells in the colony had attached MBs, our results reveal the orchestration of mechanoresponses in hESC colony through integrin and cell-to-cell contacts. As a result, hESCs in a colony subjected to locally applied cyclic forces/strains via integrin by ATC application progress as a homogeneous population from a pluripotent state with downregulation of transcription factors of Oct4 and Nanog, exhibiting EMT with a loss of E-cadherin and gain of migratory properties by N-cadherin expression, which were accompanied by Snail, Slug, as well as Ki-67 expression. It is possible that such responses to ATC induced cyclic forces are amplitude-and duration dependent. Whether a threshold of ATC application exists for these phenomena remained to be examined in further study.

In this study, we demonstrate that ATC application, by displacing integrin-bound microbubbles to hESCs, applied targeted forces to generate cyclic strains to individual cells with a subcellular resolution. Since US pulses used in ATC can be broadly applied to actuate integrin-bound MBs, our technique provides a high throughput strategy that can be used to study a large number of hESCs in situ simultaneously. This provides a distinct advantage over other established biophysical techniques such as optical tweezer and atomic force microscopy (AFM), which are limited to single cell analysis. Our results demonstrate the potential of ATC as a new biomechanical technique that could be used for mechanobiology studies and for potentially improving the differentiation efficiency of existing protocols using growth factors for differentiation of hESCs.

Future Directions

The ATC reported in this dissertation provides an important tool to study embryogenesis, but it would be more interesting to study the cellular and molecular mechanism that involved how ATC alter human embryonic stem cell fate rapidly. Beyond this feasibility study, further work is needed to explore the dose-effect relationship of magnitude and duration of mechanical forces applied to integrin of hESCs by ATC and the ensuing effects. Additionally, the definitive signaling pathways and molecular players that are involved in the rapid hESC differentiation in a colony induced by locally applied cyclic forces to integrin, and the integration of cell-cell contacts in the mechanoresponses of hESCs, will need to be elucidated. Understanding the specific germ-layers (endo-meso-ectoderm) derived from these mechanically induced differentiated hESCs will prove to be useful to shed light on how mechanical cues are involved in control hESC fate for the benefit of developmental biology and regenerative therapies.

Strikingly, application of this technology in the large-scale settings will be the future of this tool we established. Further, being able to stimulate bubbles in 3D systems, such as embryoid bodies or blasctocyt-like structures, via ATC would be the most attractive application and will open a new avenue in understanding early development and in the use of mechanical based- cell therapies.

5.3 Rapid Induction of Neural Rosettes Differentiation of Human Embryonic Stem Cells

Summary and Conclusion

Recently established *in vitro* implantation protocols by utilizing from mouse and human embryonic stem cells have expanded our knowledge about post-implantation during early development(*16, 17*, *18*). Interactions between embryonic tissue (epiblasts) and extra embryonic tissues (trophectoderm and primitive endoderm) require intricate interactions to coordinate morphogenesis during early development(*19*). During these physical interactions and cell rearrangements, epiblasts polarize and implement a rosette-like configuration(*20*). Despite the differences to form neural rosettes in different species, many contexts such as extracellular cues, physical forces regulate shaping cell polarization and rosette formation during morphogenesis at post-implantation stage of the early embryo development(*18*).

Our seminal observations that application of ATC on hESCs can elicit changes in biochemical signaling within cells. We demonstrated that ATC treated hESCs formed neural tube like rosettes in 48 hours upon supplementing these cells with neural induction medium. Our method has accelerated neural rosette formation, which it usually takes more than 10 days *in vitro* with conventional methods. Since ATC stimulate acto-myosin contractility via MBs-integrin-CSK linkage as discussed in Chapter 3, these acto- myosin cables at cell junctions cause cell rearrangements under tension and spontaneously produce an anisotropic state in the presence of neural induction medium and form rosettes. Our approach indicates acute local mechanical stimulation has profound, long-term impact for hESC differentiation since the effect of external cues were disrupted in the presence of inhibitors even neural induction medium was supplemented. With appropriate growth factors and inhibitors cues, these cells in the neural rosettes could be used to further differentiate into various neuronal and glial cells types, such as astrocytes and dopaminergic neurons.

Our results also demonstrate the potential of ATC as a new tool for biomechanical technique to be able to use in mechanobiology of hESC to understand early development, also to utilize a high throughput setting by using a large number of hESC colonies for regenerative medicine and tissue engineering.

Future Directions

It is discussed how biochemical cues in combination with ATC application formed neural rosettes in 48 hours. The duration and different biochemical cues and combination of these two is also intriguing yet still mysterious question, which can be studied in future by leveraging the ATC system. In particular, it would be interesting to investigate differentiating these cells into functional neurons or using other induction mediums in combination with altering the magnitude of ATC application, such as utilizing from mesoderm induction to differentiate these cardiomyocytes.

Beyond this feasibility study, further work is required to discover the dose-effect of magnitude and duration of ATC, and consequently the biological response of the cells to these factors. In addition, the definitive signaling pathways are needed to explore to understand molecular mechanism how integrin-bound MBs hESCs induce rapid mechanochemical conversion as detected by at local sites in the hESC cell surface. Moreover, application of ATC via E-cadherin bound MBs on the hESC will be interesting to explore and would open a new avenue in mechanical based therapies.

5.4 Thesis Conclusions and Outlook

Pluripotent stem cells are very unique resource for understanding developmental biology, to utilize in regenerative medicine, and tissue engineering. To direct and control their fate, various protocols have been established to be able to utilize these cells in cell-based therapy. Current differentiation protocols employ soluble molecules including cytokines, growth factors, and small inhibitors, yet recent experimental evidence demonstrates that stem cells are heavily influenced by insoluble biophysical signal, including matrix mechanics and topography, and external mechanical cues to regulate stem cell fate with and without any external soluble cues in shorter period of time. The effects of substrate stiffness on cell-ECM and cell-cell interactions and externally-applied mechanical forces have been well-studied in organisms such as Drosophila, Zebrafish, Frog, and other mammalian cells types, in cells such as MSCs, fibroblasts, and mouse ESC; however, researchers have started to explore how these mechanical cues alter hPSCs in the last decade. The field of mechanobiology is rapidly enlarging over the past decade based on the numbers of papers have been published per year due to serving as a hub in between biomedical engineering, material science, physics, and biology.

This dissertation showcased our work on developing and applying novel techniques to establish differentiation protocols of human embryonic stem cells by utilizing from external mechanical forces to improve large-scale expansion in the use of regenerative medicine and cell-based therapies, and to shed light into early human development. Our research established a novel mechanistic framework centering rapid differentiation of hESCs for understanding hESC cell behavior in early development. Mechanical forces via cell surface receptors (integrins), cell-cell adhesions (E-cadherin) and cell-ECM interaction, and cytoskeleton in relation to proliferation and differentiation of hESCs was our main mechanotransductive method.

Thereby, I envision that mechanobiology of hESC will be more focused study in the next decade especially considering its importance in development and potential use in large scale manufacturing for functional derivatives, specifically patient specific approaches by using human induced pluripotent stem cells (hiPSCs).

Future studies will likely focus on the role of biophysical cues on differentiation of hESCs into different germ layers and to explore the biophysical cues stimulated signaling pathways in the use of drug discovery, regenerative medicine. It remains to be determined the relative significance of endogenous and exogenous biophysical forces in two-dimensional and three-dimensional culture environments of hESCs.

Although accumulating evidence demonstrates the importance of mechanical cues during development, the study of mechanotransduction of hPSCs is still in its early stages, and we still lack the knowledge of how individual cells sense global changes in tissue and transduce these signals to alter gene expression robustly, and how combination of physical cues and biochemical signaling act together during development. The information to be gained from these studies may help tissue engineers design large scale expansion and build more stable differentiation protocols to maximize differentiation of these cells in order to utilize them in regenerative medicine and cell therapies. Further, this multidisciplinary approach, which involves the combination of stem cell biology, material sciences, bioengineering, medicine, and surgery in the uses of hPSC may improve the regulation of stem cell fate in bioartificial systems to facilitate functional engraftment and tissue regeneration *in vivo.*

5.4 References

1. M. F. Pera, B. Reubinoff, A. Trounson, Human embryonic stem cells. *J Cell Sci* **113 (Pt 1)**, 5-10 (2000).
2. P. J. Donovan, J. Gearhart, The end of the beginning for pluripotent stem cells. *Nature* **414**, 92-97 (2001).
3. J. L. Kopp, B. D. Ormsbee, M. Desler, A. Rizzino, Small increases in the level of Sox2 trigger the differentiation of mouse embryonic stem cells. *Stem Cells* **26**, 903-911 (2008).
4. H. Niwa, J. Miyazaki, A. G. Smith, Quantitative expression of Oct-3/4 defines differentiation, dedifferentiation or self-renewal of ES cells. *Nat Genet* **24**, 372-376 (2000).
5. Y. H. Loh *et al.*, The Oct4 and Nanog transcription network regulates pluripotency in mouse embryonic stem cells. *Nat Genet* **38**, 431-440 (2006).
6. N. K. Dhaliwal, K. Miri, S. Davidson, H. Tamim El Jarkass, J. A. Mitchell, KLF4 Nuclear Export Requires ERK Activation and Initiates Exit from Naive Pluripotency. *Stem Cell Reports* **10**, 1308-1323 (2018).
7. M. Oka, T. Moriyama, M. Asally, K. Kawakami, Y. Yoneda, Differential role for transcription factor Oct4 nucleocytoplasmic dynamics in somatic cell reprogramming and self-renewal of embryonic stem cells. *J Biol Chem* **288**, 15085-15097 (2013).
8. S. Saha, L. Ji, J. J. de Pablo, S. P. Palecek, Inhibition of human embryonic stem cell differentiation by mechanical strain. *J Cell Physiol* **206**, 126-137 (2006).
9. S. Saha, L. Ji, J. J. de Pablo, S. P. Palecek, TGFbeta/Activin/Nodal pathway in inhibition of human embryonic stem cell differentiation by mechanical strain. *Biophys J* **94**, 4123-4133 (2008).
10. T. Teramura *et al.*, Mechanical stimulation of cyclic tensile strain induces reduction of pluripotent related gene expressions via activation of Rho/ROCK and subsequent decreasing of AKT phosphorylation in human induced pluripotent stem cells. *Biochem Biophys Res Commun* **417**, 836-841 (2012).
11. G. F. Weber, M. A. Bjerke, D. W. DeSimone, A mechanoresponsive cadherin-keratin complex directs polarized protrusive behavior and collective cell migration. *Dev Cell* **22**, 104-115 (2012).
12. C. P. Heisenberg, Y. Bellaiche, Forces in tissue morphogenesis and patterning. *Cell* **153**, 948-962 (2013).
13. D. E. Leckband, Q. le Duc, N. Wang, J. de Rooij, Mechanotransduction at cadherin-mediated adhesions. *Curr Opin Cell Biol* **23**, 523-530 (2011).
14. S. Budnar, A. S. Yap, A mechanobiological perspective on cadherins and the actin-myosin cytoskeleton. *F1000Prime Rep* **5**, 35 (2013).
15. J. L. Maitre *et al.*, Asymmetric division of contractile domains couples cell positioning and fate specification. *Nature* **536**, 344-348 (2016).
16. I. Bedzhov, M. Zernicka-Goetz, Self-organizing properties of mouse pluripotent cells initiate morphogenesis upon implantation. *Cell* **156**, 1032-1044 (2014).
17. A. Deglincerti *et al.*, Self-organization of the in vitro attached human embryo. *Nature* **533**, 251-254 (2016).

18. S. E. Harrison, B. Sozen, N. Christodoulou, C. Kyprianou, M. Zernicka-Goetz, Assembly of embryonic and extraembryonic stem cells to mimic embryogenesis in vitro. *Science* **356**, (2017).
19. G. Reig *et al.*, Extra-embryonic tissue spreading directs early embryo morphogenesis in killifish. *Nat Commun* **8**, 15431 (2017).
20. J. D. Axelrod, D. C. Bergmann, Coordinating cell polarity: heading in the right direction? *Development* **141**, 3298-3302 (2014).